ACTA UNIVERSITATIS SZEGEDIENSIS

ACTA PHYSICA ET CHEMICA

NOVA SERIES

TOMUS XIII FASCICULI 1–2

SZEGED, HUNGARIA
1967

ACTA UNIVERSITATIS SZEGEDIENSIS

ACTA PHYSICA ET CHEMICA

NOVA SERIES

TOMUS XIII FASCICULI 1—2

SZEGED, HUNGARIA
1967

Adiuvantibus

D. GÁL, J. I. HORVÁTH, K. KOVÁCS, F. MÁRTA, GY. SIPOS, Z. G. SZABÓ et F. SZÁNTÓ

redigit

ÁGOSTON BUDÓ

Edit

Facultas Scientiarum Naturalium Universitatis Szegediensis de Attila József nominatae

Editionem curant

J. GYULAI, M. HALMOS et I. GALIBA

Nota

Acta Phys. et Chem. Szeged

Szerkeszti

BUDÓ ÁGOSTON

A szerkesztőbizottság tagjai:

GÁL D., HORVÁTH J. I., KOVÁCS K., MÁRTA F., SIPOS GY., SZABÓ Z. G. és SZÁNTÓ F.

Kiadja

a József Attila Tudományegyetem Természettudományi Kara
(Szeged, Aradi Vértanúk tere 1.)

Szerkesztőbizottsági titkárok:

GYULAI J., HALMOS M. és GALIBA I.

Kiadványunk rövidítése:

Acta Phys. et Chem. Szeged

ZERO-POINT KINETIC ENERGY OF RELATIVISTIC FERMION GASES

By J. I. HORVÁTH

Department of Theoretical Physics, Attila József University, Szeged

(Received November 15, 1966)

The general idea of the geometrization of the relativistic phase-space suggested previously is discussed in some details and the method will be denoted as hyper-geometrization. Then, after a new definition of the relativistic phase-space volume, the well-known method of the calculation of the zero-point kinetic energy of perfect fermion gases will be generalized for the case when the gaseous systems are in gravitational fields with stationary Riemannian metrics.

§. 1. *Introduction*

In order to explain the internal structure of physical fields and elementary particles, respectively, *i. e.* to understand the symmetry properties recently found in high-energy physics, we have proposed [1] to consider the relativistic phase-space as a geometrical background of physical processes. The general idea of this proposal has been suggested by the analogy between the geometry of Yukawa's bilocal theory of fields and the relativistic phase-space formalism as well as by the arguments in favour of the belief that the phase-space formalism would be adequate to represent the dynamic symmetries of elementary particle physics in a natural way.

Nevertheless, an investigation of the geometrical structure of the relativistic phase-space has been suggested — independently of the arguments mentioned above — also by the increasing interest in the relativistic generalisations of kinetic and statistic theories of gases having the plasma physics [2—9] and modern astrophysical theories [9, 10] in mind. More recently [11] it was demonstrated that the proposed geometrization of the phase-space formalism [1] can very advantageously be used as a geometrical background at the foundation of the relativistic gas theory.

In the present investigation a new attempt will be suggested to clarify our way of thinking and after a short rewiew of previous results [1, 11] the definition of the relativistic phase-space volume, the zero point kinetic energy of perfect fermion gases will be calculated in Riemannian spaces to resolve a problem of the neutrino astrophysics [9, 10].

§. 2. *On the hyper-geometrization of the relativisiic phase-space*

The concept of the space-time represents the geometrisation of the space and time relations of the physical systems considered. While in the framework of the special theory of relativity only the kinematic aspects of the space and time relations are characterized and the space-time continuum as an underlying geometrical background of the physical events has been considered, in Einstein's theory of

gravitation the space-time continuum has a significantly different meaning, namely, its geometrical structure is determined by the gravitational interactions, therefore, the space-time continuum represents a geometrization of the gravitational field, too.

Somewhat analogous geometrization of the kinematic and dynamic relations has been introduced in the framework of the phase-space formalism of the non-relativistic gas theory suggested earlier by the kinetic and statistic theories of Boltzmann. This means, however, that having a relativistic generalization of the phase-space formalism in mind, the concept of the relativistic phase-space has to reveal the geometrization — in other terms: a geometrical mapping — of the space-time *and* dynamic relations of the physical systems considered.

More concretely: the concept of space-time means the geometrization of the space and time relations based on the four-dimensional group of co-ordinate transformations and the concept of the non-relativistic phase-space means a geometrization of the dynamical relations based on the contact transformations of dynamics. The requirement seems be natural that in the case of the relativistic kinetic and statistic theories of gases the geometrical structure of the relativistic phase-space has to reveal the geometrization of the space-time *and* dynamical relations of the considered system based again on the four-dimensional group of co-ordinate transformations as it will be formulated below.

If a relativistic phase-space formalism has to be developed, one must introduce in every point of the four-dimensional space-time continuum a local momentum space which is, however, only three-dimensional due to the familiar normalization condition of the four-momenta; hence, the relativistic phase-space of the gaseous particles is $(4+3)$-dimensional. In fact, the „points", *i. e.*, the „radius vectors" of the momentum-space are potentially arbitrary but, actually, as the tangents of the world lines of the particles they are governed in all points of the space-time by the equations of motions, *i. e.*, by the dynamical space and time relations of the system considered. Under these circumstances the momentum-space means the internal degrees of freedom of system dynamics localized at every point of the space-time and determined unambiguously by the potentially arbitrary initial values of motion.

In terms of the phase-space formalism the trajectories of the gaseous particles reflect their dynamical history and depend on the initial values mentioned. As a matter of fact, the dynamical relations of the system at every point of the space-time continuum are determined by the tangents of the trajectories (world-lines), *i. e.*, by the actual momentum of the particle considered. Therefore, the dynamical relations of the system depending on the dynamical history of its constituents can be geometrized only if a geometry could be introduced in which the geometrical quantities at every point of the space considered are dependent on the directions, too. Such a geometrical framework means the geometry of the general line-element space where all the geometrical quantities in every point $x \equiv \{x^\mu\}$ of the space are dependent on the homogeneous direction coordinates $v \equiv \{v^\mu\}$ [12].

In fact, beside the space and time relations, the dynamical relations of the systems are geometrized in the framework of the line-element geometry by their dependence on the directions which means a second step in the geometrization, therefore this idea may be denoted as a kind of „hyper-geometrization" based on a geometry of an adequate four-dimensional anisotropic space.

§. 3. *Invariant volume-element of the relativistic phase-space*

The natural geometrical model of an anisotropic space is the line-element geometry [1, 11, 12] which is the geometry of an ensemble of line-elements $\{x^\mu, v^\mu\}$ rather than of points as in current geometries [1]. $\{x^\mu\}$ mean the position coordinates of the line-elements and by the contravariant vector $\{v^\mu\}$ with the transformation law

$$x^{\mu'} = x^{\mu'}(x^\mu); \quad v^{\mu'} = \frac{\partial x^{\mu'}}{\partial x^\mu} v^\mu \quad \left(\Delta \overset{\text{def}}{=} \det \left| \frac{\partial x^{\mu'}}{\partial x^\mu} \right| \neq 0 \right) \tag{3.1}$$

the direction of the line-element $(x, v) \equiv \{x^\mu, v^\mu\}$ is determined. Since only a direction is defined by the vector $\{v^\mu\}$, the components v^μ are not independent of each other and only their proportions have meaning; *i. e.*, they, as homogeneous direction co-ordinates, may be regarded.

The geometric anisotropy means that all of the geometrical quantities, particularly, the components of the metrical fundamental tensor $g_{\mu\nu}$ — the most important geometrical quantity determining the geometrical structure of the line-element space — depend not only on the space point $\{x^\mu\}$ but also on the homogeneous direction coordinates $v = \{v^\mu\}$, *i. e.*, after all on the line-element: $g_{\mu\nu} = g_{\mu\nu}(x, v)$ being a homogeneous function of the variable v^μ of zero degree.

The one-parametric sequence of the line-elements

$$x^\mu = x^\mu(t), \; v^\mu = v^\mu(t) \qquad (t_1 \leqq t \leqq t_2) \tag{3.2}$$

is defined as a curve of the space $\mathscr{L}$ for the direction field $v^\mu(t)$. The length of the arch of our curve $x^\mu = x^\mu(t)$ for the regarded fields of directions $v^\mu = v^\mu(t)$ is defined by

$$s = \int_{t_1}^{t_2} \{g_{\mu\nu}(x, v) \dot{x}^\mu \dot{x}^\nu\}^{1/2} dt \quad \left(\dot{x}^\mu \overset{\text{def}}{=} \frac{dx^\mu}{dt} \right). \tag{3.3}$$

Now, let a scalar, so-called *fundamental function*

$$F(x, v) \overset{\text{def}}{=} \{g_{\mu\nu}(x, v) v^\mu v^\nu\}^{1/2} \tag{3.4}$$

be introduced, which is a homogeneous function of the variables v^μ of first order, then a vector of unit length can be defined in the direction of the line-element (x, v) by

$$l^\mu \overset{\text{def}}{=} v^\mu / F \tag{3.5}$$

which is naturally also a homogeneous function of zero degree of v^μ-s.

Due to the well known normalization condition of the four-momenta mentioned above[2]:

$$g_{\mu\nu} p^\mu p^\nu = m_0^2 \tag{3.6}$$

by the components p^μ of the four-momenta merely a direction is determined in the space-time continuum, therefore the identification

$$l^\mu \equiv p^\mu / m_0 \tag{3.7}$$

[1] The Greek indices have to be run over 0, 1, 2, 3 and the Latin ones over 1, 2, 3. Further, Einstein's summation convention will be used.

[2] The velocity of light *in vacuo* as the unit of velocity is introduced!

may be suggested and the $(4+3)$-dimensional set of "points" $\{x^\mu, p^\mu\}$ as the relativistic *phase-space* can be regarded. As usual, let the ensemble of the co-ordinates $\{x^\mu\}$ be called as *co-ordinate-space* or — in order to avoid any confusion with the space part of the space-time — *configuration-space* and that of the momentum components $\{p^\mu\}$ in every point $\{x^\mu\}$ of the configuration space as *momentum-space*. This means, however, that the framework of the line-element geometry is indeed a well fitted geometrical basis for the relativistic gas theories.

The components of the metrical foundamental tensor are in pseudo-Euclidian space-time usually constant (with the signature: $+\ -\ -\ -$) and in Riemannian space they are depending on the co-ordinates $\{x^\mu\}$. Now, if a certain direction is distinguished in the momentum-space — *e. g.*, the considered gaseous system streams with constant velocity — the momentum-space and the phase-space, respectively, loses its isotropy and the components of the metrical fundamental tensor depend on the homogeneous direction co-ordinates $\{v^\mu\}$, too; *i. e.*, $g_{\mu\nu}=g_{\mu\nu}(x^\mu, v^\mu)=$ $=g_{\mu\nu}(x^\mu, p^\mu)$. This general case will, however, not be treated below [1, 11] and actually only the Riemannian metric $g_{\mu\nu}=g_{\mu\nu}(x^\mu)$ will be used.

In order to define the local momentum-space in a covariant way under the group $\mathscr{G}_x$ of the general co-ordinate transformations (3.1), first of all let the *inhomogeneous direction co-ordinates*

$$\xi_i \overset{\text{def}}{=} \overset{\mu}{\lambda_i} p_\mu / m_0 \tag{3.8}$$

be introduced referring them at any point $\{x^\mu\}$ of the configuration-space to an orthonormal triad with space-like axes $\overset{\mu}{\lambda_i}$ $(i=1, 2, 3)$, then the orientations of the triads at different points of the configuration-space has to be co-ordinated.

The orthonormality of the space-like triad-axes means, of course,

$$g_{\mu\nu}\overset{\mu}{\lambda_i}\overset{\nu}{\lambda_k} = -\delta_{ik} \qquad (i, k = 1, 2, 3). \tag{3.9}$$

One can immediately see that if the triad-axes $\overset{\mu}{\lambda_i}$ are in the rest system $\mathscr{K}^0$ of the gaseous particles orthogonal to the four-momentum $\{p^\mu_{(0)}\} \equiv \{p^0_{(0)}, 0, 0, 0\}$, *i. e.*

$$\overset{\mu}{\lambda_i}_{(0)} p_{(0)\mu} = 0 \qquad (i=1, 2, 3) \tag{3.10}$$

(where $\overset{\mu}{\lambda_i}_{(0)}$-s denote the components of the triad axes in the frame $\mathscr{K}^0$) and the sign of p^0 — corresponding to the sign of the energy of the particles — is fixed, the inhomogeneous direction co-ordinates, being the cosine of the angles between the radius vector p^μ and the triad-axes $\overset{\mu}{\lambda_i}$, *i. e.*

$$\vartheta_i \overset{\text{def}}{=} \arccos\{\overset{\mu}{\lambda_i} p_\mu / m_0\} \tag{3.11}$$

determine uniquely the directions characterized by the momentum vectors $\{p^\mu\}$ at the points $\{x^\mu\}$ of the configuration-space.

Let the three by pairs orthogonal unit vectors $\overset{\mu}{\lambda_i}$ be called in the following as *λ-triad.* Of course, the λ-triad as a *new local frame of reference* and the inhomogeneous direction co-ordinates as the *independent components of the radius vectors of the momentum-space* may be used.

Owing to the definition (3.8) of the inhomogeneous direction co-ordinates they are invariants of the transformations (3.1) of the group $\mathscr{G}_x$. Nevertheless, the ξ_i-s are not only depending on the momentum components p^μ but also on the *a priori* orientation of the λ-triad introduced. As a matter of fact, by changing the directions of the triad-axes intrinsic transformations of the local momentum-space can by introduced which cannot be induced by any change of the co-ordinates in the configuration-space. By these transformations of the momentum-space — denoted further by $\mathscr{G}_\xi$ — internal dynamical degrees of freedom of the gas system can be characterized. Therefore, let the „co-ordinates" $\{\xi_i\}$ of the local momentum-space be called as *internal co-ordinates* and the "co-ordinates" $\{x^\mu\}$ of the configuration-space as *external co-ordinates* of the system considered.

In order to determine the handedness of the λ-triad unambigously, keeping the relations (3.9) and (3.10) in mind, it seems to be deemed proper to suppose that in the rest frame of reference $\mathscr{K}^0$ in the configuration-space the axes of the right-handed λ-triad have consecutively the same directions as those of the spatial axes of the original tetrad distinguishing $\mathscr{K}^0$; *i. e.*, they are explicitly given by

$$\{\lambda^\mu_{1(0)}\} \equiv \{0, 1, 0, 0\}, \quad \{\lambda^\mu_{2(0)}\} \equiv \{0, 0, 1, 0\}, \quad \{\lambda^\mu_{3(0)}\} \equiv \{0, 0, 0, 1\}. \tag{3.12}$$

Let the right-handed λ-triad be called in the following as λ^+-*triad*, and the left handed one as λ^--*triad*. It is obvious that by settling the handedness of the λ-triads in this way the vectors λ^μ_i are unambigously determined in any frame of reference.

This is the reason that, for sake of simplicity, our argumentation will be mostly developed in the system $\mathscr{K}^0$; namely, the results obtained can be transformed into all frames of reference without any difficulty. However, we have to bear, in all circumtances, in mind that a special choice of the orientation of the λ-triad means simultaneously a special choice of a distinguished frame of reference in the configuration-space. In fact, the rest frame of reference $\mathscr{K}^0$ meets a natural distinction of the frames; this is the reason for favouring it in the following.

As a matter of fact, the group $\mathscr{G}_\xi$, *i. e.*, the group of internal transformations of the momentum-space can be generated by the rotations of the λ-triad around its origin and by the reflexions on different symmetry elements of the triad. Consider, first of all, the rotations of the λ-triad which can be characterized by the Eulerian angles $\{\varphi, \psi, \vartheta\}$:

$$\lambda'^\mu_i = M^k_i \lambda^\mu_k, \tag{3.13}$$

where the well-known matrix-elements $M^k_i = M^k_i(\varphi, \psi, \vartheta)$ fulfil the orthogonality relations

$$M^k_i M^k_j = \delta_{ij} \quad \text{and} \quad M^r_i M^s_i = \delta^{rs}. \tag{3.14}$$

Due to the definition (3.8) of the internal (inhomogeneous direction) co-ordinates their transformation law can be obtained as follows:

$$\xi_{i'} = \lambda'^\mu_i p_\mu / m_0 = M^k_i \lambda^\mu_k p_\mu / m_0 = M^k_i \xi_k. \tag{3.15}$$

More generally we have:

$$\xi'_i = D^k_i \xi_k. \tag{3.16}$$

As the orthogonality relations (3. 10) have to remain valid also the new triad axes

$\lambda'^{\mu}_{(0)}$ are orthogonal to $p^{\mu}_{(0)}$, therefore the group $\mathcal{G}_{\xi}$ is isomorphic to the three-dimensional rotary-reflexion group.

In order to settle the orientation of the λ-triad at any or at different points of the space-time continuum it seems to be simple to use the framework of the orthonormal tetrad formalism of the Riemannian spaces discussed in details by SYNGE [13] especially favourable for our purposes.

As an orthonormal tetrad, four by pairs orthogonal unit vectors $\Lambda^{\mu}_{(\alpha)}$ are denoted where the indices in parantheses like (α) mean a label distinguishing the particular axes. The covariant components of the same tetrad are

$$\Lambda_{(\alpha)\mu}=g_{\mu\nu}\Lambda^{\nu}_{(\alpha)}. \tag{3.17}$$

Three of the axes are, of course, space-like and one is time-like. We shall always so label the axes that $\Lambda^{\mu}_{(0)}$ is time-like.

The conditions of orthonormality may be written in the form:

$$\Lambda^{\mu}_{(\alpha)}\Lambda_{(\beta)\mu}=\eta_{(\alpha\beta)}, \tag{3.18}$$

where

$$\eta_{(00)}=-\eta_{(11)}=-\eta_{(22)}=-\eta_{(33)}=\eta, \quad \eta_{(\alpha\beta)}=0 \qquad (\alpha\neq\beta) \tag{3.19}$$

$$\eta_{(\alpha\beta)}=\eta^{(\alpha\beta)}$$

is a diaxonal matrix; it satisfies the relation

$$\eta^{(\alpha\beta)}\eta_{(\beta\gamma)}=\delta^{\alpha}_{\gamma} \tag{3.20}$$

being, in language of matrix algebra, a square root of unity.

One has to emphasize that the labels on the vectors have no tensorial meaning; nevertheless, by means of the η-matrix the framework of the tensor calculus can be introduced. Let the raising and lowering of the labels be defined by

$$\Lambda^{(\alpha\mu)}=\eta^{(\alpha\beta)}\Lambda^{\mu}_{(\beta)} \quad \text{and} \quad \Lambda^{(\alpha)}_{\mu}=\eta^{(\alpha\beta)}\Lambda_{(\beta)\mu}, \tag{3.21}$$

then owing to eqs. (3.20) we have

$$\Lambda^{\mu}_{(\alpha)}=\eta_{(\alpha\beta)}\Lambda^{(\beta)\mu} \quad \text{and} \quad \Lambda_{\alpha(\mu)}=\eta_{(\alpha\beta)}\Lambda^{(\beta)}_{\mu}, \tag{3.22}$$

respectively. Finally, the relations

$$\Lambda^{\mu}_{(\alpha)}\Lambda^{(\beta)}_{\mu}=\delta^{\beta}_{\alpha} \quad \text{and} \quad \Lambda^{\mu}_{(\alpha)}\Lambda^{(\alpha)}_{\nu}=\delta^{\mu}_{\nu} \tag{3.23}$$

can be obtained. The two tetrads $\Lambda^{(\alpha)}_{\mu}$ and $\Lambda^{(\alpha)\mu}$ are closely connected: their space-like axes are the same and their time-like ones are opposed to one another, *i. e.*, they are different in their handedness.

Let us give at a space-time point $\{x^{\mu}\}$ two orthonormal tetrads, $\Lambda^{\mu}_{(\alpha)}$ and $\Lambda'^{\mu}_{(\alpha)}$, they can be connected by a Lorentz transformation with the so-called *Lorentz matrix*

$$L^{(\alpha)}_{(\alpha')} \overset{\text{def}}{=} \Lambda^{(\alpha)}_{\mu}\Lambda'^{\mu}_{(\alpha)} \tag{3.24}$$

being the unit matrix if the two tetrads coincide. Owing to eqs. (3.23) and (3.24) at every space-time point the equivalent Lorentz transformations:

$$\Lambda'^{\mu}_{(\alpha)}=L^{(\alpha)}_{(\alpha')}\Lambda^{\mu}_{(\alpha)} \quad \text{and} \quad \Lambda^{(\alpha)}_{\mu}=L^{(\alpha)}_{(\beta')}\Lambda'^{(\beta)}_{\mu} \tag{3.25}$$

can be introduced, being independent of any changes of the space-time co-ordinates. These Lorentz transformations may be interpreted as the "internal" changes of the orientation of the tetrads.

Now, let us suppose that in the local rest frame of reference $\mathscr{K}^0$ of the gaseous particles, distinguished by an original tetrad $\Lambda^{*\mu}_{(\alpha)}$, we have

$$p^{\mu}_{(0)} \stackrel{\text{def}}{=\!=} \Lambda^{*\mu}_{(0)}, \quad \lambda^{\mu}_{i} \stackrel{\text{def}}{=\!=} \Lambda^{*\mu}_{(i)} \qquad (i = 1, 2, 3), \tag{3.26}$$

then one can immediately see that the λ^{+}-triad as the space-like part of the Lorentz-covariant $\Lambda^{*\mu}_{(\alpha)}$ tetrad and the λ^{-}-triad as the space-like part of the Lorentz-contravariant $-\Lambda^{*(\alpha)\mu}$ tetrad has to be defined.

As a matter of fact, any changes of the orientation of the λ-triad generating the group of internal transformations $\mathscr{G}_{\xi}$, is the spatial subgroup of the infernal Lorentz transformations (3.24).

Associated with each point of a curve $x^{\mu} = x^{\mu}\sigma$ in space-time an orthonormal tetrad can be introduced with particularly considerable features formed by the *unit tangent*

$$t^{\mu}_{(0)} \stackrel{\text{def}}{=\!=} \frac{dx^{\mu}}{d\sigma}, \tag{3.27}$$

as well as by the *first, second* and *third normals to the curve* denoted by $\eta^{\mu}_{(1)}$, $\eta^{\mu}_{(2)}$ and $\eta^{\mu}_{(3)}$, respectively. These by pairs orthogonal unit vectors are determined by means of the well-known Frenet-Serret formulae:

$$\begin{cases} \dfrac{D}{d\sigma} t^{\mu}_{(0)} = \varrho_1 n^{\mu}_{(1)}, \qquad \dfrac{D}{d\sigma} n^{\mu}_{(2)} = \varrho_3 n^{\mu}_{(3)} - \varrho_2 n^{\mu}_{(1)}, \\ \dfrac{D}{d\sigma} n^{\mu}_{(1)} = \varrho_2 n^{\mu}_{(2)} + \varrho_1 t^{\mu}_{(0)}, \qquad \dfrac{D}{d\sigma} n^{\mu}_{(3)} = -\varrho_3 n^{\mu}_{(2)}, \end{cases} \tag{3.28}$$

where the scalars, ϱ_1, ϱ_2 and ϱ_3 are the first, second and third curvatures of the curve considered. In the case of time-like curves, *i. e.*, in the case of curves with time-like unit tangents, we have:

$$g_{\mu\nu} t^{\mu}_{(0)} t^{\nu}_{(0)} = 1, \quad g_{\mu\nu} n^{\mu}_{(i)} n^{\nu}_{(i)} = -1 \qquad (i = 1, 2, 3). \tag{3.29}$$

This so-called *normal tetrad* $\{t^{\mu}_{(0)}, n^{\mu}_{(i)}\}$ *to the curves* will be used below when the orientation of the tetrads at different distinct space-time points will be compared.

Considering at any two distinct points of the Riemannian space-time continuum a tetrad and λ-triad, respectively, their orientation has to be compared by means of the framework of the general parallel transport along the world lines of the particles.

The world lines of the particles are time-like curves with equations $x^{\mu} = x^{\mu}(\sigma)$. It is well-known that a vector is said to undergo *parallel transport* along a curve if its absolute derivative vanishes.

$$\frac{DV^{\mu}}{d\sigma} \stackrel{\text{def}}{=\!=} \frac{dV^{\mu}}{d\sigma} + \left\{ \begin{matrix} \mu \\ \varkappa\, \lambda \end{matrix} \right\} V^{\varkappa} \frac{dx^{\lambda}}{d\sigma} = 0. \tag{3.30}$$

In the following it seems to be more favoured to use a particular kind of parallel transports of a vector V^{μ} — called usually Fermi—Walker transport ([14, 15] and [13] as well) — along the world lines of the particles defined by the equation

$$\frac{DV^{\mu}}{d\sigma} = \frac{\varrho_1}{m_0} V_{\varkappa} (p^{\mu} n^{\varkappa}_{(1)} - p^{\varkappa} n^{\mu}_{(1)}), \tag{3.31}$$

where attention was paid to the fact that in the case of particles world lines $x^{\mu} = x^{\mu}(\sigma)$ the unit tangent is just the four-momentum of the particles normalized to unity:

$$t^{\mu}_{(0)} = \frac{dx^{\mu}}{d\sigma} = p^{\mu}/m_0. \tag{3.32}$$

The important features of the Fermi—Walker transport are that

(*i*) the unit tangent $t^{\mu}_{(0)}$ itself automatically undergoes Fermi—Walker transport, as it can be checked on the basis of eqs. (3.31) and (3.28) immediately;

(*ii*) it resembles parallel transport in the conservation of magnitude and scalar product;

(*iii*) if the Fermi—Walker transport is applied to the normals $m_{(i)}$ which are orthogonal to the tangent $t^{\mu}_{(0)}$ at some point of the curve considered, they remain, of course, orthogonal to $t^{\mu}_{(0)}$ and to each other. This means, however, that the normal tetrad $\{t^{\mu}_{(0)}, n^{\mu}_{(i)}\}$ under Fermi—Walker transport remains normal tetrad along any curves.

As a matter of fact, the comparison of the orientations of two orthonormal tetrads at two distinct points $\{x^{\mu}\}$ and $\{y\}^{\mu}$ of the Riemannian space-time can be mastered in the following way:

Let the two considered points be connected by a world-line with a unit tangent the direction of which, *e. g.*, at the point $\{x^{\mu}\}$ coincides with that of the $t^{\mu}_{(0)}$ axis of the tetrad considered. Then, let the orthonormal tetrad with its origin, *e. g.*, at $\{x^{\mu}\}$ be undergone Fermi—Walker transport as long as its origin coincides with $\{y^{\mu}\}$. In this way a virtual tetrad is unambiguously oriented, which, as a basis to determine the orientation of the second tetrad — with its origin originally at $\{y^{\mu}\}$ — can be used by means of the method for the comparison of tetrads at the same space-time point in terms of the internal Lorentz transformations.

The comparison of the λ-triads of different space-time points, having their definition (3.26) in mind, based on that of the tetrads is straightforward and we have not to enter upon it. However, then the inhomogeneous direction co-ordinates $\{\xi_i\}$ of the local momentum-spaces, originally defined at different space-time points, can be „synchronized" and the relativistic phase-space in Riemannian space-time can be defined as a direct product of the configuration- and the momentum-spaces, respectively.

Finally, we have to mention that the definition of the inhomogeneous direction co-ordinates — the framework of which, having the invariant characterization of the internal degrees of freedom of physical fields in mind, was suggested several years ago [16] — seems to be very close to that of the spatial set of Fermi co-ordinates [14] the advantages of which from other points of view were emphasized by SYNGE [13].

In order to define the invariant volume-element of the relativistic phase-space, we have (*i*) to keep in mind the familiar definition of the corresponding scalar density of the Riemannian space-time, (*ii*) to propose a reasonable scalar density in the momentum-space, then we have the possibility to construct an adequate invariant under the transformations of a certain group to be defined below. We would have several possibilities to carry out this program. However, it seems to be reasonable to accept such a definition of the relativistic phase-space volume-element which at a certain instant, *i. e.*, on a space-like surface of the space-time continuum is reduced into the familiar phase-space volume-element of the non-relativistic theory.

As a matter of fact, we have to suggest the following definition of the hyper-surfaces in the framework of general line-element geometry:

As hyper-surface of the geometrized relativistic phase-space the ensemble of the line-elements $\{x^{\mu} = x^{\mu}(u^i); p^{\mu}\}$ *or* $\{x^{\mu} = x^{\mu}(u^i); \xi_i\}$ $(i = 1, 2, 3)$ *will be denoted, where* $\{u^i\}$ *and* $u^i = \text{const.}$ *mean respectively the parameters and the parametric lines of the three-dimensional hyper-surface of the co-ordinates of the line-elements.*

Let the set of quantities

$$\varepsilon_{\alpha\beta\gamma\delta} \overset{\text{def}}{=} \begin{cases} +1, & \text{if } \{\alpha, \beta, \gamma, \delta\} \text{ means an even permutation of the numbers } \{0, 1, 2, 3\}, \\ -1, & \text{if } \{\alpha, \beta, \gamma, \delta\} \text{ means an odd permutation of the numbers } \{0, 1, 2, 3\}, \\ 0, & \text{if at least two of the indices } \{\alpha, \beta, \gamma, \delta\} \text{ agree} \end{cases} \tag{3.33}$$

be introduced, which are *per definitionem* anti-symmetric in all their indices, and let the pseudo-tensor

$$\eta_{\alpha\beta\gamma\delta} \overset{\text{def}}{=} \sqrt{-g}\, \varepsilon_{\alpha\beta\gamma\delta} \quad (g \overset{\text{def}}{=} \det |g_{\mu\nu}|) \tag{3.34}$$

with the law of transformation

$$\eta_{\alpha'\beta'\gamma'\delta'} = \operatorname{sgn}\{\Delta\} \frac{\partial x^\alpha}{\partial x^{\alpha'}} \frac{\partial x^\beta}{\partial x^{\beta'}} \frac{\partial x^\gamma}{\partial x^{\gamma'}} \frac{\partial x^\delta}{\partial x^{\delta'}} \eta_{\alpha\beta\gamma\delta} \tag{3.35}$$

be defined, then the normal vector to the hyper-surface of the configuration-space in the form

$$\gamma_\alpha \overset{\text{def}}{=} \eta_{\alpha\beta\gamma\delta} \frac{\partial x^\beta}{\partial u^1} \frac{\partial x^\gamma}{\partial u^2} \frac{\partial x^\delta}{\partial u^3} \tag{3.36}$$

can be obtained, where $\partial x^\beta / \partial u^i$ mean the tangents to the parametric lines $u^i = \text{const.}$ of the surface considered.

The length of the normal vector ν_α one calculates in a straightforward way:

$$\nu_\alpha \nu^\alpha = g^* \tag{3.37}$$

with

$$g^*_{ik} \overset{\text{def}}{=} g_{\alpha\beta} \frac{\partial x^\alpha}{\partial u^i} \frac{\partial x^\beta}{\partial u^k} \quad \text{and} \quad g^* \overset{\text{def}}{=} \det |g^*_{ik}|. \tag{3.38}$$

This means, however, that the unit normal vector to the hyper-surface $\{x^\mu = x^\mu(u^1, u^2, u^3); p^\mu\}$ is given by

$$n_\alpha = \nu_\alpha / \sqrt{|g^*|}. \tag{3.39}$$

Let us suppose in the following that the vectors ν_α and n_α, respectively, are time-like vectors, *i. e.*, $g^* > 0$; then the set of tangents of the hyper-surface and the hyper-surface itself will be called space-like.

Keeping this familiar definitions in mind, the *oriented hyper-surface elements* can be introduced also in the case *of the relativistic* configuration-space by means of the definition

$$df_\varrho \overset{\text{def}}{=} \nu_\varrho\, du^1 du^2 du^3 = n_\varrho\, df \tag{3.40}$$

with

$$df \overset{\text{def}}{=} \sqrt{|g^*|}\, du^1 du^2 du^3 \tag{3.41}$$

being the invariant measure of the hyper-surface element.

Considering the curve $x^\varrho = x^\varrho(s)$ of the configuration-space (s being again the parameter of the length of arch of the line-element geometry), let us suppose that *the unit tangent of the curve coincides in the crossing point of the curve and the hyper-surface with the unit normal vector of the hyper-surface, i. e.,*

$$\frac{dx^\varrho}{ds} = n^\varrho \quad \text{or} \quad dx^\varrho = n^\varrho\, ds, \tag{3.42}$$

then the analytical definition of *the invariant volume-element of the configuration-space can in general be given by*

$$dV \overset{\text{def}}{=} \frac{\sqrt{-g}}{\sqrt{|g^*|}}\, dx^\varrho\, df_\varrho = \frac{\sqrt{-g}}{\sqrt{|g^*|}}\, n^\varrho n_\varrho\, df\, ds = \frac{\sqrt{-g}}{\sqrt{|g^*|}}\, df\, ds. \tag{3.43}$$

In the particular important special case of the parametrization

$$x^0 \equiv s,\ x^i \equiv u^i \qquad (i=1,2,3) \tag{3.44}$$

the formally well-known formula:

$$dV = \sqrt{-g}\, dx^0\, dx^1\, dx^2\, dx^3 \overset{\text{def}}{=} \sqrt{-g}\, d^4x \tag{3.45}$$

can be obtained.

Due to the definition (3.8) of the inhomogeneous direction co-ordinates $\{\xi_i\}$, they are invariants of the group of the transformations of the co-ordinates. However, if instead of the line-element $\{x^\mu, p^\mu\}$, the line-element $\{x^\mu, p^\mu + Dp^\mu\}$ is considered, the inhomogeneous direction co-ordinates are, of course, changed and in the general (anisotropic) cases it is rather troublesome to determine their infinitesimal changes. But, in the special case when the metrical fundamental tensor does not depend on the direction co-ordinates, one can immediately see that

$$d\xi_i = m_0^{-1} \lambda_i^\mu \{(p_\mu + Dp_\mu) - p_\mu\} = Dp_\mu \lambda_i^\mu / m_0, \tag{3.46}$$

where Dp_μ denotes the covariant differential of p_μ.

Owing to the obvious invariance of $d\xi_i$ against any co-ordinate transformation, the invariant volume-element of the local momentum-space at arbitrary but fixed point of the configuration-space can, of course, be defined as follows:

$$dP \overset{\text{def}}{=} m_0^3 d\xi_1 d\xi_2 d\xi_3 \overset{\text{def}}{=} m_0^3 d^3\xi, \tag{3.47}$$

where the factor m_0^3 has to be introduced in order to save the correct physical dimensions of the volume-element of the momentum-space.

Although dP is an invariant of the group $\mathscr{G}_x$, it will generally change if the internal transformations

$$\xi_{i'} = \xi_{i'}(\xi_i) \tag{3.48}$$

of the group $\mathscr{G}_\xi$ are considered. Bearing in mind that the transformations $\mathscr{G}_\xi$ are homogeneous linear orthogonal transformations — *i. e.*, they are isomorphic to the three-dimensional subgroup of the Lorentz transformations (3.24) — of the type

$$\xi_{i'} = D_i^k \xi_{k'} \tag{3.49}$$

we have

$$d^3\xi' \equiv d_1'\xi\, d_2'\xi\, d_3'\xi = \frac{\partial(\xi_1', \xi_2', \xi_3')}{\partial(\xi_1, \xi_2, \xi_3)}\, d\xi_1 d\xi_2 d\xi_3 = \operatorname{sgn}\{D\}\, d^3\xi \tag{3.50}$$

and, as a matter of fact, dP will be under the group $\mathscr{G}_\xi$ of the internal transformations a pseudo-scalar. Indeed, the invariant volume-element of the local momentum-space depends on the orientation of the basic λ-triad.

The underlying general group $\mathscr{G}$ in the background of the concept of the relativistic phase-space — corresponding to the relativistic generalization of the

group of the contact transformations of classical dynamics — is, of course, the direct product of the groups of the external and internal transformations, *i. e.*,

$$\mathscr{G} = \mathscr{G}_x \times \mathscr{G}_\xi . \tag{3.51}$$

This means, however, that as the relativistic phase-space volume-element in terms of the parametrization (3.44) the expression

$$d\Omega \overset{\text{def}}{=} m_0^3 \sqrt{-g}\, d^4x\, d^3\xi \tag{3.52}$$

can be introduced being a pseudo-scalar of the group $\mathscr{G}$. The scalar factor m_0^3 is again considered to keep the correct physical dimensions of the phase-space volume-element.

In fact, the relativistic phase-space volume-element may be oriented; let it be denoted as a positive one if the underlying λ-triad is right-handed.

At a given instant of time, *i. e.*, on the hyper-plain $x^0 = \text{const.}$ of the configuration-space, the phase-space volume-element is reduced into the form

$$d\Omega_0 \overset{\text{def}}{=} m_0^3 \sqrt{-g}\, dx^1 dx^2 dx^3 d\xi_1 d\xi_2 d\xi_3 = m_0^3 \sqrt{-g}\, d^3x\, d^3\xi \tag{3.53}$$

being the direct generalization of the well-known expression of the non-relativistic gas theory. For sake of simple speaking $d\Omega_0$ will be called in the following as the *momentary expression of the phase-space volume-element.*

Finally, owing to the general definition (3.8) of the inhomogeneous direction co-ordinates $\{\xi_i\}$, let the explicit forms of the relativistic phase-space volume-element be obtained in two important cases, in special frames of reference defined in different underlying metrical space-times:

(*i*) Considering a pseudo-Euclidian space-time continuum with the metrical fundamental tensor

$$\gamma_{00} = -\gamma_{11} = -\gamma_{22} = -\gamma_{33} = 1; \quad \gamma_{\mu\nu} = 0 \quad (\mu \neq \nu), \tag{3.54}$$

let us first suppose that the axes of the λ^+-triad due to its orientation in the rest frame of reference $\mathscr{K}^0$ are given by (3.12), then based on the definitions (3.46) of the scalar differentials $d\xi_i$ of the inhomogeneous direction co-ordinates one obtains

$$d\xi_i = -dp^i/m_0 = dp_i/m_0. \tag{3.55}$$

This means, however, that the relativistic phase-space volume-element is given in this case by

$$d\Omega = dx^0\, dx^1\, dx^2\, dx^3\, dp_1\, dp_2\, dp_3 \overset{\text{def}}{=} d^4x\, d^3p_{\text{cov}} \tag{3.56}$$

and its momentary expression, *i. e.*, its expression on the $x^0 = \text{const.}$ hyper-plain can be put in the form

$$d\Omega_0 = d^3x\, d^3p_{\text{cov}}; \tag{3.57}$$

the very familiar expression of the non-relativistic phase-space volume-element.

(*ii*) In our case, investigated below, the background space-time continuum is Riemannian. In order to obtain the phase-space volume-element and its momentary expression, respectively, one has to use explicitly the framework of the theory of external forms [6, 12]. Namely, in terms of the method of the external forms, the phase-space volume-element can be written as follows:

$$d\Omega = m_0^3 \sqrt{-g}\, dx^0 \wedge dx^1 \wedge dx^2 \wedge dx^3 \wedge d\xi_1 \wedge d\xi_2 \wedge d\xi_3 \tag{3.58}$$

with the temporarily more favourable abbreviation of the commutators, *e. g.*, A and B:

$$A \wedge B \overset{\text{def}}{=} AB - BA. \tag{3.59}$$

Having the above introduced frame of reference and orientation of the λ-triad in mind we have

$$d\xi_i = Dp_i = m_0^{-1}(dp_i - \{_i{}^{\mu}{}_{\lambda}\}p_{\mu}\,dx^{\lambda}), \tag{3.60}$$

where $\{_i{}^{\mu}{}_{\nu}\}$ denotes the components of the Christoffel-symbols. Nevertheless, due to identity

$$dx^{\mu} \wedge dx^{\nu} \equiv 0, \tag{3.61}$$

finally the expressions

$$d\Omega = \sqrt{-g}\,d^4x\,d^3p_{\mathrm{cov}} \tag{3.62}$$

and

$$d\Omega_0 = \sqrt{-g}\,d^3x\,d^3p_{\mathrm{cov}}, \tag{3.63}$$

respectively, can be obtained.

§. 4. The zero-point kinetic energy of perfect fermion gases

In addition to the natural theoretical interest in the generalization of important physical concepts, the investigations to deal with the definitions of the energy and momentum of particles on the Fermi level in the case of relativistic fermion gases in Riemannian space-time continuums are also suggested by problems more recently raised in the neutrino-astronomy [9, 10].

Considering a *completely degenerate fermion gas, i. e.*, — for the sake of simplicity — a perfect system of fermions at zero point of the absolute temperature, the fermions are distributed over the different quantum states in such a way that the total energy E of the gas has its smallest possible value. Due to the fundamental feature of fermion gases, — *i. e.*, to Pauli's exclusion principle,— no more than one fermion may be in any one state, the fermions fill all states with energies between the smallest (equal to zero) and some largest value which is determined by the number N of the fermions. Let us suppose that the fermion gas is in a volume V_0 of the configuration space, then the smallest possible value of its total energy — the so-called *zero point kinetic energy* E_0 — can simply be calculated based on the framework of the non-relativistic phase-space method having in the background the Euclidian geometry in mind.

Let us suppose that the intrinsic dynamical properties of the completely degenerate fermion gas considered are isotropic, then the number of quantum states of translational motion of a particle with a momentum whose absolute value lies between $\mathbf{p} \equiv p$ and $p + dp$ is:

$$dn = 4\pi p^2\,dp\,dV_0/(2\pi\hbar)^3, \tag{4.1}$$

where the familiar convention has been taken into account that the volume of the phase-space corresponding to each degree of freedom is just equal to the Planck's constant $h \equiv 2\pi\hbar$.

Let the highest value of the energy be called as *Fermi energy* ε_F, the corresponding momentum as *Fermi momentum* p_F as well as the energy state itself as *Fermi-level*, then the number of filling all states in the momentum interval $(0, p_F)$ is given by

$$N = \gamma V_0(2\pi\hbar)^{-3}\int_0^{p_F} dp^2\,dp = \gamma V_0 p_F^3/6\pi^2\hbar^3, \tag{4.2}$$

where γ denotes the number of the internal degrees of freedom in each quantum state (having usually only the spin degeneracy in mind). The only unknown quantity in relation (4.2) is the Fermi momentum; therefore, we have

$$p_F = \hbar(6\pi^2 N/\gamma V_0)^{1/3} \equiv \hbar(6\pi^2\varrho/\gamma)^{1/3} \tag{4.3}$$

based on which in the familiar way for the Fermi energy

$$\varepsilon_F = \frac{p_F^2}{2m_0} = \frac{\hbar^2}{2m_0}\left(\frac{6\pi^2 N}{\gamma V_0}\right)^{2/3} = \frac{\hbar^2}{2m_0}\left(\frac{6\pi^2}{\gamma}\bar{\varrho}\right)^{2/3} \tag{4,4}$$

and for the zero point kinetic energy

$$E_0 = \frac{3\hbar^2}{10m_0} N \left(\frac{6\pi^2}{\gamma}\bar{\varrho}\right)^{2/3}, \tag{4.5}$$

respectively, can be obtained, where

$$\bar{\varrho} = N/V_0 \tag{4,6}$$

denotes the *mean value of the density of fermions* in the configuration-space.

Keeping in mind the general definitions (3.62) and (3.63) of the relativistic phase-space volume-element and its momentary value, respectively, all of the classical concepts and results summarized above may be directly generalized for a relativistic and dynamically anisotropic system of fermions in space-time continuum with general structure, too, characterized by the metrical fundamental tensor $g_{\mu\nu}(x, p)$.

However, for the sake of simplicity let the relativistic neutrino gas be considered in Riemannian spaces with spherical symmetry. First the somewhat more general case of fermions with non-vanishing rest mass, $m_0 \neq 0$, will be discussed, then the results will be specialized for the neutrino gas by the limiting process $m_0 \to 0$.

Owing to the classical results summarized above the Fermi momentum and energy of the gaseous particles depend on the mean density N of fermions in the three-dimensional configuration-space. This mean density can naturally be defined either in a closed universe or in open universes having in mind the framework of infinite systems of fermions, *i. e.*, the limits $N \to \infty$ and $V_0 \to \infty$ with the restriction $\bar{\varrho} = \text{const}$. Both cases will be discussed in Riemannian space-time continuums with particularly interesting metrical structures.

Due to the spherical structure of the space-time continuum and to the dynamical isotropy of systems of the considered particles on the $x^0 = \text{const}$. hyper-plain the spherical polar co-ordinates $\{r, \vartheta, \varphi\}$ and $\{p, \theta, \varphi\}$ will, of course, be introduced in the configuration- and local momentum-spaces, respectively. This means that the momentary relativistic phase-space volume of the degenerate relativistic fermion gas considered has to be defined by

$$\Omega_0 = \int_\alpha^R dr \int_0^\pi d\varphi \int_0^{2\pi} d\varphi \int_0^{p_F} dp \int_0^\pi d\theta \int_0^{2\pi} d\Phi \sqrt{-g}\, p^2 \sin\theta, \tag{4.7}$$

where the upper limit R of the configuration-space integral means either the radius of the universe or in the case of open universe the spherical symmetric space-time domain taken into account before the limiting process $R = (3V_0/4\pi)^{1/3} \to \infty$ and the lower one is determined by its metrical properties.

Keeping in mind the volume-element dP of the local momentum-space defined by eq. (3.47), the absolute value of the three-momentum has to be calculated from the normalization condition of the covariant four-momentum components:

$$g^{\mu\nu}(x) p_\mu p_\nu = m_0^2, \tag{4.8}$$

since the momentum components with covariant transformation character have to be considered in the actual version (3.57) of dP.

In the particular cases considered in the following the components of the metrical fundamental tensor may generally be given as follows:

$$g_{00} = -h_0(r),\ g_{11} = h_1(r),\ g_{22} = h_2(r),\ g_{33} = h_3(r)\sin^2\vartheta;\ g_{\mu\nu} = 0 \qquad (\mu \neq \nu). \tag{4.9}$$

The reason that here the signature $(-+++)$ was introduced instead of the usual one, is that the hyper-surface $x^0 = \text{const.}$ is space-like. This means, however, that

$$g = -h_0 h_1 h_2 h_3 \sin^2\vartheta \quad \text{and} \quad \sqrt{-g} = \{h_0 h_1 h_2 h_3\}^{1/2}\sin\vartheta, \tag{4.10}$$

respectively, furthermore

$$g^{00} = -h^{-1}(r),\quad g^{11} = h_1^{-1}(r),\quad g^{22} = h_2^{-1}(r),\quad g^{33} = h_3^{-1}(r)\sin^{-2}\vartheta; \tag{4.11}$$
$$g^{\mu\nu} = 0 \qquad (\mu \neq \nu).$$

Therefore, the normalization condition can be put into the form:

$$-h_0^{-1}p_0^2 + \{h_1^{-1}p_1^2 + h_2^{-1}p_2^2 + h_3^{-1}\sin^{-2}\vartheta p_3^2\} = -m_0^2 \tag{4.12}$$

and the definition of p may finally be given by

$$p \overset{\text{def}}{=} \{h_1^{-1}p_1^2 + h_2^{-1}p_2^2 + h_3^{-1}\sin^{-2}\vartheta p_3^2\}^{1/2} = \{\varepsilon^2 h_0^{-1}(r) - m_0^2\}^{1/2}, \tag{4.13}$$

where it was taken into accont that in our system of units

$$p_0 \equiv \varepsilon \tag{4.14}$$

denoting by ε the energy of the particles.

In order to introduce the inhomogeneous direction co-ordinates $\{\xi_i\}$ we have to normalize the basic vectors of the λ^+-triad. In terms of the parametrization (3.44) starting from the local rest frame of reference $\mathscr{K}^0$, *i. e.*, bearing the components of the triad axes (3.12) in mind, it can be obtained on the one hand

$$\begin{cases} \overset{1}{\lambda}{}^1 = h_1^{-1/2}(r), \quad \overset{2}{\lambda}{}^2 = h_2^{-1/2}(r), \quad \overset{3}{\lambda}{}^3 = h_3^{-1/2}(r)\sin^{-1}\vartheta \\ (\text{all the other components of } \overset{i}{\lambda}{}^{\mu}\text{-s are vanishing}) \end{cases} \tag{4.15}$$

and on the other

$$\xi_1 = h_1^{-1/2}(r)p_1/m_0, \quad \xi_2 = h_2^{-1/2}(r)p_2/m_0, \quad \xi_3 = h_3^{-1/2}(r)p_3/m_0\sin\vartheta, \tag{4.16}$$

respectively. This means, however, that due to eq. (4.13) the absolute value of the three-momentum may be substituted by the absolute value ξ of the inhomogeneous direction co-ordinates defined by

$$p \equiv \xi = \left\{\frac{\varepsilon^2}{m_0^2}h_0^{-1}(r) - 1\right\}^{1/2} \tag{4.17}$$

and finally the momentary relativistic phase-space volume in eq. (4.7) on the $x^0 = \text{const.}$ hyper-plain can be written in the from:

$$\Omega_0 = m_0^3 \int_\alpha^R dr \int_0^\pi d\vartheta \int_0^{2\pi} d\varphi \int_0^{\xi_F} d\xi \int_0^\pi d\theta \int_0^{2\pi} d\Phi \{h_0 h_1 h_2 h_3\}^{1/2}\sin\vartheta\xi^2\sin\theta =$$
$$= \frac{(4\pi)^2}{3} m_0^3 \int_\alpha^R dr \{h_0 h_1 h_2 h_3\}^{1/2} \left\{\frac{\varepsilon_F^2}{m_0^2}h_0^{-1} - 1\right\}^{3/2}, \tag{4.18}$$

where ξ_F and ε_F mean the values of ξ and ε, respectively, on the Fermi level of the momentum-space. Due to the definition of the three-dimensional volume in the configuration-space, we have

$$V_0 = 4\pi \int_\alpha^R dr \{h_0 h_1 h_2 h_3\}^{1/2}, \tag{4.19}$$

and one can write instead of eq. (4.2)

$$N = \gamma \frac{(4\pi)^2}{3} \left(\frac{m_0}{2\pi\hbar}\right)^3 \int_\alpha^R dr \{h_0 h_1 h_2 h_3\}^{1/2} \left\{\frac{\varepsilon_F^2}{m_0^2} h_0^{-1}(r) - 1\right\}^{3/2}. \tag{4.20}$$

Owing to the mean density (4.6) of the relativistic fermion gas, its density $\varrho(r)$ on the hyper-plain $x^0 = \text{const.}$ of the configuration-space may be defined by

$$\frac{N}{V_0} = \frac{\gamma}{V_0} \frac{(4\pi)^2}{3} \left(\frac{m_0}{2\pi\hbar}\right)^3 \int_\alpha^R dr \{h_0 h_1 h_2 h_3\}^{1/2} \left\{\frac{\varepsilon_F^2}{m_0^2} h_0^{-1}(r) - 1\right\}^{3/2} = 4\pi \int_\alpha^R dr r^2 \varrho(r). \tag{4.21}$$

Indeed, let the three-dimensional density $\varrho(r)$ be introduced by

$$\varrho(r) \stackrel{\text{def}}{=} \frac{8}{V_0} \frac{4\pi}{3} \left(\frac{m_0}{2\pi\hbar}\right)^3 \frac{1}{r^2} \{h_0 h_1 h_2 h_3\}^{1/2} \left\{\frac{\varepsilon_F^2}{m_0^2} h_0^{-1}(r) - 1\right\}^{3/2}. \tag{4.22}$$

So far the Fermi energy of the particles in unknown and is terms of $\bar{\varrho}$ is only implicitly determined by eq. (4.21). In order to calculate it explicitly one has to carry out the r-integration in eq. (4.21)

Finally, it seems to be worthwhile to introduce the three-dimensional energy density of the fermion gas being the corresponding $T_0^0(r)$ component of the energy-momentum tensor of the system. Due to the definition of the zero point kinetic energy this may be carried out by means of the relation:

$$\begin{aligned} E_0 &= \int_\alpha^R dr \int_0^\pi d\vartheta \int_0^{2\pi} d\varphi \int_0^{\varepsilon_F} d\varepsilon r^2 \varrho(r) \varepsilon(r) = \\ &= 2\pi \varepsilon_F^2 \int_\alpha^R dr r^2 \varrho(r) = -4\pi \int_\alpha^R dr \{h_0 h_1 h_2 h_3\}^{1/2} T_0^0(r) \end{aligned} \tag{4.23}$$

based on which the definition

$$T_0^0(r) \stackrel{\text{def}}{=} -\frac{2\pi}{3} \frac{8}{V_0} \left(\frac{m_0}{2\pi\hbar}\right)^3 \varepsilon_F^2 \left\{\frac{\varepsilon_F^2}{m_0^2} h_0^{-1}(r) - 1\right\}^{3/2} \tag{4.24}$$

can be suggested.

We are particularly interested in the special case of relativistic neutrino gas. This means that we have to carry out the limiting process $m_0 \to 0$ in the formulae obtained above.

First of all, one observes that due to eqs. (4.6) and (4.21), furthermore, to the fact that owing to the spin degeneracy in the case of neutrinos $\gamma = 2$, the mean

density of the neutrino gas on the hyper-plain $x^0 = \text{const.}$ of the configuration-space is determined in terms of

$$\bar{\varrho} = \frac{4\varepsilon_F^3}{3\pi V_0 \hbar^3} \int_\alpha^R dr h_0^{-1} \{h_1 h_2 h_3\}^{1/2}; \tag{4.25}$$

i. e., the Fermi energy is given by means of $\bar{\varrho}$ as

$$\varepsilon_F = \hbar \left[\frac{3\pi}{4} \bar{\varrho} \int_\alpha^R dr \{h_0 h_1 h_2 h_3\}^{1/2} \right]^{1/3} \left[\int_\alpha^R dr h_0^{-1} \{h_1 h_2 h_3\}^{1/2} \right]^{-\frac{1}{3}}. \tag{4.26}$$

As to the three-dimensional density (4.22) of the neutrino gas and to its three-dimensional energy density (4.23) on the hyper-plain $x^0 = \text{const.}$ of the configuration-space we have:

$$\varrho(r) = \frac{\varepsilon_F^3}{3\pi^2 V_0 \hbar^3} \frac{1}{r^2 h_0} \{h_1 h_2 h_3\}^{1/2} \tag{4.27}$$

Table I

	Einstein's universe	Schwartzschild's solution	Special solution with cylindrical symmetry
h_0	1	$1-\alpha/r$	$1-\alpha/r$
h_1	$(1-r^2/R^2)^{-1}$	$(1-\alpha/r)^{-1}$	$(1-\alpha/r)^{-1}$
$h_2 = h_3$	r^2	r^2	$r^2(1-\alpha/r)^{-1}$
$\{h_1 h_2 h_3\}^{1/2}$	$r^2(1-r^2/R^2)^{-\frac{1}{2}}$	$r^2(1-\alpha/r)^{-\frac{1}{2}}$	$r^2(1-\alpha/r)^{-\frac{3}{2}}$
α	0	$2M$	$2M$
$\varepsilon_F(R)$	—	$\hbar\left(\frac{3\pi}{4}\bar{\varrho}\right)^{1/3}\left\{1+\frac{9}{4}\frac{\alpha}{R}\right\}^{1/3}$	$\hbar\left(\frac{3\pi}{4}\bar{\varrho}\right)^{1/3}\left\{1+\frac{15}{4}\frac{\alpha}{R}\right\}^{1/3}$
ε_F	$\hbar\left(\frac{3\pi}{4}\bar{\varrho}\right)^{1/3}$	$\hbar\left(\frac{3\pi}{4}\bar{\varrho}\right)^{1/3}$	$\hbar\left(\frac{3\pi}{4}\bar{\varrho}\right)^{1/3}$
$\varrho(r)$	$\frac{\varepsilon_F^3}{3\pi^2 V_0\hbar^3}\left\{1-\frac{r^2}{R^2}\right\}^{-\frac{1}{2}}$	$\frac{\varepsilon_F^3}{3\pi^2 V_0\hbar^3}\left\{1-\frac{\alpha}{r}\right\}^{-\frac{3}{2}}$	$\frac{\varepsilon_F^3}{3\pi^2 V_0\hbar^3}\left\{1-\frac{\alpha}{r}\right\}^{-\frac{5}{2}}$
$T_0^0(r)$	$\frac{\varepsilon_F^5}{6\pi^2 V_0\hbar^3}$	$\frac{\varepsilon_F^5}{6\pi^2 V_0\hbar^3}\left\{1-\frac{\alpha}{r}\right\}^{-\frac{3}{2}}$	$\frac{\varepsilon_F^5}{6\pi^2 V_0\hbar^3}\left\{1-\frac{\alpha}{r}\right\}^{-\frac{3}{2}}$

and

$$T_0^0(r) = -\frac{\varepsilon_F^5}{6\pi^2 V_0 \hbar^3} h_0^{-3/2}(r), \tag{4.28}$$

respectively.

In order to obtain the final results in the case of different Riemannian space-time continuums the explicit expressions of the metrical fundamental tensor in eqs. (4.9) have to be taken into account. These are summarized in *Table I.*

References

[1] *Horváth, J. I.:* Acta Phys. et Chem. Szeged, **9**, 3 (1963).
[2] *Synge, J. L.:* The Relativistic Gas (North-Holland, Amsterdam, 1957).
[3] *Clemmow, P. C., A. J. Wilson:* Proc. Cambr. Phil. Soc. **53**, 222 (1957).
[4] *Ken-Iti Goto:* Progr. Theor. Phys. **20**, 1 (1958).
[5] *Abonyi, I.:* Magy. Fiz. Folyóirat **8**, 13 (1960); **13**, 367 (1965).
[6] *Chernikov, N. A.:* Soviet Physics; Doklady **2**, 248 (1957); **5**, 764 (1960); **7**, 397, 414, 428 (1962); Reprint (Dubna, 1962).
[7] *Zaslavsky, G. M., S. S. Moiseyev:* ZhETP **42**, 1054 (1962); ZhTP **33**, 782 (1963).
[8] *Israel, W.:* Journal of Math. Phys. **4** ,1163 (1963).
[9] *Fodor, L., Zs. Kövesy, G. Marx:* Acta Phys. Hung. **17**, 171 (1964).
[10] *Marx, G.:* ITP Budapest Report. No. 218 (1966).
[11] *Horváth, J. I.:* Wiss. Zs. d. Friedrich-Schiller-Univer. Jena, **15**, 149 (1966).
[12] *Horváth, J. I., A. Moór:* Indag. Math. **17**, 421, 581 (1955).
[13] *Synge, J. L.:* Relativity: the General Theory (North-Holland, Amsterdam, 1960).
[14] *Fermi, E.:* Rend. Acc. Linc. (1) **31**, 21, 51 (1922).
[15] *Walker, A. G.:* Proc. Roy. Soc. Edinburgh, **52**, 345 (1932).
[16] *Horváth, J. I.:* Suppl. del Nuovo Cimento (10) **9**, 444 (1958).

К ВОПРОСУ ВЫХОДА АНТИСТОКСОВОЙ ФЛУОРЕСЦЕНЦИИ

Л. КОЗМА

Институт Экспериментальной Физики Университета им. А. Йожефа, г. Сегед

(Поступило в редакцию 15-ого ноября, 1965 г.)

Экспериментально исследовалось зависимость квантового выхода от длины волн возбуждающего света и от температуры трех производных фталимида и уранилового стекла. Полученные результаты согласуются раньше полученными данными, относящиеся к органическим красителям.

Исследования, продолжаемые в последние времена и дающие противоположенные друг другу результаты [1]—[5], требуют распространения исследований зависимости квантового выхода антистоксовой флуоресценции от длины волн возбуждающего света на системы, имеющие отклоняющиеся от органических красителей характеристики. Для объяснения экспериментально полученной зависимости от температуры функции $\eta(\lambda)$, выражающей зависимость квантового выхода от длины волн возбуждающего света [1]—[3], оказывается целесообразным исследовать такие системы, в которых не возникают второстепенные процессы (н. п. разложение димеров, изменение концентрации разных форм ионов, присутствующих в растворе, и т. д.) ведущие к увеличению выхода в области антистоксового возбуждения.

С этой целью мы исследовали антистоксовую флуоресценцию уранилового стекла и трех производных фталимида, растворенных в этаноле, с помощью методов, разработанных в [1], [6]. Подробно исследовали влияние температуры на функцию $\eta(\lambda)$ и на спектры поглощения $k(\lambda)$ и излучения $f_q(\lambda)$. В случае уранилового стекла изменение температуры не вызывал изменения состава системы. Использование фталимидов предметом исследований оправдывается тем, что их легко тщательно очистить, а с другой стороны в растворе находятся только однооброзные нейтральные формы молекул.

На рис. 1*а* изображены спектры поглощения и люминесценции уранилового стекла, измеренные при температура 263 и 363 °К. Результаты измерений показывают, что с повышением температуры на длинноволновой области коэффициент поглощения увеличивается, у более коротких волн полосатый характер спектров теряется, и в то же время число фотонов, которые выпускаются в области по длинным волнам второй полосы спектра люминесценции увеличивается. Эти опыты согласуются с результатами, полученными в растворе ураниловых соединений [7], и можно их объяснить изменением, вызванным увеличением температуры, расспределения на колебательных уровнях.

Мы определили зависимость квантового выхода от длины волн возбуждающего света при четырех разных температурах, которую изобразили на рис. 1*б* относительными единицами. В стоксовой области спектра функция $\eta(\lambda)$ постоянна и даже температура не изменяет ее хода, но в антистоксовой

области выход быстро падает с увеличением длины волн возбуждения. Такие же результаты получили Соломин [8] и Аленцев [9]. Под влиянием увеличения температуры в антистоксовой области $\eta(\lambda)$ относительно увеличивается. По нашему мнению одинаковое изменение $\eta(\lambda)$ и $k(\lambda)$ с увеличением темпе-

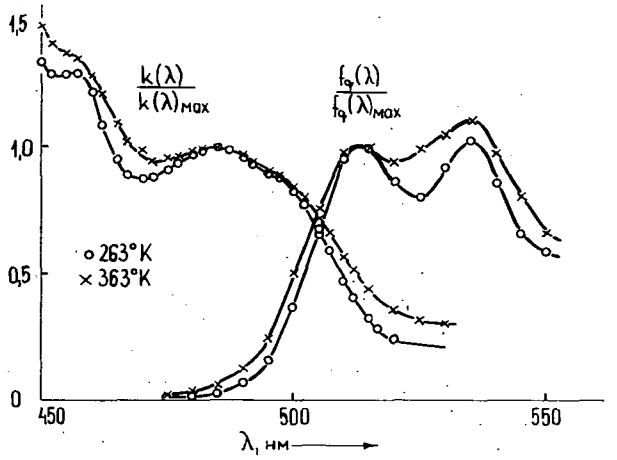

Рис. 1а

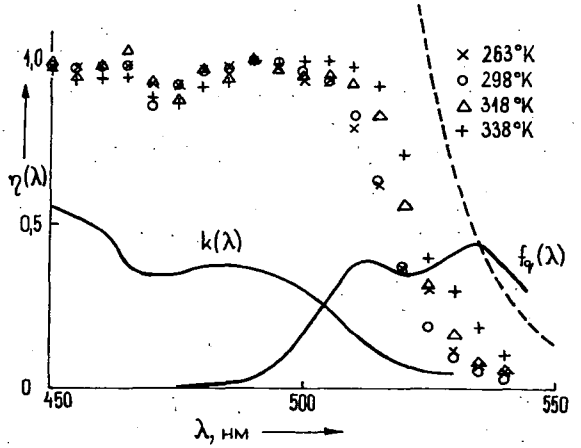

Рис. 1б

ратуры можно объяснить по данному нами раньше способу т. е. относительным увеличением активного поглощения. В системе не могут происходить второстепенные процессы. Замечаем, что уменьшение выхода длины волны 470 нм связано с переходами на второе возбужденное состояние. Мы вычисляли функцию по формуле (6) работы [10], которую получили термодинамическим путем, над которой не может повышаться $\eta(\lambda)$. Эта функция, изоб-

ражена на рис. 1*б* (— — —) и вычислена по спектрам люминесценции, относящимся к температуре 298 °К, показывает, что и по структурным спектрам как и по сплошным спектрам [11] можно дать высший предел функции $\eta(\lambda)$.

Мы исследовали растворы 3-аминофталимида, 3-монометиламинофталимида и 3-диметиламино-N-метилфталимида в этиловом спирте при концентрации $1 \cdot 10^{-2}$ моль/л. Результаты показывают, что в случае всех трех систем функция $\eta(\lambda)$ быстро падает в антистоксовой области спектра. Вследствие слабого перекрытия спектров падение выхода наблюдается в той области спектров, где значение коэффициэнтов поглощения очень маленькое. Из этого следует, что при этих веществах падение выхода можно наблюдать только с помощью таких экспериментальных методов, которые довольно чувствительны при маленьких значениях коэффициентов поглощения. На рис. 2

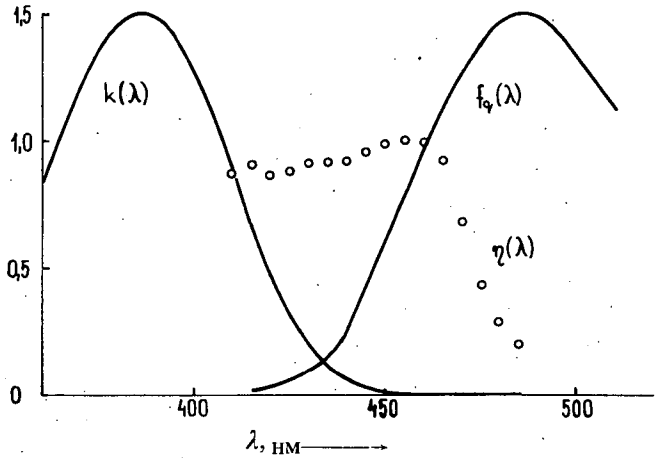

Рис. 2

представлены результаты, относящиеся к 3-аминофталимиду при температуре 298° К, которые практически совпадают с кривыми $\eta(\lambda)$, $k(\lambda)$ и $f_q(\lambda)$, полученными при температурах 263 и 338 °К. То же самое наблюдается у двух других исследованных производных фталимида. Значит, у этих систем температура не вызывает изменения ни спектра поглощения, ни функции выхода. Те же самые результаты мы получили раньше у растворов аурофосфина и флавофосфина [3].

По вышеупомянутым можно сказать, во-первых: антистоксовое падение квантового выхода обнаруживается и у систем большой чистоты, в которых люминесцируют нейтральные молекулы, также и у ионов UO_2^{++}, находящихся в твердой среде. Во-вторых: изменение температуры вызывает подобное влияние в хода функции $\eta(\lambda)$ и спектра $k(\lambda)$.

* * *

Автор выражает благодарность профессору А. Будо за постоянное внимание к данной работе и профессору И. Кечкемети за полезные советы при проведении эксперимента и при обработке результатов.

Литература

[1] *Ketskeméty, I., J. Dombi, J. Hevesi, R. Horvai, L. Kozma:* Acta Phys. et Chem. Szeged. **7**, 88 (1961).
[2] *Kozma, L., J. Hevesi, R. Horvai:* Acta Phys. et Chem. Szeged **10**, 79 (1964).
[3] *Хевеши, Я., Л. Козма:* Опт. и спектр., **19**, 434 (1965).
[4] *Гуринович, Г. П., Е. К. Круглик, А. Н. Севченко:* ДАН СССР, **167**, 1269 (1966).
[5] *Севченко, А. Н., Е. К. Круглик:* Международная конференция по люминесценции. Будапешт, 1966.
[6] *Ketskeméty, I., J. Dombi, R. Horvai, J. Hevesi, L. Kozma:* Acta Phys. et Chem. Szeged **7**, 17 (1961).
[7] *Володко, Л. В., А. Н. Севченко, Д. С. Умрейко:* Изв. АН СССР **24**, 749 (1960); Опт. и спектр. **17**, 356 (1964).
[8] *Соломин, С. С.:* ДАН СССР, **31**, 741 (1941).
[9] *Аленцев, М. Н.:* Канд. дисс., Тр. ФИАН СССР **5**, 500 (1951).
[10] *Budó, A., I. Ketskeméty:* Acta Phys. Polon. **26**, 385 (1964).
[11] *Budó, A., I. Ketskeméty:* Acta Phys. et Chem. Szeged **11**, 77 (1965).

THE QUANTUM YIELD OF FLUORESCENCE IN THE ANTI-STOKES REGION

L. Kozma

The dependence of the quantum yield on the exciting wavelength and the temperature has been experimentally studied in three phtalimiden compounds and in uran glass. The results are in a good accordance with earlier experimental data referring to organic dyestuffs.

ON THE PHOTOCONDUCTIVITY OF GaP CRYSTALS

By J. GYULAI

Research Group for Luminescence and Semiconductors of the Hungarian Academy of Sciences, Szeged

V. K. SUBASHIEV and G. A. CHALIKYAN

Institute of Semiconductors, Academy of Sciences USSR, Leningrad

(Received November 30, 1966)

The anomalous photoconductivity response of very high-ohmic GaP crystals was investigated. On base of the experiments it can be concluded that the effect is connected with the different mobilities in the corresponding minima of the conduction band. Based on calculations it is shown that the presence of the effect is connected with very short lifetimes.

Investigation of the photoconductivity response curves (PCR) of GaP brought some interesting new effects: first the anomalous photoconductivity response (APC)[1], observed firstly by D. F. NELSON, L. F. JOHNSON and M. GERSHENZON [1], and successively investigated by the authors [2], [3], and furthermore, an interesting oscillation effect, attributed to interactions between excess carriers and longitudinal optical phonons [4]. The present article gives some more details on our work concerning the problem of APC, the conclusions having been published in [2], [3].

Experimental methods

The GaP crystals investigated were vapour-grown whiskers (very high-ohmic, dark conductivity $\sigma_d(296°K) \approx 3 \cdot 10^{-12} \Omega^{-1}\,cm^{-1}$; dimensions $0{,}6 \times 0{,}6 \times 0{,}05\ cm^3$) and platelets (dark conductance $\Sigma_d(296°K) \approx 3 \cdot 10^{-10} \Omega^{-1}$; dimensions $0{,}8 \times 0{,}1 \times 0{,}1\ cm^3$). The whiskers were triangular in cross-section. Contacts were soldered Sn contacts with suitable impurities.

The PCR measurements were carried out at either 296°K or 77°K, with and without additional steady illumination. PCR curves were taken by two independent Xe-lamp—monochromator systems, one for d. c. measurements and an other for measurements using mechanically chopped light (chopping frequency ≈ 1350 c/s). In d. c. measurements a Zeiss SPM1 monochromator and a megohmmeter JUPITER, (type JM 242) were used, while under a. c. conditions the monochromatic light was produced by a 3MP—2 monochromator, and the signals in this latter case were detected by a calibrated selective amplifier system (ME3, type У2—6 amplifier, ME3, type СД—1 phase-sensitive detector coupled with an automatic potentiometer). In the experiments performed at 77°K, we have used a finger type Dewar. In both arrangements it was, of course, possible to measure the incident light intensity.

[1] The APC is an effect involving a second, and sometimes big rise in PCR spectral curves far beyond the absorption edge.

As in d. c. measurements PCR was taken point by point, the light energy was measured at every wave-length by a movable mirror rendering possible to focus the light energy onto a thermocouple. In a. c. measurements, the exciting light passed through an inclined quartz plate, which reflected a fraction of it onto a PbS-cell, coupled with a selective measuring amplifier system. The apparatus was previously calibrated against a thermocouple having been set in the place of the sample.

For the additional steady illumination a stabilized tungsten lamp was used, followed by suitable filters to produce various wave-lengths: glass filters, a continuouly adjustable Zeiss-interference filter, Ge or Si filters.

If not mentioned otherwise, PCR curves were taken by regulating the slits of the monochromator so as to keep the incident light energy approximately constant over the investigated spectral range. (The incident photon flux (Q) was calculated on basis of this constant energy, and changes in conductivity ($\Delta\sigma$) were related to these values, *i. e.* $\Delta\sigma/Q$ was calculated.) In a. c. measurements $\Delta\sigma$ was calculated according to the formula $\Delta\sigma = v/V_0 R_L$ [5], where v is the measured a. c. voltage, V_0 the voltage applied to the crystal (in our case 750 V), R_L the input resistance of the amplifier, while in d. c. measurements changes in conductance ($\Delta\Sigma$) were used instead of $\Delta\sigma$.

Experimental results

In order to get new informations about APC, first of all we have systematically investigated the effect of double injection. Steady illumination of wave-lengths ranging from 2,5 ev to 0,35 ev, was employed. On Fig. 1 the effect of long wave-length illumination (Si-filter) is to be seen (temperature 296°K). At room temperature strengthening the intensity of steady illumination, we generally obtained the following effect: first PCR rose both in the range of indirect and direct transitions. Then from a certain intensity, PCR in the indirect region remained almost constant, while APC gradually disappeared approaching this constant level of PCR in the region of indirect transitions. This feature of PCR curves was also found when using steady light of shorter wave-lengths (Fig. 2. red filter, Fig. 3. blue filter). This fact, *i. e.* the disappearing of APC with increasing intensity of steady illumination, seemed to be in contradiction with the explanation suggested in [1], according to which the level of APC ought to mean some level of saturation with increasing intensity of steady illumination.

At this point there still remained two possible ways of explanation which determined the means of our further experiments. According to the first

i) APR would be an effect simply correlated with the decrease of penetration depth in the region of direct transitions.

The values of the absorption coefficient, k, of GaP available for us [6] did not contradict such an effect, though less in magnitude. According to the second

ii) APR would be due to the fact that in the region of direct transitions, electrons are excited into the [000] minimum of the conduction band (Fig. 4a.), where the mobility (provided a scattering by acoustic modes) is about 15 times larger than in the [100] minimum.

The first idea was that if APC were simply a „geometric" effect, it could have been provoked using an inclined light ray in PCR measurements, producting thus the diminution of penetration depth even at energies corresponding to indirect

transitions. Unfortunately, the refraction index of GaP ($n=3{,}1$) is rather large so as to make this effect hardly observable. Using a light inclined by 60° to normal incidence, its deviation within the substance did not exceed 15°, corresponding to an effective diminution of penetration depth only by a factor 1,06. It was surprising and pointed at the sensitivity of the measuring circuitry that some resulting change of about 1,1 times could be observed at all. Of course, it was not possible to draw quantitative conclusions from this effect.

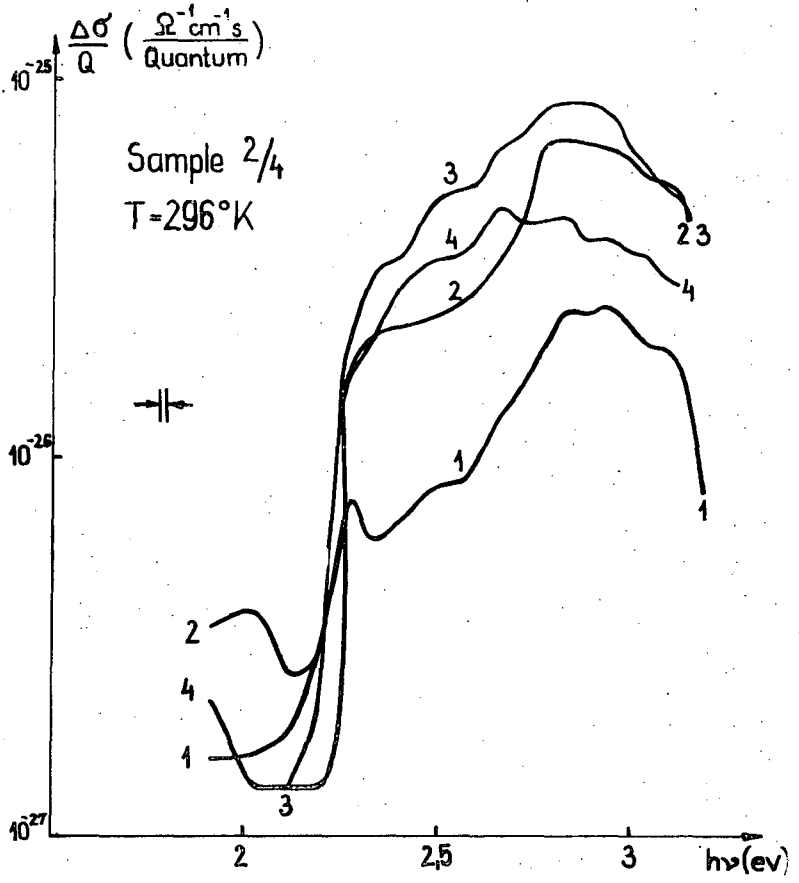

Fig. 1. PCR spectral curves. $Q \approx 5 \cdot 10^{12}$ quantum/s. Secondary illumination through Si filter ($\lambda > 1{,}1\mu$) of various intensities (curve *1*: 0 quantum/s; *2*: $9 \cdot 10^{12}$ quantum/s; *3*: $3{,}5 \cdot 10^{13}$ quantum/s; *4*: $2 \cdot 10^{14}$ quantum/s)

The experiment which seemed of great importance, and at last led to the most probable interpretation of APC was the following. We have measured PCR under special conditions, namely, choosing the incident intensity of exciting light so as to produce an approximately constant near-surface density of generation. This

constant generation rate can be approximated by keeping $Qk = const.$ over the whole experimental range. (The least value of Q, for large k depends on the energy reserves of the illumination system.)

Condition $Qk = const.$ ensures the uniform density of generation on the surface and, at other points of the sample, a decreasing generation density with increasing $h\nu$.

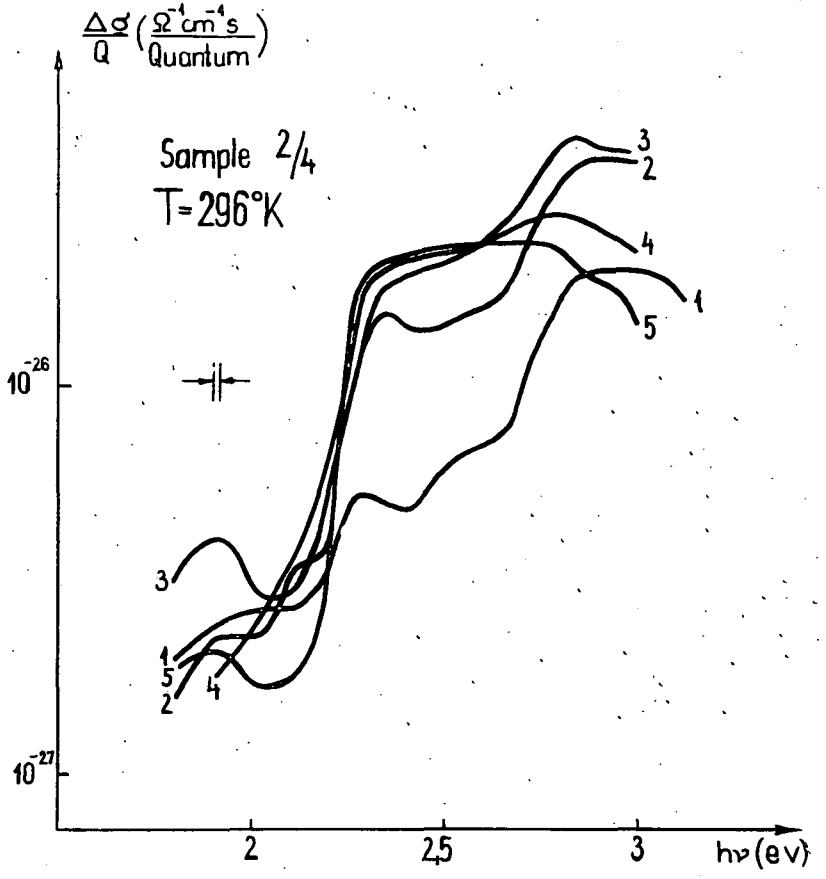

Fig. 2. PCR spectral curves. $Q \approx 3 \cdot 10^{12}$ quantum/s. Secondary illumination through red filter (type KC-10, $\lambda > 0{,}6\mu$) of various intensities (curve *1*: 0 quantum/s; *2*: $3 \cdot 10^{13}$ quantum/s; *3*: $1{,}8 \cdot 10^{14}$ quantum/s; *4*: $4{,}8 \cdot 10^{14}$ quantum/s; *5*: $1 \cdot 10^{15}$ quantum/s)

The result of this experiment is to be seen in Fig. 5. For comparison, the PCR of sample 1/1, of relatively low resistance, which does not show APC, is also to be seen in the figure.

It is also to be mentioned that at the highest employed injection rates ($Q > 10^{15}$ quantum/s), a strong peak appeared in PCR at 296°K, coinciding with the beginning of indirect band gap [4]. In this case APR was less expressed (Fig. 6.). At lower levels of illumination or at reduced temperatures this peak was inobservable.

Investigation of PCR at reduced temperatures also presented some interesting features. Obviously, the thermal ionization of the centres in crystals 2/4 and 2/6 was such that at 77°K a strong impurity PCR was observed (Figs. 7., 8.). The steady illumination, even at the least intensities employed, ionized these centres and APC appeared in a more expressive form compared with room temperature measurements.

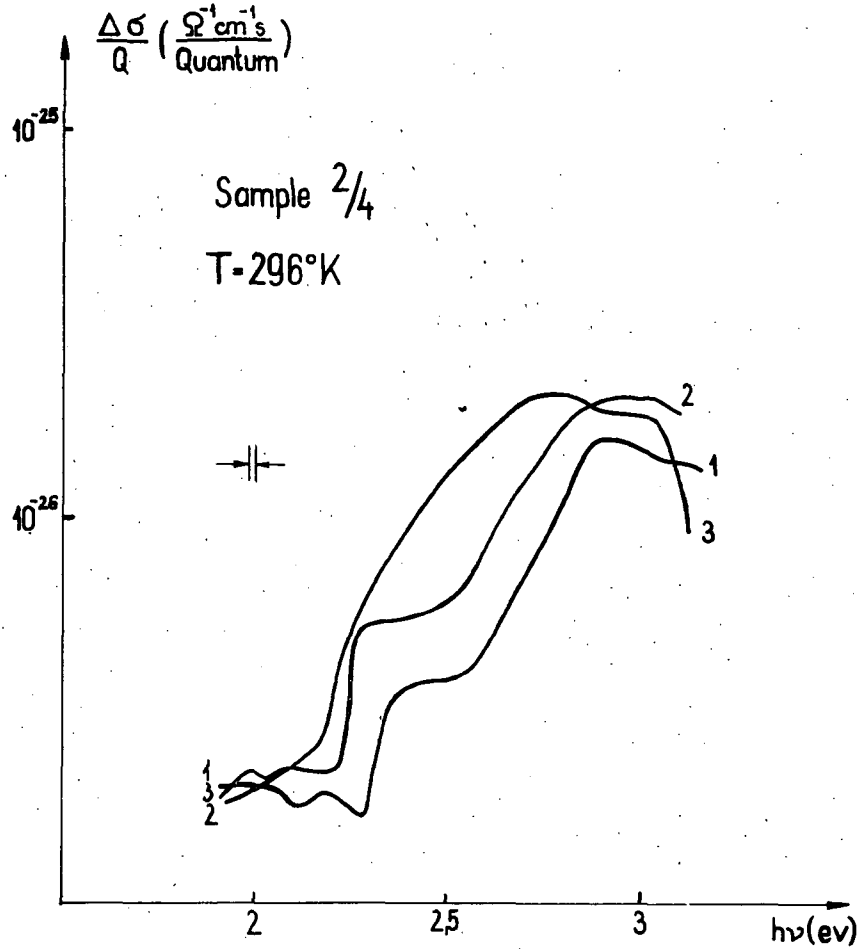

Fig. 3. PCR spectral curves. $Q \approx 8 \cdot 10^{12}$ quantum/s. Secondary illumination through blue filter (type CC5+C3C14, $0{,}38\mu < \lambda < 0{,}48\mu$) of various intensities (curve *1*: 0 quantum/s; *2*: $1{,}5 \cdot 10^{14}$ quantum/s; *3*: $9 \cdot 10^{14}$ quantum/s)

The PCR *versus* incident photon flux curves taken at two characteristic wavelengths show linear PCR at room temperature, even in the range of APC, *i. e.* in the region of direct transitions, though some superlinearity was observed at

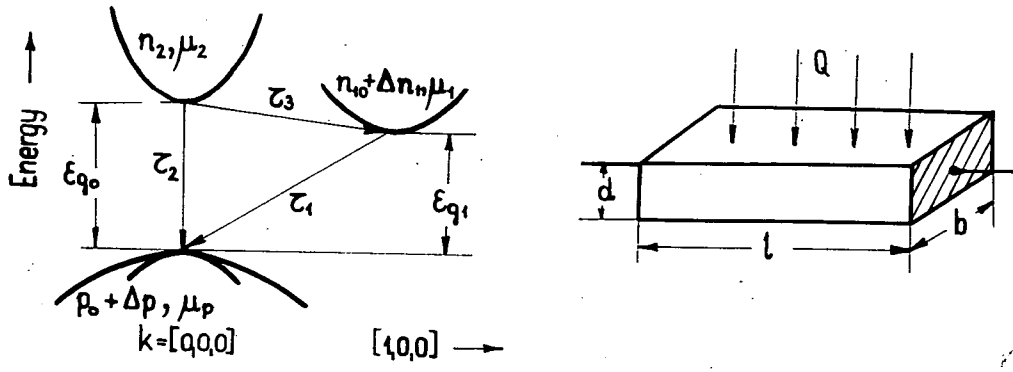

Fig. 4a. Energy band model for GaP. *4b.* Schematic diagram for calculation of APC

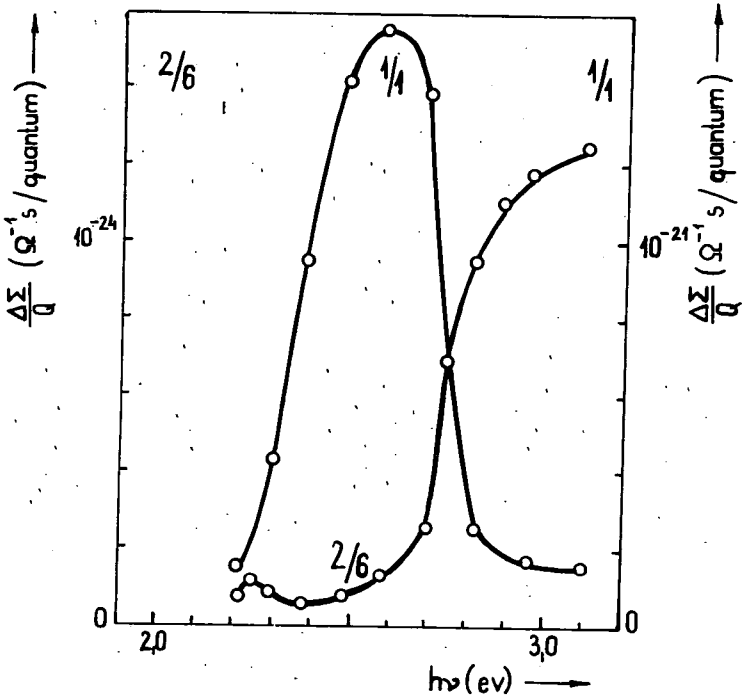

Fig. 5. PCR spectral curves (d. c. method) taken at uniform near-surface densities of generation

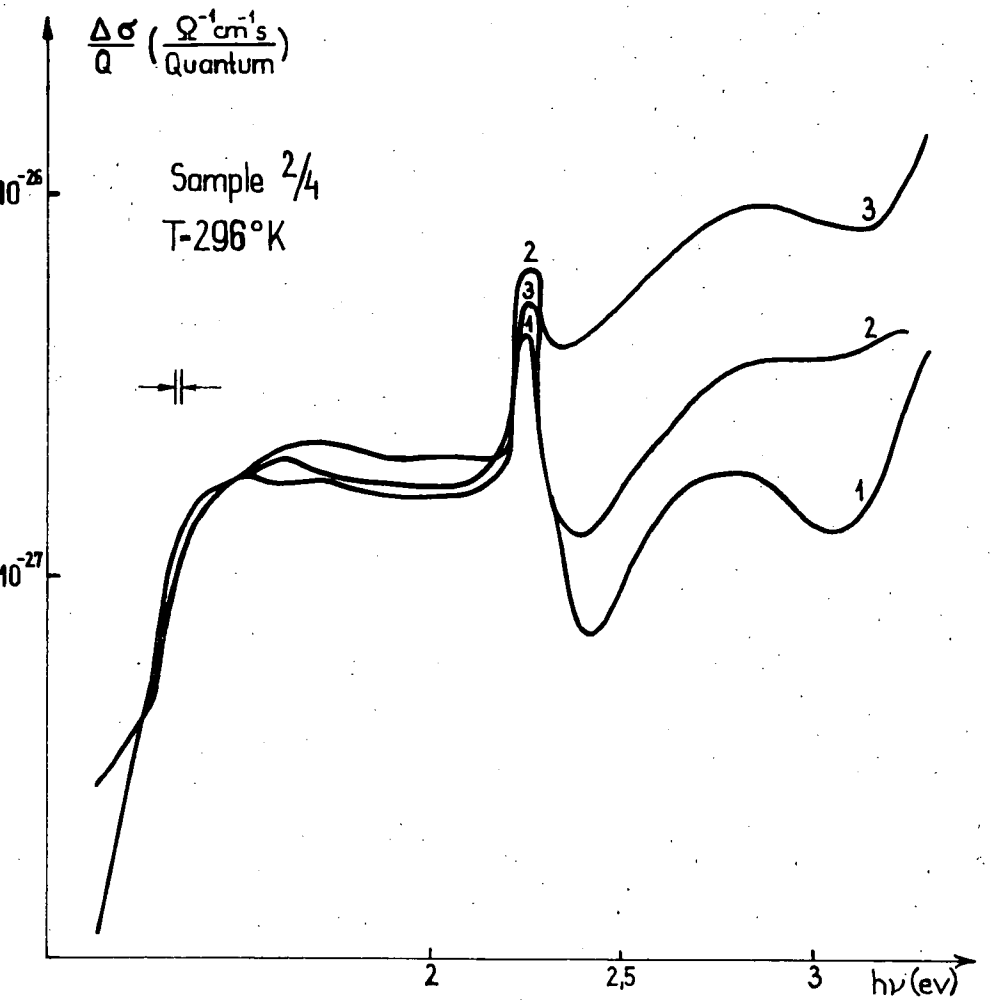

Fig. 6. PCR spectral curves. $Q > 10^{15}$ quantum/s. Secondary illumination through Si filter ($\lambda > 1{,}1\mu$) of various intensities (curve *1*: 0 quantum/s; *2*: $7 \cdot 10^{13}$ quantum/s; *3*: $1{,}8 \cdot 10^{14}$ quantum/s)

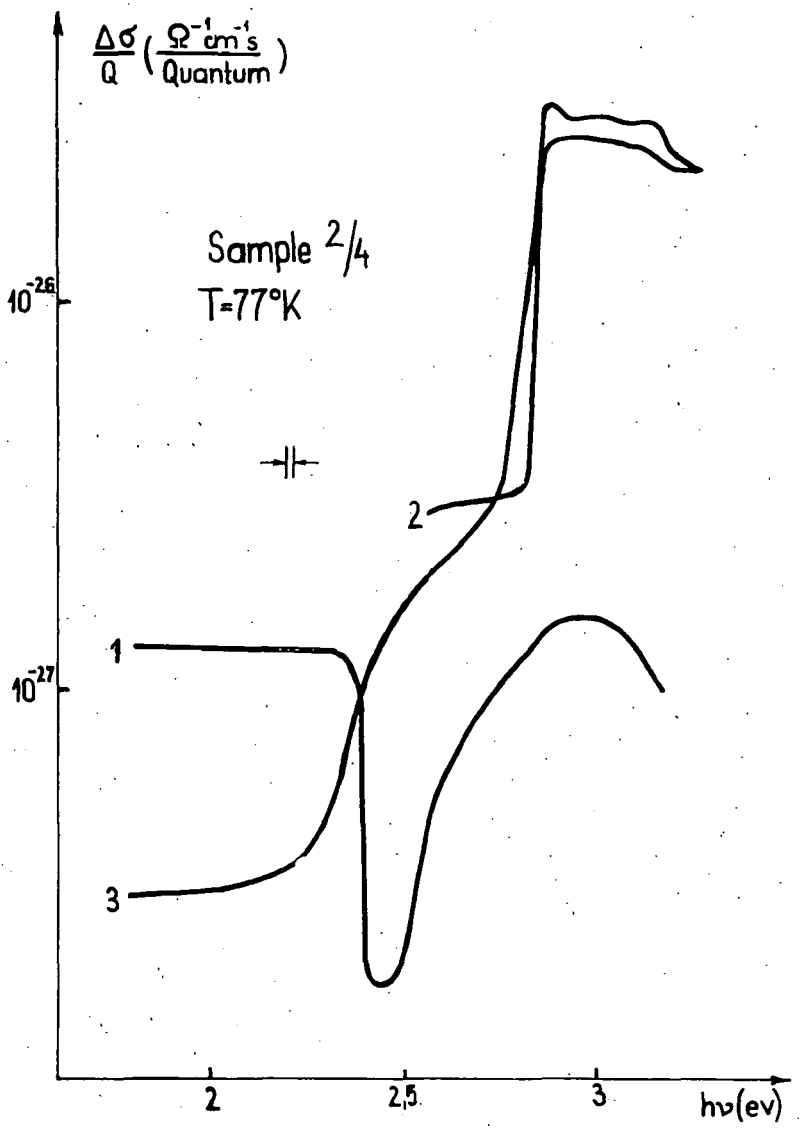

Fig. 7. PCR spectral curves. $Q \approx 10^{14} \div 10^{15}$ quantum/s. Secondary illumination through Si filter ($\lambda > 1{,}1\,\mu$) of various intensities (curve *1*: 0 quantum/s; *2*: $7 \cdot 10^{13}$ quantum/s; *3*: $1{,}8 \cdot 10^{14}$ quantum/s)

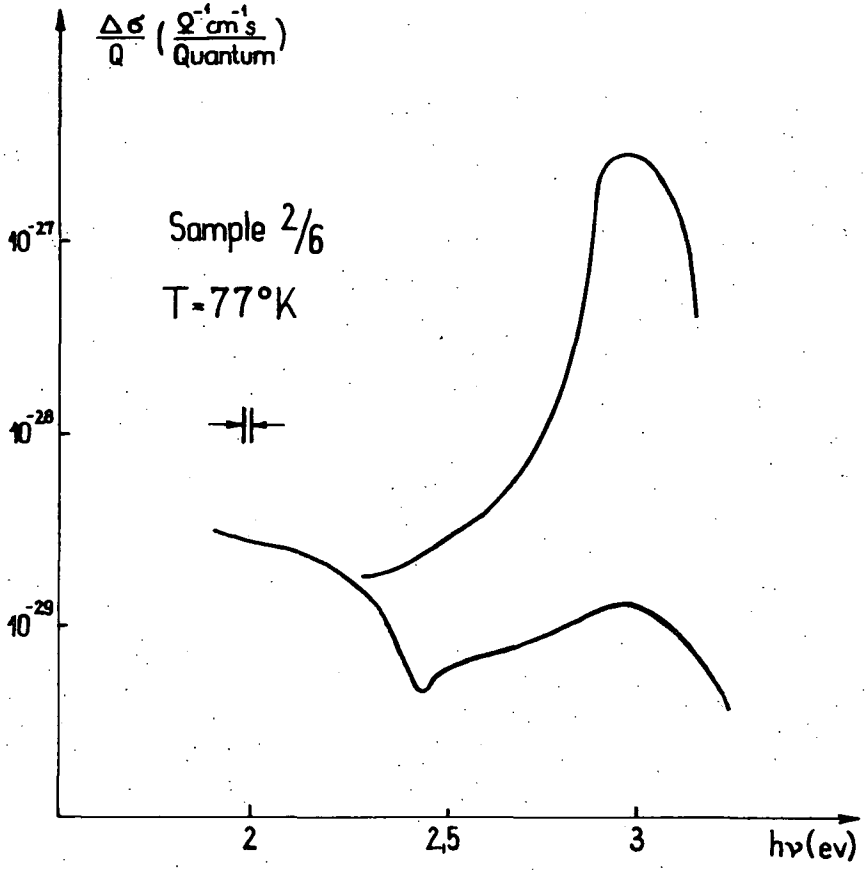

Fig. 8. PCR spectral curves. $Q \approx 10^{13}$ quantum/s. Secondary illumination through Si filter ($\lambda > 1{,}1\mu$) of various intensities (curve *1*: 0 quantum/s; *2*: $1 \cdot 10^{14}$ quantum/s)

$\lambda = 478$ nm and at $T = 77°K$ (Figs. 9., 10.). This superlinearity can be interpreted as in CdS [7] by the actual relative position of the Fermi level at 77°K and the recombination centres involved.

Discussion

The PCR curves taken with double illumination, as pointed out, are in contradiction with the explanation suggested in [1]. The experiment involving constant near-surface density of generation enabled us to decide between the explanations i) and ii). Namely, the existence of APC under this special condition would be in contradiction with explanation i), while it is consistent with explanation ii). Inversely, explanation ii) does not lead to any contradiction with known experimental facts, therefore it is to be considered as the most probable explanation of APC.

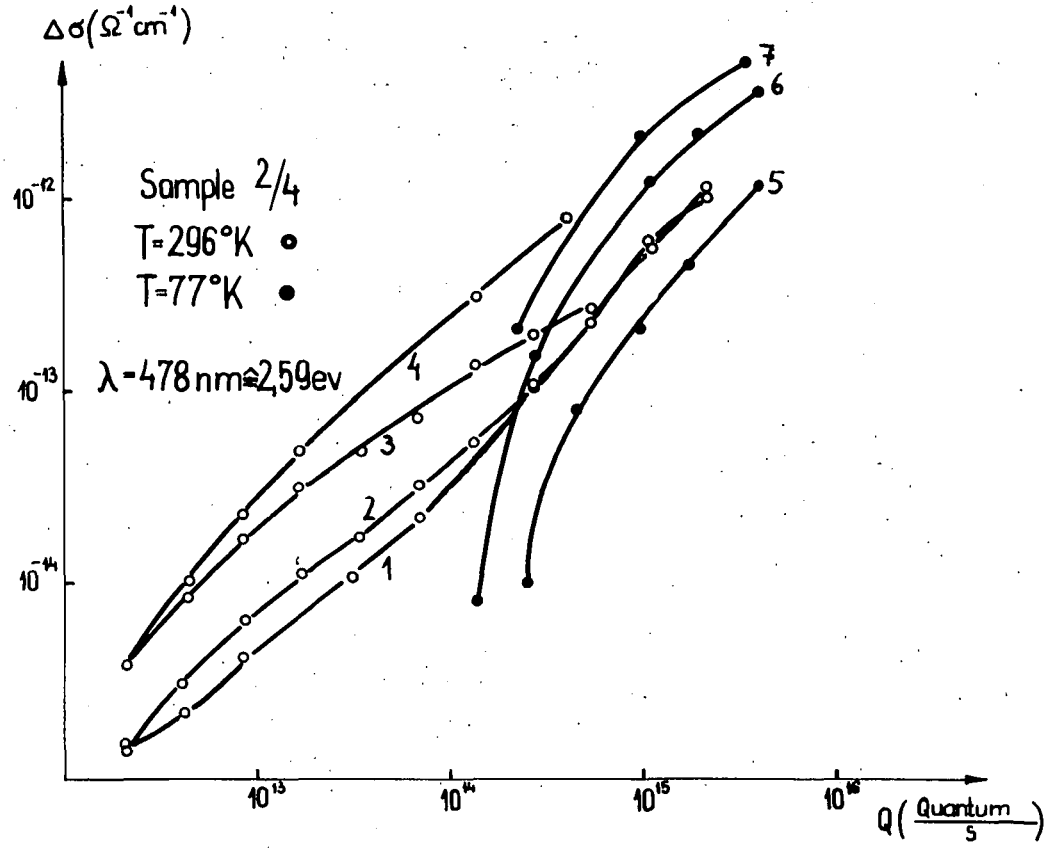

Fig. 9. Dependence of $\Delta\sigma$ on illumination intensity (Q) in the region of indirect transitions. Secondary illumination through glass filter (type ИКС-2, $\lambda > 0{,}95\mu$) of various intensities (curve *1*: 0 quantum/s; *2*: $6{,}3 \cdot 10^{13}$ quantum/s; *3*: $3 \cdot 10^{14}$ quantum/s; *4*: $7 \cdot 10^{14}$ quantum/s; curve *5*: 0 quantum/s; *6*: $7 \cdot 10^{13}$ quantum/s; *7*: $1{,}8 \cdot 10^{14}$ quantum/s)

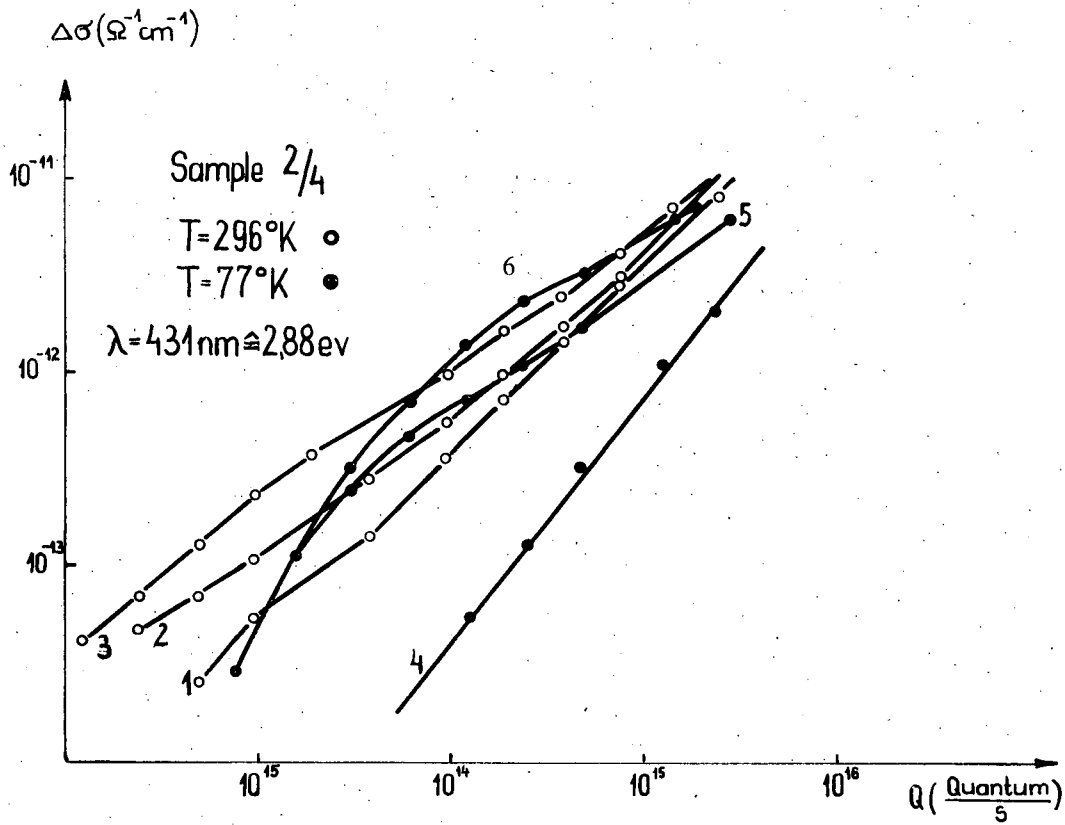

Fig. 10. Dependence of $\Delta\sigma$ on illumination intensity (Q) in the region of direct transitions. Secondary illumination through glass filter (type ИКС-2, $\lambda > 0{,}95\mu$) of various intensities (curves *1* and *4*: 0 quantum/s; *2* and *5*: $6{,}6 \cdot 10^{13}$ quantum/s; *3* and *6*: $1{,}8 \cdot 10^{14}$ quantum/s)

On Fig. 4a. the band scheme of GaP is to be seen. Using the notations of the figure and those of Fig. 4b., the conductivity change by illumination ($\Delta\sigma = \sigma_l - \sigma_d$) can be expressed as

$$\Delta\sigma = \frac{b}{l} q \int_0^d (\mu_1 \Delta n_1 + \mu_2 n_2 + \mu_p \Delta p)\, dx \qquad \text{(steady state)},$$

(q charge on the electron).

A) In the region of indirect transitions ($\varepsilon_{g1} \leqq h\nu \leqq \varepsilon_{g0}$) we have $n_2 = 0$, $\Delta n_1/\tau_1 = \Delta p/\tau_p$. Using $\Delta n_1/\tau_1 = G = (Q/lb)k \exp(-kx)$, for very low values of diffusion coefficient

$$\Delta\sigma_{\text{indir.}} = \frac{b}{l} q \int_0^d (\mu_1\tau_1 + \mu_p\tau_p) G\, dx.$$

B) For direct transitions ($h\nu \geqq \varepsilon_{g0}$), where $\Delta n_1/\tau_1 + n_2/\tau_2 = \Delta p/\tau_p$, $n_2/\tau_2 + n_2/\tau_2 = G$ and $n_2/\tau_3 = \Delta n_1/\tau_1$, we have

$$\Delta\sigma_{\text{dir.}} = \frac{b}{l} q \left[\int_0^d \left(\mu_1 + \mu_p \frac{\tau_p}{\tau_1} \right) \Delta n_1\, dx + \int_0^d \frac{G\tau_3}{\tau_1 + \tau_3} (\mu_2\tau_2 + \mu_p\tau_p)\, dx \right],$$

or, by $\Delta p/\tau_p = G$, $n_2 = G\tau_2\tau_3/(\tau_2 + \tau_3)$ and $\Delta n_1/\tau_1 = G\tau_2/(\tau_2 + \tau_3)$,

$$\Delta\sigma_{\text{dir.}} = \frac{b}{l} q \int_0^d \left[\mu_1\tau_1 + \mu_p\tau_p + \frac{\mu_2\tau_2 - \mu_1\tau_1}{\tau_2 + \tau_3} \tau_3 \right] G\, dx.$$

The *amount of APC* can thus be calculated using the ratio

$$\frac{\Delta\sigma_{\text{dir.}}}{\Delta\sigma_{\text{indir.}}} = \frac{\int_0^d \left[\mu_1\tau_1 + \mu_p\tau_p + \frac{\mu_2\tau_2 - \mu_1\tau_1}{\tau_2 + \tau_3} \tau_3 \right] G\, dx}{\int_0^d [\mu_1\tau_1 + \mu_p\tau_p] G\, dx}.$$

Supposing τ_1, τ_2 and τ_3 to be independent of generation density and thus of x, we have

$$\frac{\Delta\sigma_{\text{dir.}}}{\Delta\sigma_{\text{indir.}}} = 1 + \frac{\mu_2\tau_2 - \mu_1\tau_1}{\mu_1\tau_1 + \mu_2\tau_2} \frac{\tau_3}{\tau_2 + \tau_3} \equiv a.$$

Taking $a \approx 10$ for APC, this value can be explained by *e. g.* $\mu_2 = 15\mu_1$, $\tau_2 \approx \tau_1 \approx \tau_3$ and $\mu_p\tau_p \ll \mu_1\tau_1$. This explanation is in good agreement with the fact that APC takes place only in crystals of very low PCR, *i. e.* of very short lifetimes.

The lifetime *e. g.* in sample 2/4 can also be calculated approximately by the relation

$$\tau = \frac{h\nu}{q} \frac{l}{b} v/V_0 R_L I_A \mu,$$

where I_A the absorbed light energy and μ the drift mobility of majority carriers (supposing $\mu = 10^2$ cm^2 volt^{-1} s^{-1}). Using the signal at 431 nm, the formula yielded $\tau \approx 5 \cdot 10^{-9}$ s, in a very good agreement with [1].

* * *

Thanks are due to Prof. A. BUDÓ, member of the Hungarian Academy of Sciences for rendering possible to perform some experiments in this institute, furthermore, to A. A. VOLFSON (Leningrad) for allowing to use his apparatus in a. c. measurements. One of the authors (J. Gy.) is indebted to the Hungarian Academy of Sciences for a scholarship.

References

[1] *Nelson, D. F., L. F. Johnson, M. Gershenzon:* Phys. Rev. **135**, A 1399 (1964).
[2] *Subashiev, V. K., J. Gyulai, G. A. Chalikyan:* Report on the Photoconductivity Conference, Odessa, 1965.
[3] *Gyulai, J., V. K. Subashiev, G. A. Chalikyan:* Phys. stat. sol. **17**, K49 (1966).
[4] *Наследов, Д. Н., В. В. Негрескул, С. И. Рагауцан, С. В. Слободчиков:* Ф. Т. Т. **7**, 3671 (1965).
[5] *Рывкин, С. М.:* Фотоэлектрические явления в полупроводниках (Физматгиз, Москва, 1963), p. 40.
[6] *Subashiev, V. K., S. A. Abagyan:* Proc. Intern. Conf. Phys. Semicond. (Dunod, Paris, 1964) p. 225.
[7] *Bube, R. H.:* Photoconductivity of Solids (J. Wiley, New York, 1960) p. 288.

О ФОТОПРОВОДИМОСТИ ФОСФИДА ГАЛЛИЯ

Й. Гьюлаи, В. К. Субашиев, Г. А. Чаликян

Была исследована аномальная фотопроводимость очень высокоомных кристаллов фосфида галлия. Из экспериментальных результатов получается, что аномальная фотопроводимость связана разными подвижностями в разных минимумах зоны проводимости. По расчетам было показано, что наличие эффекта самое вероятно в кристаллах с очень мален - кими величинами времени жизни носителей.

ON DIFFUSE REFLECTION SPECTRA OF V_2O_5

By I. HEVESI

Institute of Experimental Physics, Attila József University, Szeged

(Received November 30, 1966)

Diffuse reflection spectra of powders prepared from V_2O_5 single crystals show a correlation between the range of linear increase in the spectrum and the range of exponential drop in the tail to the absorption edge of V_2O_5 single crystals. Comparative data are presented.

Band gap width and position of the absorption edge of semiconductors can be estimated with a relatively simple method by using their diffuse reflection spectra $R(\lambda)$ [1]. The evaluation is based on the fact, that the sharp decrease in absorption of powdered semiconductor particles in the neighbourhood of the absorption edge goes hand in hand with a steep increase in reflectivity. The onset of the linear part of the curve, which at the same time represents the region of greatest slope in the reflectivity curve, can be brought into connection with the onset of the exponential drop in the long wave tail to the absorption edge in a number of semiconductors. Though the use of the steepest part of the diffuse absorption spectrum as the base of determining the optical band gap is somewhat arbitrary, this method can give valuable informations, especially in the beginning of more detailed investigations on a semiconductor, while in other cases it is useful for comparing or checking the results.

In our investigations we used single crystals of V_2O_5, which are characterized by relatively low melting point and great band gap width. In determining the band gap of such semiconductors mainly optical methods can be taken into account rather than thermical ones. In two publications [2—3] dealing with optical absorption of V_2O_5 single crystals more in detail, we were able to state that the long wave tail to the absorption edge shows an exponential drop both with photon energy and temperature in accordance with URBACH's rule. The onset of the exponential drop was found to be at about $\lambda = 520\ m\mu$ and $\lambda = 515\ m\mu$ for light polarized parallel to the c axis and to the a axis, respectively. It was to be expected that the onset of the linear part in the diffuse reflection spectrum $R(\lambda)$ of V_2O_5 would to be found near the wavelengths mentioned. This supposition has been confirmed by our measurements.

Diffuse reflection spectra were obtained with the aid of a double beam grating spectrophotometer Type Optica Milano CF4DR, the reflectance head of which was provided with an integrating sphere. The V_2O_5 single crystal plates were ground to powders of different size distribution ($I > II > III \sim 10\ \mu$, see Fig. 1) in an agate pestle and mortar. One of two holders fixed on and easily removable from the surface of the integrating sphere contained the V_2O_5 single crystal powder to be measured, the other containing MgO powder used as reference standard, both

slightly compressed. Reflection spectra of the powdered samples were measured in the spectral range 350 mμ to 650 mμ.

Fig. 1 presents automatically recorded diffuse reflection spectra of three powders of different size distribution. Reflection shows a steep increase in the wavelength range 500 mμ to 580 mμ for each of the three samples. Though the steep increase in reflection becomes the more pronounced the smaller the size of the particles in the powder is, no essential differences can be found in the position

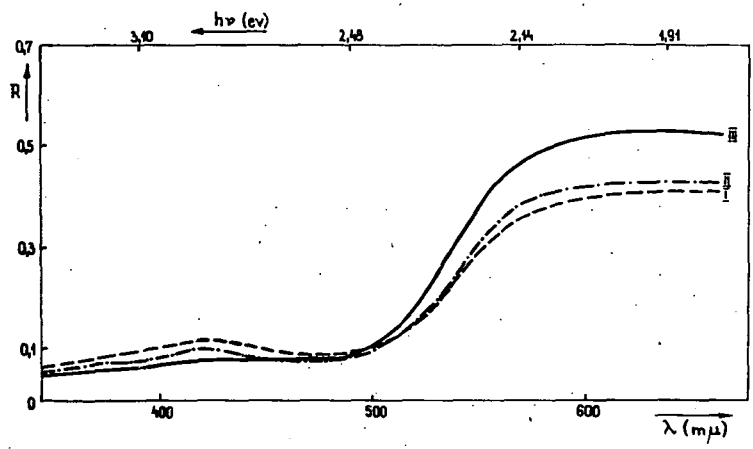

Fig. 1. Diffuse reflection spectra of V_2O_5

of the onset of the linear section in the curves. In the short wave range of the spectrum, *i. e.* in the region of low and nearly constant reflection, a band with a maximum at $\lambda = 425$ mμ can be observed. This increase in reflection is rather pronounced with thick single crystals, while it becomes indistinct with decreasing size of the particles in powdered samples.

On the base of diffuse reflection spectra of V_2O_5 it can be stated that the wavelength range of the linear increase in the spectra $R(\lambda)$ essentially coincides with that of the exponential drop in the tail to the absorption edge of V_2O_5 single crystals, and the onset of the linear increase in the reflection spectrum (~ 530 mμ) is to be found near the onset of exponential drop. Determining the band gap with the method given above, a value of 2,34 eV ($\triangleq 530$ mμ) has been obtained. The agreement of this figure with the values $E_g^{\parallel} = 2{,}30$ eV and $E_g^{\perp} = 2{,}32$ eV found in V_2O_5 single crystals at room temperature according to the polarization of light relative to the crystal axes, on the supposition of direct forbidden transitions [2—3], justifies the above estimate.

* * *

The author is indebted to Prof. A. BUDÓ, member of the Hungarian Academy of Sciences, for his steady interest in the course of this work.

References

[1] *Fochs, P. D.:* Proc. Phys. Soc., **69**, 70 (1956).
[2] *Bodó, Z., I. Hevesi:* Phys. stat. sol. **20**, K 45 (1967).
[3] *Hevesi, I.:* to be published in Acta Phys. Hung.

О СПЕКТРАХ ДИФФУЗНОГО ОТРАЖЕНИЯ МОНОКРИСТАЛЛОВ ПЯТИОКИСИ ВАНАДИЯ

И. Хевеши

В работе исследованы спектры диффузного отражения порошков полученных из монокристаллов пятиокиси ванадия. Установлена связь между экспоненциальным участком края основной полосы поглощения и резко возрастающим участком спектров диффузного отражения. Приведены данные для сравнения.

THE THERMAL DECOMPOSITION OF *n*-PROPYL NITRITE

By F. MÁRTA and L. SZIROVICZA

Institute of General and Physical Chemistry, Attila József University, Szeged

(Received December 1, 1966)

A recent investigation of the thermal decomposition of ethyl nitrite has been extended to include the analogous decomposition of *n*-propyl nitrite. The order of the reaction was found to be 1,25, and the overall activation energy 36,6 kcal. The products of the decomposition were found to be nitric oxide, nitrous oxide, propionaldehyde, propanol, water and formaldehyde. The effect of nitric oxide, propionaldehyde, propylene and hyrogen on the rate of the decomposition and on the product-distribution has also been investigated. The results are compared with those of the decomposition of ethyl nitrite and a similar mechanism is suggested which is able to explain the main features of the reaction.

Among various authors there is a general agreement that the alkoxyl radicals play an important role in the gas-phase pyrolysis of alkyl nitrites. The authors are of different opinion, however, concerning the reactions of alkoxyl radicals. The abstraction of hydrogen atom by these radicals from the parent nitrite molecule postulated by STEACIE and his co-workers [1], RICE and RODOWSKAS [2] can be neglected in the light of LEVY's results [3].

The decomposition of alkoxyl radicals has also been postulated by many authors [1, 2, 3, 4, 5]. According to their assumption the aldehyde of lower carbon number than the corresponding alkoxyl radical should be present in the products of the decomposition of nitrites. In the case of the decomposition of ethyl nitrite, for instance, the products should contain formaldehyde when the decomposition of ethoxyl radicals takes place. This product was found neither by LEVY [6] nor during the experiments carried out in this laboratory [7, 8, 9]. It seems very likely that a fission of alkoxyl radicals having higher carbon number than the ethoxyl radicals may occur during the pyrolysis of alkyl nitrites. This assumption seems to be supported by LEVY [10] who found formaldehyde in the decomposition products of *n*-propyl nitrite, but detailed analyses of the decomposition products were not made. From this point of view it seemed worth-while investigating the thermal decomposition of *n*-propyl nitrite which was carried out in the temperature range of 190—220°C and at initial pressures of 60—180 torr.

Experimental

The apparatus and the procedures were the same as described earlier [7, 8]. The samples extracted from the reaction vessel were analyzed by a Carlo Erba Fr. Mod. C. Gas Chromatograph on a column of 80 cm long and of 5 mm internal diameter packed with 20% of ethyl cyano ether supported on fire brick of 80 mesh. All the reactants were carefully purified. Propyl nitrite, nitric oxide and propylene were produced and purified as described earlier [7, 8]. Propionaldehyde was produced

by oxidation of propanol with chromic acid. The fraction obtained by several fractional distillation was subjected to repeated distillation at low temperatures under vacuum. Hydrogen taken from a steel flask was deoxygenated with pyrophoric copper on a silica gel carrier [11]. The gas was then transferred into the storing bottle through traps cooled with liquid air.

Results

(a) *Effect of initial pressure and of temperature on the decomposition of propyl nitrite*

For the investigation of the effect of initial pressure experiments were carried out at 200°C and at pressures of 60, 100, 140, and 180 torr. The results are shown in Fig. 1.

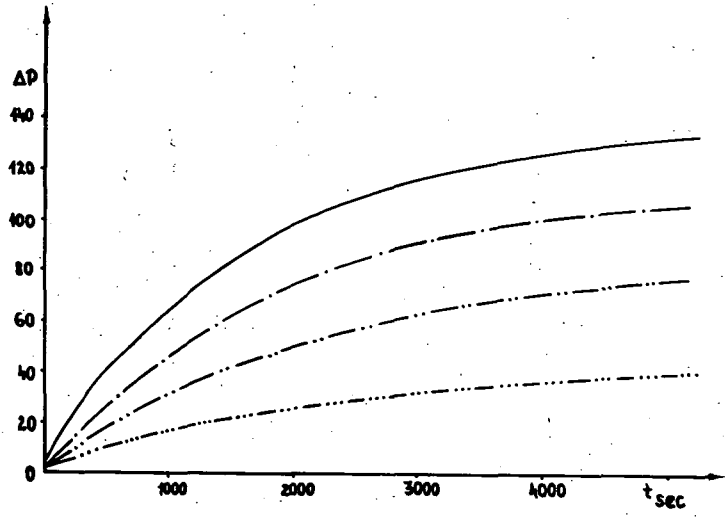

Fig. 1. ΔP—t curves at 200°C and at initial pressures of 60, 100, 140, 180 torr, —···—, —·—, —·—, —, respectively

From the results of experiments carried out at different initial pressures the order of the reaction was determined. Applying the van't Hoff's method, the overall order was found to be 1,25. The rate constants calculated on the basis of first and 3/2 order rate equation show a definite trend of decrease and increase resp., as can be seen from Table I. For the characterization of the rates it seemed more reasonable — taking into consideration the observed discrepancies — to use the times belonging to the same stages of the reaction instead of the rate constants.

The effect of temperature has been investigated for all of the already mentioned initial pressures at temperatures of 190, 200, 210, and 220°C. The results of these experiments are illustrated in Fig. 2.

The activation energy was determined from the temperature dependence of one eight, one quarter and half-times shown in Fig. 3.

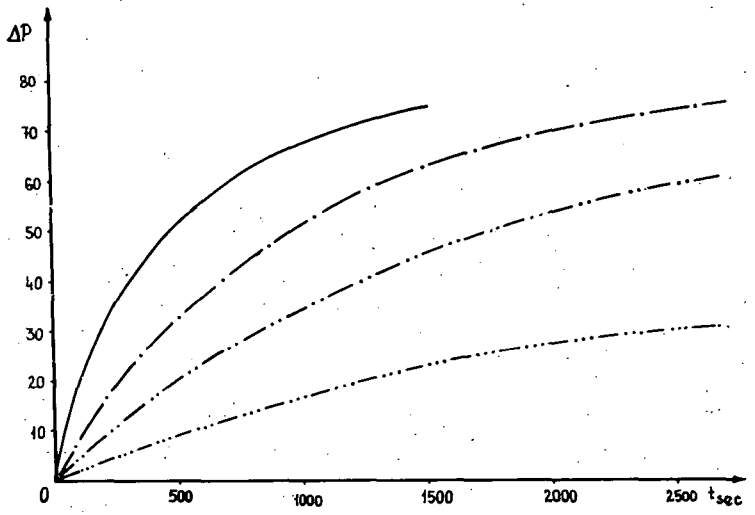

Fig. 2. ΔP—t curves at an initial pressure of 100 torr and at temperatures: —...— 190°, —..— 200°, —.— 210°, — 220 °C

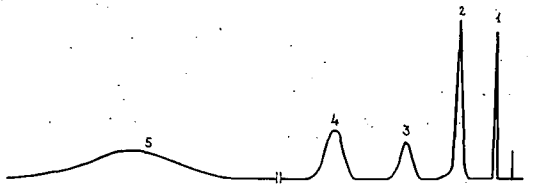

Fig. 4. The chromatogram of the products at a conversion of 94,6%, $P_0 = 100$ torr; $T_0 = 200$ °C, carrier gas: helium,

Sensitivities:

(1) $NO + N_2O$	128 mV
(2) propylnitrite	128 mV
(3) formaldehyde	32 mV
(4) propionaldehyde	32 mV
(5) propyl alcohol	32 mV

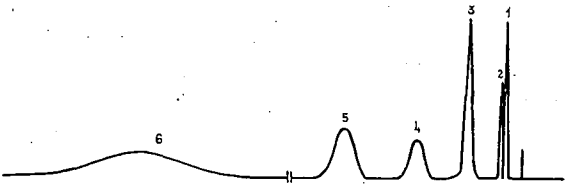

Fig. 5. The chromatogram of the products at a conversion of 94,6%, $P_0 = 100$ torr, $T_0 = 200$ °C, carrier gas: nitrogen,

Sensitivities:

(1) NO	32 mV
(2) N_2O	32 mV
(3) propylnitrite	32 mV
(4) formaldehyde	4 mV
(5) propionaldehyde	4 mV
(6) propanol	4 mV

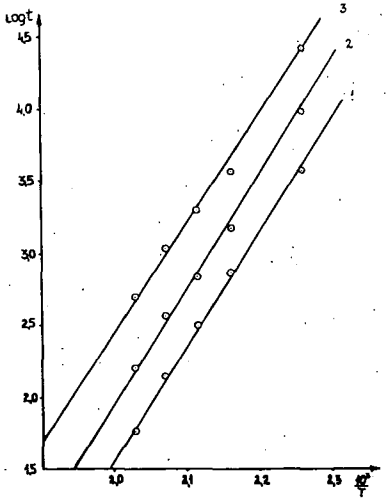

Fig. 3. Dependence of the one eight (1), one quarter (2), and half times (3) on the temperature

Table I
Rate constants calculated according to first and 3/2 orders

t_{sec}	% decomp.	$10^{-4} \cdot k_1$	$10^{-5} \cdot k_{3/2}$
404	15	4,05	4,21
509	18	3,94	4,21
622	21	3,85	4,08
826	27	3,84	3,80
1105	33	3,52	3,89
1586	43	3,56	4,02
1905	48	3,45	4,08
2675	59	3,34	4,22
3087	64	3,28	4,31
3578	68	3,18	4,28
4581	75	3,02	4,36

The values of activation energy and that of the activation constant were found to be 36,6 kcal and $3{,}16 \times 10^{13}$ resp., in good agreement with the data to be found in the literature.

(b) *The products of the reaction and their effect on the decomposition*

The products of the reaction we were able to identify gas chromatographically were nitric oxide, nitrous oxide, propionaldehyde, propanol, formaldehyde and water. With the exception of water quantitative analyses of these products were made at different stages of the reaction. Using helium as carrier gas it was possible to determine the yield of propionaldehyde, propanol, formaldehyde, propil nitrite and the sum of nitrogen oxides from one sample as is shown in Fig. 4.

Nitrogen oxides could be separated and determined on a column packed with molecular sieve 5A, and on the column mentioned earlier but using nitrogen as carrier gas. The chromatogram obtained in the latter case is shown in Fig. 5.

The changes in the partial pressures of the products and of propyl nitrite determined from the analysis are shown in Fig. 6. From the results of the analysis the material-balance of the products of the decomposition was determined and listed in Table II.

The effect of products such as nitric oxide and propionaldehyde as well as that of hydrogen and propylene on the decomposition of propyl nitrite has also been studied.

Table II
Material balance of the decomposition products of propyl nitrite
$P_0 = 100$ torr; $T = 200°C$

Product	Partial pressure
Nitrous oxide	6,1
Nitric oxide	89,1
Residue of propyl nitrite	5,4
Formaldehyde	5,8
Propionaldehyde	49,3
Propyl alcohol	16,4
Water	6,1
Total:	178,2
Manometrically measured	186,0
Diviation	4,5%

Table III
The Effect of nitric oxide on the values of half-times

P_{NO} torr	$t_{\frac{1}{2}}$ sec
0	2100
5	2250
10	2380
20	2700
30	3400

The results of the experiment carried out in the presence of added nitric oxide may be summarized as follows:

(a) The order of the reaction was not influenced by added nitric oxide

(b) The final pressure change slightly decreased increasing the amount of nitric oxide

(c) The rate of the decomposition decreased as can be seen from Table III.

(d) The yield of nitrous oxide and propionaldehyde increased and that of formaldehyde and propanol decreased as can be seen from Table IV.

Table IV

Material balance of products in the presence of added nitric oxide and propionaldehyde of 100 torr

Product	Partial pressure of products in the presence of	
	Nitric oxide	propionaldehyde
Nitrous oxide	10,2	3,1
Nitric oxide	72,1	92,1
Residual propyl nitrite	5,4	4,2
Formaldehyde	1,0	6,1
Propylaldehyde	52,1	47,9
Propyl alcohol	14,8	16,3
Water	10,2	3,1
Total:	165,8	172,8
Manometrically measured	172,0	184,0
Diviation	4,2%	6,1%

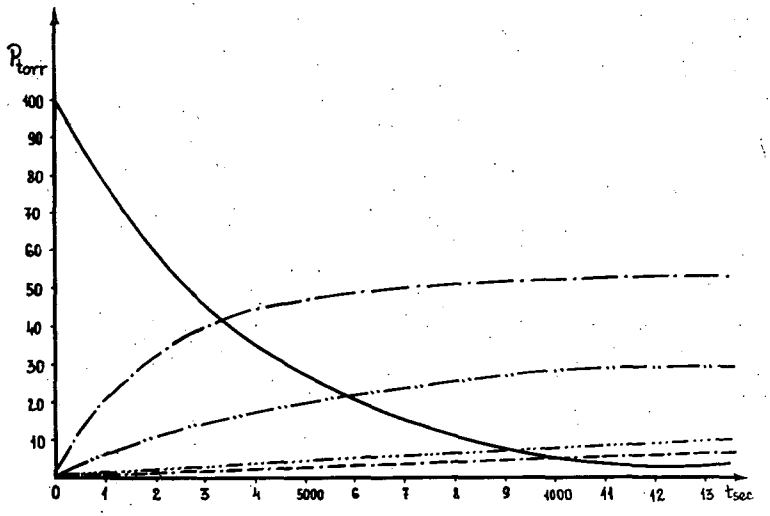

Fig. 6. Plot of the partial pressure of the products against time ——— propylnitrite; —.— NO; —..— propionaldehyde; —...— propanol; — —. formaldehyde

In the experiments carried out in the presence of added propionaldehyde it was found that

(a) The order of the reaction remained unchanged

(b) The final pressure change was roughly the same as in the absence of propionaldehyde

(c) The rate of the decomposition increased as is shown in Table V.

(d) The yield of the products altered only slightly with the exception of nitrous oxide the yield of which was reduced as can be seen from Table IV.

Table V
The effect of propionaldehyde on the values of half-times

$P_{propionaldehyde}$ torr	$t_{\frac{1}{2}}$ sec
0	2100
5	1900
10	1650
20	1500
50	1340
100	1010

The hydrogen and propylene had not any appreciable effect on the rate and on the order of the decomposition; their effect on the product-distribution is illustrated in Table VI.

During the pyrolysis the formation of tarry products was observed and this was greately increased in the presence of added propylene. The analysis of these tarry products led to the following results regarding their composition: C = 47,91%, H = 5,37%, N = 13,97%, O = 32,75%.

Table VI
Effect of propylene and hydrogen on the yields of products at 25% conversion

Products	—	Propylene (100 torr)	Hydrogen (100 torr)
Nitrous oxide and Nitric oxide	9,5	10,8	10,0
Propyl nitrite	82,5	82,4	87,8
Formaldehyde	1,5	1,0	0,2
Propionaldehyde	4,8	2,4	2,4
Propyl alcohol	1,9	1,8	2,0

Discussions

From the results described above it appears that nitrous oxide is a significant product of the reaction. This result is in an apparent disagreement with the results of LEVY [10] who found that nitrous oxide appears as a product only in the presence of added nitric oxide. The kinetic feature of the decomposition of *n*-propyl nitrite is very similar to that of ethyl nitrite with the difference that formaldehyde becomes a product due to the decomposition of propoxyl radical.

The main features of the reaction may be interpreted by the following sequence of steps:

$$C_3H_7ONO \overset{k_1}{\underset{k_2}{\rightleftarrows}} C_3H_7O + NO \tag{1.2}$$

$$C_3H_7O + NO \xrightarrow{k_3} C_2H_5CHO + HNO \tag{3}$$

$$C_3H_7O + HNO \xrightarrow{k_4} C_3H_7OH + NO \tag{4}$$

$$C_3H_7O + C_2H_5CHO \xrightarrow{k_5} C_3H_7OH + C_2H_5CO \tag{5}$$

$$CH_3CH_2CH_2O \xrightarrow{k_6} CH_3CH_2 + CH_2O \tag{6}$$

$$2\,HNO \xrightarrow{k_7} N_2O + H_2O \tag{7}$$

Application of the steady-state treatment to this mechanism gives rise to the following expression for the concentration of propoxyl radical:

$$[C_3H_7O] = \frac{k_1[C_3H_7ONO]}{(k_2+k_3)[NO]+k_4[HNO]+k_5[C_2H_5CHO]+k_6}, \tag{8}$$

The rate of disappearance of propyl nitrite is given by the expression:

$$-\frac{d[C_3H_7ONO]}{dt} = k_1[C_3H_7ONO]-k_2[NO][C_3H_7O] \tag{9}$$

if expression (8) is substituted into expression (9) the resulting rate expression will be:

$$-\frac{d[C_3H_7ONO]}{dt} = \tag{10}$$

$$= k_1[C_3H_7ONO]\left\{1-\frac{k_2[NO]}{(k_2+k_3)[NO]+k_4[HNO]+k_5[C_2H_5CHO]+k_6}\right\}$$

and by rearrangement of (10)

$$-\frac{d\ln[C_3H_7ONO]}{dt} k_1\left\{1-\frac{k_2}{k_2+k_3+k_4\frac{[HNO]}{[NO]}+k_5\frac{[C_2H_5CHO]}{[NO]}+\frac{k_6}{[NO]}}\right\}, \tag{11}$$

From rate expression (11) it can be seen that the overall rate of the reaction is determined by the ratio of $[C_2H_5CHO]/[NO]$; on increasing the concentration of propionaldehyde or that of nitric oxide the rate of the decomposition increases or decreases resp., as it was found experimentally.

Since neither ethane nor carbon monoxide were found among the products, one has to assume that the species C_2H_5 and C_2H_5CO together with NO and CH_2O must have disappeared in the reaction leading to the formation of tarry products.

Comparing the decomposition of ethyl nitrite and that of propyl nitrite it turns out that the nitric oxide has roughly the same effect on the product-distribution in both cases, but the propionaldehyde has much smaller influence on the product-distribution than the acetaldehyde had in the case of ethyl nitrite. The mechanism is suitable for the explanation of the product-distribution influenced by nitric oxide but not for that of propionaldehyde.

In the presence of added nitric oxide the rate of step (2) is increased and this results in the decrease of the stationary concentration of the propoxyl radical. The rates of step (3) and (7) remain essentially unchanged, because the decrease in the concentration of propoxyl radicals is compensated by the increase in the concentration of nitric oxide. The rates of steps (4), (5) and (6), however, decrease and consequently the yield of propanol and formaldehyde decreases. The rate of step (6) is decreased mainly because the higher pressure due to the presence of nitric oxide does not favour the unimolecular decomposition of propoxyl radicals. This assumption is proved by the fact that hydrogen results in the decrease of the yield of formaldehyde, too. These circumstances lead to the consequence that the propoxyl radicals are consumed mainly by step (3) bringing about an increase in the yield of propionaldehyde and nitrous oxide.

According to the mechanism the rate of step (5) should increase in the presence of added propionaldehyde bringing about the disappearance of the propoxyl radicals mainly by step (5) instead of step (3) and (6), and resulting in a decrease in the yield of nitrous oxide and formaldehyde and an increase in that of propanol.

During the experiments, however, it was found that while the yield of nitrous oxide was reduced in agreement with the mechanism the yield of formaldehyde and that of propanol was essentially not altered in apparent disagreement with the mechanism. Further experiments are needed to elucidate this discrepancy.

References

[1] *Steacie, E. W. R., G. T. Show:* J. Chem. Phys. **3**, 344 (1935).
[2] *Rice, F. O., F. L. Rodowskas:* J. Am. Chem. Soc. **57**, 350 (1935).
[3] *Levy, J. B.:* J. Am. Chem. Soc. **78**, 1780 (1956).
[4] *Steacie, E. W. R., R. S. Katz:* J. Chem. Phys. **5**, 125 (1937).
[5] *Adler, D. G., M. W. Pratt, P. Gray:* Chem. Ind. **1955**, 1517.
[6] *Levy, J. B.:* J. Am. Chem. Soc. **75**, 1801 (1953).
[7] *Márta, F., L. Seres:* Acta Phys. et Chem. Szeged, **12**, 35 (1966).
[8] *Márta, F., L. Seres:* Acta Phys. et Chem. Szeged, **12**, 47 (1966).
[9] *Márta, F., L. Seres:* Acta Phys. et Chem. Szeged, **12**, 113 (1966).
[10] *Levy, J. B.:* Ind. Eng. Chem. **48**, 762 (1956).
[11] *Márta, F., L. Seres:* Ber. Bunsenges. physik. Chem. **70**, 921 (1966).

ТЕРМИЧЕСКОЕ РАЗЛОЖЕНИЕ *n*-ПРОПИЛНИТРИТА

Ф. Марта и Л. Сировица

Авторы включали в серию изучения термического разложения этилнитрита подобный процесс разложения *n*-пропилнитрита. Порядок реакции оказался 1,25 а среднее значение энергии активации 36,6 ккал. Продукты разложения были окись и двуокись азота, пропиональдегид, пропанол, вода и формальдегид. Изучалось влияние двуокиси азота, пропиональдегида, пропилена и водорода на скорость разложения и на перераспределение продуктов. Полученные результаты сравнивались с теми же разложения этилнитрита и авторы предлагают подобный механизм объяснить главные черты реакции.

ÜBER DIE PERMANGANAT-OXALAT REAKTION

von E. HORVÁTH und M. GÉCSEG

Institut für Allgemeine und Physikalische Chemie
der Attila-József-Universität, Szeged

(Eingegangen am 14 Dezember, 1965)

Es wurde die Reaktion zwischen $KMnO_4$, $NaMnO_4$, NH_4MnO_4, $AgMnO_4$ und Oxalat bei verschiedenen Temperaturen, in Lösungen mit verschiedenen p_H-Werten untersucht. Obwohl sich die aus grafischer Darstellung erhaltene Reaktionsordnung nahe bei 1 ergab, erhalten wir mit der Gleichung für Reaktionen erster Ordnung keine annehmbare Werte für die Geschwindigkeitskonstante. Es wurde gezeigt, daß die Reaktionsgeschwindigkeit durch den p_H des Mediums, durch die Temperatur und das angewandte Kation stark beeinflußt wird.

Einleitung

Die Ergebnisse der bis 1958 vollendeten Untersuchungen über die Permanganat-Oxalat Reaktion wurden von GUPTA und GHOSH [1] zusammengefaßt. In den S-förmigen d[Oxidant]/dt Kurven kann man drei Teile unterscheiden. Die Induktionsperiode wird zur allmählichen Reduktion des Mn(VII) zu Mn(II), die Endperiode zum monomolekularen Zerfall der Mn(II)-Oxalat-Komplexe zugeordnet. Die Hauptperiode entspricht der Reaktionsserie, die nach dem Erreichen der entsprechenden Mn(II)-Konzentration beginnt.

GUPTA und GHOSH [1] haben die Reaktion des $KMnO_4$ mit Oxalat mittels spektrophotometrischen und jodometrischen Methoden in Systemen von verschiedenen p_H-Werten erforscht. Sie fanden, daß unter den erforschten Systemen das von $p_H = 2{,}06$ das günstigste für die Reduktion des Permanganats ist. In großem Säureüberfluß beschleunigt sich die Reaktion, doch die Induktionsperiode verschwindet nicht. Mn^{++}-Ionen beschleunigen die Anfangsreaktion, in den späteren Perioden, in Lösungen von kleiner Acidität, wirken sie aber als Inhibitoren. Nach einigen Minuten vermindert sich die Permanganat-Konzentration schneller, als die der gegenwärtigen Oxidanten. Das zeigt, daß in dem System neben Mn(VII) auch andere Oxidationsmittel vorhanden sind. So nehmen sie an, daß während der Reaktion auch Mn(VI), MnO_2, H_2O_2 usw. entstehen werden.

Wir haben die Reaktionen des $KMnO_4$, $NaMnO_4$, NH_4MnO_4 und $AgMnO_4$ mit Oxalat bei verschiedenen Temperaturen und in Lösungen von verschiedenen p_H-Werten untersucht.

Experimenteller Teil

Die bei den Untersuchungen verwendeten Lösungen wurden aus analysenreinen Chemikalien angefertigt. NH_4MnO_4 und $AgMnO_4$ wurden nach den Vorschriften der Literatur [2] hergestellt.

0,2 M Oxalsäure- und 0,2 N Kaliumoxalat-Lösungen wurden in verschiedenen Verhältnissen vermischt und so Grundlösungen von 1,9 bzw. 2,1 bzw. 2,8 bzw. 3,8 p_H-Werten hergestellt.

80 ml der Oxalat-Ionen erhaltenen Lösung wurde mit 10 ml destilliertes Wasser und 10 ml Permanganat-Lösung vermengt. Die Reaktionslösung wurde stark gerührt. Nach je 2 Minuten wurde 5 ml dieser Lösung zu einer Mischung von 1 ml 2,0 N Schwefelsäure und 5 ml 7% KJ-Lösung gegeben und das ausgesonderte J_2 mit $Na_2S_2O_3$-Lösung titriert.

Der p_H der Lösungen wurde nach 1 bzw. 20 Minuten mit einem Radiometer PHM 22 gemessen.

Die Permanganat-Konzentrationen waren 10^{-3} bzw. $2\cdot10^{-3}$ bzw. $4\cdot10^{-3}$ M. Die Reaktionslösung wurde zu $25\pm0{,}1$ °C thermostiert. Im Falle von 10^{-3} M Permanganat-Konzentrationen wurden die Messungen auch bei 30, 35 und 40 °C durchgeführt.

Die spektrophotometrische Messungen wurden mit einem BECKMAN DU Spektrophotometer, bei 25°C, mit Quarzküvetten von 1 cm durchgeführt.

Besprechung der Versuchsergebnisse

a) *Zusammenhang zwischen Reaktionsgeschwindigkeit und Permanganat-Konzentration*

Zur Feststellung der Reaktionsordnung haben wir die Reaktionsgeschwindigkeit bei konstanter Oxalat-Konzentration und Temperatur (25°C) mit Permanganat-Lösungen von 10^{-3} bzw. $2\cdot10^{-3}$ bzw. $4\cdot10^{-3}$ M Konzentrationen, bei verschiedenen H^+-Konzentrationen untersucht. Fig. 1 zeigt die bei Grundlösung mit $p_H=2{,}8$ erhaltenen d[Oxidant]/dt Kurven.

Nach den Daten der Kurven wird die Reaktion in Lösungen mit gleichen Kationen beschleunigt, wenn die Permanganat-Konzentration zunimmt, die $dc/dt_{max}-c$ Kurven sind linear.

Als Richtungstangente der $\log dc/dt-\log c$ Kurven ergab sich 1,06—1,16, so kann man die Reaktion in guter Näherung als eine erster Ordnung ansehen. Die mit dieser Gleichung erhaltenen Geschwindigkeitskonstanten zeigen aber einen bestimmten Gang. Tabelle I enthält die k-Werte im Falle von $KMnO_4$ in der erwähnten Grundlösung ($p_H=2{,}8$).

Eine solche Änderung der Geschwindigkeitskonstante kann teils der p_H-Wirkung, teils der Anwesenheit der während der chemischen Umwandlung entstehenden Oxidationsmittel zugesagt werden. Wir haben nämlich beobachtet, wenn der p_H oberhalb 2,1 ist, wird die Reaktion langsamer; und nach unseren p_H-Messungen nimmt die H^+-Konzentration während des Ablaufes der Reaktion nur wenig, aber eindeutig ab. Anderseits verweisen GUPTA und GHOSH und auch frühere Verfasser [1] auf die Gegenwart von Zwischen- und Nebenprodukten mit Oxidationswirkung, durch die die titrimetrischen Ergebnisse natürlich stark beeinflußt werden. Wir haben Extinktionsmessungen bei der, in dem sichtbaren Spektralgebiet liegende, die MnO_4^- -Ionen charakterisierende Wellenlänge durchgeführt, um der Reaktion so folgen zu können. Die aus diesen Daten gerechnete jeweilige Permanganat-Konzentration ergab kleinere, als die nach jodometrischen Messungen erhaltenen Werte. Das ist leicht zu verstehen, daß man mit photometrischen Messungen bei

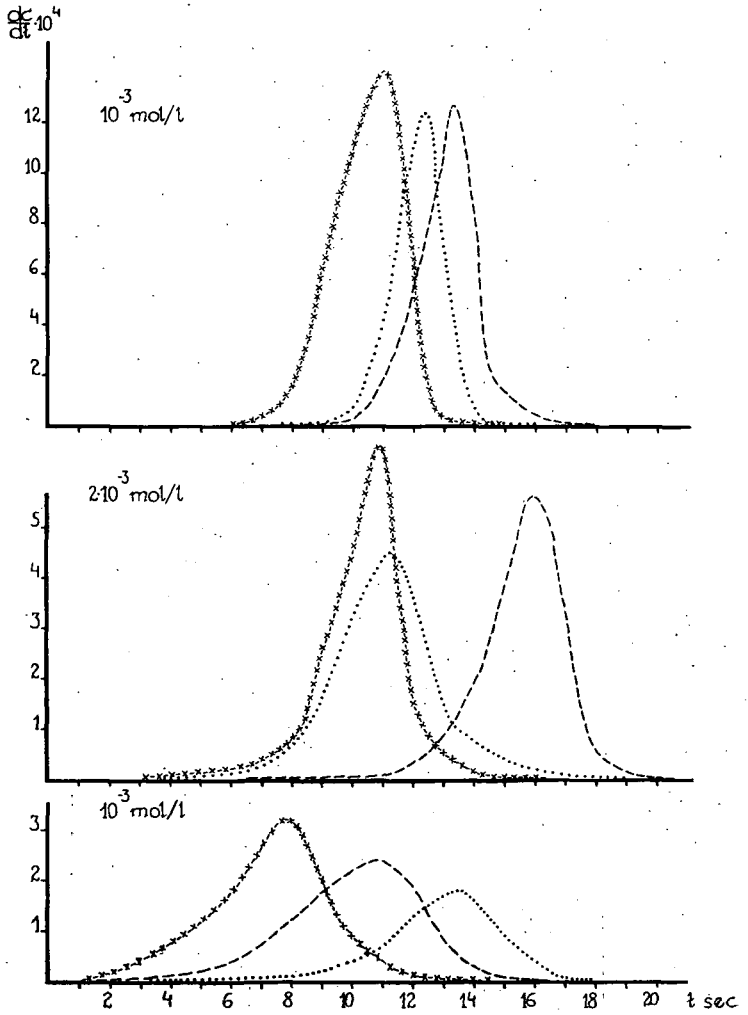

Fig. 1. Konzentrationeinfluß und Kationenwirkung.
..... $KMnO_4$; ---- $NaMnO_4$; -x-x-x NH_4MnO_4

Tabelle I

sec.	$k \cdot 10$		
	10^{-3} M	$2 \cdot 10^{-3}$ M	$4 \cdot 10^{-3}$ M
2	0,989	1,912	2,282
4	1,692	1,870	2,075
6	1,282	1,859	1,884
8	1,192	1,567	1,857
10	1,157	1,376	1,642
12	1,045	1,245	1,082
14	0,955	1,163	1,152
16	0,912	1,017	1,026
18	0,806	0,898	0,915
20	0,729	0,814	0,828

guter Ernäherung die Änderung der Permanganat-Konzentration folgen kann, während man bei der Titration Konzentrationsänderung der gesamten Oxidationsmittel mißt.

a) p_H-*Effekt*

Nach den in den Grundlösungen von 1,9 bzw. 2,1 bzw. 2,8 bzw. 3,8 p_H ausgeführten Messungen ergab sich für alle Permanganaten, daß der p_H um 2,1 das günstigste für die Reaktion ist. Bei niedrigeren oder höheren p_H-Werten wird der Prozeß wesentlich langsamer. Das ist an Fig. 2 gut zu sehen, welche bei Lösungen von 10^{-3} M Konzentration die $dc/dt - t$ Kurven darstellt. Die Daten der Tabelle II zeigen, daß sich der p_H bei dieser Konzentration unter dem Einfluß der Permanganaten in 1 Min. Reaktionszeit nicht verändert. Auch nach 20 Minuten kann man keine bedeutende p_H-Änderung beobachten.

Tabelle II
p_H-Änderung der Reaktionslösungen

Kation	p_H der Grundlösung	1,9		2,1		2,8		3,8	
	Reaktionszeit sec.	1	20	1	20	1	20	1	20
	Mol/liter								
K^+	10^{-3}	1,9	1,95	2,1	2,2	2,8	2,9	3,8	3,85
	$2 \cdot 10^{-3}$	2,0	2,2	2,3	2,4	2,9	3,1	3,8	4,0
	$4 \cdot 10^{-3}$	2,2	2,4	2,3	2,6	2,98	3,4	3,95	4,2
Na^+	10^{-3}	1,9	1,95	2,1	2,15	2,8	2,9	3,8	3,85
	$2 \cdot 10^{-3}$	2,1	2,3	2,4	2,5	3,2	3,4	4,1	4,3
	$4 \cdot 10^{-3}$	2,4	2,5	2,5	2,6	3,2	3,5	4,1	4,2
NH_4^+	10^{-3}	1,9	1,95	2,1	2,25	2,9	2,95	3,8	3,85
	$2 \cdot 10^{-3}$	1,9	1,95	2,1	2,25	2,9	3,0	3,8	3,85
	$4 \cdot 10^{-3}$	1,95	2,1	2,1	2,2	2,9	3,0	3,85	3,9

Betrachten wir aber die p_H-Änderung bei verschiedenen Konzentrationen, so ist es zu sehen, daß unter den 10^{-3} bzw. $4 \cdot 10^{-3}$ M $KMnO_4$- und $NaMnO_4$-Lösungen eine p_H-Zunahme von etwa 0,5 Einheit zu beobachten ist. Dagegen ist bei NH_4MnO_4-Lösung diese Änderung sehr gering, zwischen 0,05—0,15 Einheiten.

Wir nehmen an, daß der Einfluß der Kationen auf den p_H der Lösungen und so, nach dem oben gesagten, auch auf die Reaktionsgeschwindigkeit, teils auf den Stabilitätsunterschied der untersuchten Verbindungen, teils auf die verschiedenen Funktionen, die die erwähnten Kationen in den verschiedenen Ladungsüberführungsprozessen haben, zurückzuführen ist.

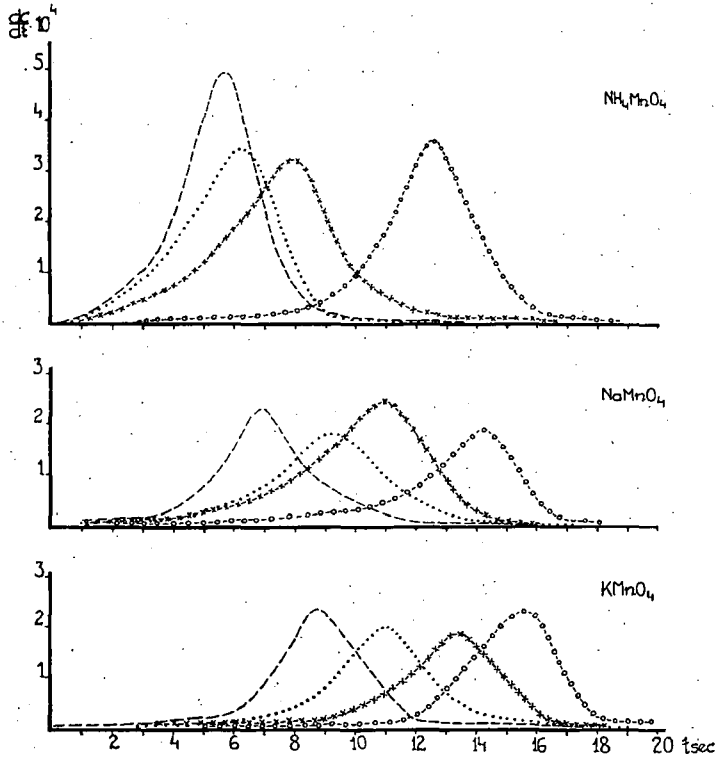

Fig. 2. p_H-Abhängigkeit der Reaktion. p_H der Grundlösung: .... 1,9; - - - -2,1; -x-x-x 2,8; -o-o-o 3,8

Um den Einfluß der Kationen zu erklären, wäre es erwünscht, die kinetischen Messungen mit verschiedenwertigen Kationen erhaltenen Permanganaten durchzuführen. Diese Messungen wurden auch geplant, doch wegen präparativen Schwierigkeiten nicht durchgeführt.

c) *Temperaturabhängigkeit*

Wir haben die Temperaturabhängigkeit der Reaktion bei verschiedenen Permanganaten mit 10^{-3} M Konzentration, in Lösungen von 1,9 p_H untersucht.

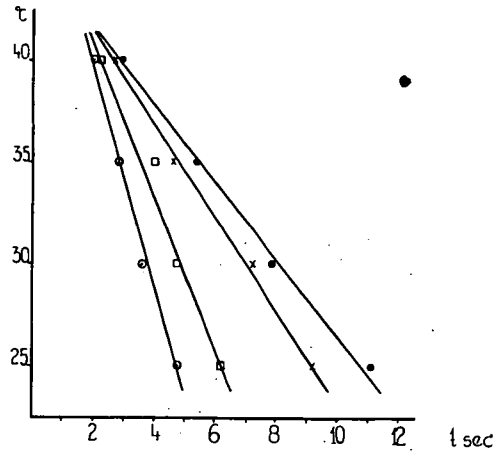

Fig. 3. Temperatureinfluß und Kationenwirkung. ·$KMnO_4$; × $NaMnO_4$; □NH_4MnO_4; ⊙$AgMnO_4$

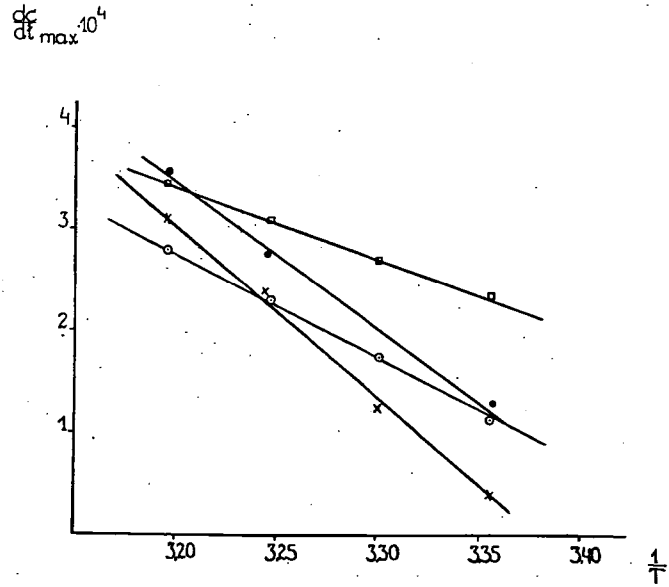

Fig. 4. · $KMNO_4$; × $NaMnO_4$; □ NH_4MnO_4; ⊙ $AgMnO_4$

Es wurde gefunden, daß die Reaktionszeit, die zum Erreichen der maximalen Reaktionsgeschwindigkeit benötigt wird, in der Kationenreihe K^+, Na^+, NH_4^+, Ag^+ bei jeder Temperatur abnimmt.

Auch das Maß des Temperatureinflußes nimmt in der oberen Kationenreihe ab. Nach den Daten der Fig. 3 ist zu erwarten, daß bei etwa 43°C dieser Unterschied der Kationenwirkung verschwinden wird.

Obwohl eine einheitliche Reaktionsordnung nicht zu erhalten war, ist die $dc/dt_{max} - 1/T$ Korrelation bei allen Kationen in guter Übereinstimmung linear (Fig. 4).

Wegen der Unsicherheit der Reaktionsordnung, und wegen des bestimmten Ganges der Reaktionskonstanten fanden wir es unbegründet, Aktivierungsenergien und andere thermodinamische Konstanten auszurechnen.

* * *

Die Verfasser sind Herrn Professor F. MÁRTA, Direktor des Instituts für Allgemeine und Physikalische Chemie der Attila-József-Universität, Szeged, für sein lebhaftes Interesse an der Arbeit zu aufrichtigem Dank verpflichtet.

Literatur

[1] *Gupta, Y. K., Ghosh, S.:* Z. phys. Chem. (Leipzig) **208**, 368 (1958); **209**, 310 (1958); **210**, 1 (1959).
[2] *Brauer, G.:* Handbuch der Präparativen Anorganischen Chemie (Stuttgart, 1954) S. 1091.

О РЕАКЦИИ ПЕРМАНГАНАТА С ОКСАЛАТОМ

Э. Хорват и М. Гечег

Исследовалась реакция $KMnO_4$, $NaMnO_4$, NH_4MnO_4, A_gMnO_4 с оксалатом, при различных температурах в растворе с переменным P_H. Хотя порядок реакции, получавшийся на основе графического изображения оказался приблизительно равным единице, используя уравнение скорости первого порядка, мы не получили приемлемых констант скорости. Было установлено что скорость реакции в значительной мере зависит от P_H среды, от температуры, а также от примененного катиона.

ИЗУЧЕНИЕ ХИМИЧЕСКИХ ПРЕВРАЩЕНИЙ ДИОЛОВ И ОРГАНИЧЕСКИХ ОКИСЕЙ. XVI

Апализ продуктов и экспериментальные данные по термический и каталитический превращений β-окисей

М. БАРТОК

Кафедра органической химии Университета им. Аттилы Йожефа, г. Сегед

(Поступило в редакцию 2-го мая, 1965)

Настоящее сообщение занимается микрореакторной техникой превращенями β-окисей и также дается анализ продуктов полученных при термическом разложении и каталитическом превращении, изученных в препаративных масштабах. Данные опытов приведены в таблицах.

1. Анализ продуктов реакции при использовании микрореактора

Идентификация продуктов реакции и расчет состава катализатов был проведен на основании полученных хроматограмм. Причем, предварительно на основании исследвания литературных данных была детально разработана методика анализа получающихся сложных смесей (подбор станциоарной жидкой фазы, параметров колонки, условий разделения, качественный анализ и количественный расчет хроматограмм).

а) *Подбор колонок*

Следует отметить, что продукты превращения β-окисей содержат, помимо насыщенных и ненасыщенных углеводородов, также алифатические карбонильные и некоторые циклические соединения, а интервал температур кипения их весьма велик. Поэтому нами была использована комбинация двух хроматографических колонок — газовой и газожидкостной и в результате первого опыта определен состав низкокипящих продуктов реакции, а в результате второго — высококипящих.

Для разделения газообразных продуктов использовалась колонка с окисью алюминия. Для анализа насыщенных и ненасыщенных углеводородов в качестве жидкой фазы применяли β,β'-оксидипропионитрил, и для кислородсодержащих соединений -трикрезилфосфат. Максимальные температуры анализов для β,β'-оксидипропионитрила и трикрезилфосфата составляли 60 и 150°, соответственно. Поэтому для анализа при высоких температурах в качестве жидкой фазы использовали апиезон *L* и силиконовое масло.

б) *Качественный анализ*

Качественный анализ был в значительной мере облегчен предварительными опытами, которые проводились для подбора колонок. Идентификацию пиков проводили при одинаковых экспериментальных условиях по эталонным веществам. В случаях отсутствия эталонов использовались литературные данные [1]. Формальдегид не идентифицировался так как в данных экспериментальных условиях он полимеризовался и оставался в колонке в виде параформальдегида.

Очень важно подчеркнуть тот экспериментальный факт, что при использовании микрореакторной техники („импульсное" включение) и Pt/T-катализатора, оказалось возможным определить присутствие промежуточных продуктов — альдегидов, ненасыщенных спиртов. Эти продукты нельзя было уловить на Pt/C катализаторах, потому что на последних, процессы протекают с большой скоростью. Непосредственная причина этого в том, что газноситель уменьшает контактное время и что Pt/C катализатор имеет меньшую активность.

В нескольких случаях нами были изучены превращения альдегидов, кетонов и ненасыщенных углеводородов в аналогичных экспериментальных условиях. Таким образом мы смогли сделать некоторые выводы об образовании вторичных продуктов. С этой же целью были изучены превращения аллильного спирта и пропанола.

В Таблице мы приводим несколько характерных физических констант и время выхода хроматографически идентифицированных продуктов термического разложения и каталитического превращения β-окисей.

Примечания к таблице

1. Вследствие применения микрореактора и расшифровки состава катализатов с помощью адсорбционной и газожидкостной хроматографии в нескольких случаях физические константы полученных соединений могли быть определены только в результате соответствующих опытов „препаративного" масштаба.

2. Продукты крекинга и изомеризации углеводородов детально не исследовались.

3. Формальдегид в изученных условиях полимеризуется.

4. В случае 2-алкилзамещенных-β-окисей расщепление, ведущее к образованию этилена, протекает лишь в незначительной степени.

5. Время удерживания вычисляли от момента ввода пробы до максимума пика.

6. Физические константы взяты из Словаря органических соединений, Москва, 1949.

7. В том случае, когда температура определения показателя преломления не приведена, она составляла 20°.

8. В том случае, когда температура определения плотности не приведена, следует читать d_4^{20}.

9. Соответствующие рисунки находятся в сообщениях серии XVII—XXVI.

Таблица

Свойства соединений, полученных при исследовании термических и каталитических превращений β-окисей

№	β-Окись	Вещества	Т. кип. °С (мм Hg)	n_D^t	d	№ стати № Рис. № пика	Удерживаемое время, мин.
1	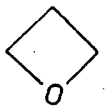	Этан	– 88,63	—	0,5719⁰	XXII/11/2	1,7
		Этилен	–105	—	0,226⁰	XXII/11/3	2,7
		Пропан	– 44,5	—	0,536⁰	—	—
		Пропиональдегид	47,5	1,3636	$0{,}79664^{25}_{25}$	—	—
		Акролеин	52	1,39975	0,8410	—	—
		Аллиловый спирт	96	1,41345	$0{,}8573^{15}$	—	—
		Пропиловый спирт	97,4	1,38499	0,8035	XXII/14/8	3,0
2	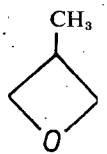	Пропан	– 44,5	—	0,536⁰	XXIII/9/2	2,4
		Пропилен	– 47,8	—	—	XXIII/9/3	3,9
		2-Метилпропан	– 10,2	—	—	XXIII/12/3	2,8
		2-Метилпропен	– 6,6	—	—	—	—
		2-Метилпропаналь	63	1,3730	0,7938	XXIII/3/1	1,5
		2-Метилаллиловый спирт	–113,8	1,4252	$0{,}8524^{20}$	XXIII/3/4	3,4
		2-Метилакролеин	– 68,4	1,4144	$0{,}837^{20}$	XXIII/3/2	1,9
3	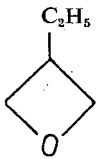	Бутан	– 0,4	—	0,60⁰	XXIII/13/2	3,0
		Бутен-1	– 6,1	—	—	—	—
		2-Метилбутан	30	$1{,}35796^{15}$	0,62007	XXIII/13/3	8,9
		2-Метилбутен-1	32	$1{,}378^{16}$	0,6668⁰		
		2-Метилбутаналь	92	1,38960	0,80294		
4	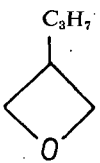	Пентан	36	1,35769	0,62632	XXIII/14/2	0,8
		Пентен-1	39	1,3711	0,6563		
		2-Метилпентан	62,3	1,3735	0,6599		
		2-Метилпентен-1	61,5	1,3921	0,6817		
		2-Метилпентаналь	119				

№	β-Окись	Вещества	Т. кип. °С (мм Hg)	n_D^t	d	№ стати № Рис. № пика	Удерживаемое время, мин.
5	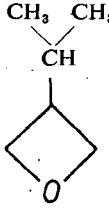	2-Метилбутан	30	$1{,}35196^{15}$	0,62007	XXIII/10/2	0,65
		3-Метилбутен-1	20,1	$1{,}3675^{16}$	$0{,}648^{0}$	XXIII/10/3	0,75
		2,3-Диметилбутан	58	1,3750	0,6612	XXIII/10/4	1,2
		2,3-Диметилбутен-1	56	1,3995	0,6803		
		2,3-Диметилбутаналь	116	$1{,}3998^{25}$	$0{,}8097^{25}$	XXIII/6/1	1,4
		2-изопропилаллиловый спирт				XXIII/6/4	2,3
6	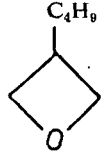	Гексан	68,95	1,37506	0,6603	XXIII/11/2	1,2
		Гексен-1	63,35	1,3870	$0{,}6734^{20}$	XXIII/11/3	1,8
		2-Метилгексан	90	1,3851	0,6789		
		2-Метилгексен-1	91,1	1,4040	0,7000		
		2-Метилгексаналь	141 (725)	$1{,}4088^{25}$		XXIII/7/1	2,5
7	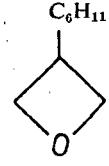	Винилциклогексан	131	$1{,}455^{19}$	$0{,}8166^{19}$		
		Этилбензол	135,5	1,49594	$0{,}8669^{4}$		
		Стирол	145	1,5462	0,9090		
		2-Циклогексилпропаналь					
8	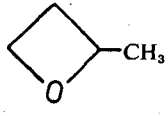	Этилен	105		$0{,}226^{0}$	XXIV/16/2′	1,0
		Пропан	−44,5		$0{,}536^{0}$	XXIV/16/3	1,7
		Пропилен	−47,8			XXIV/16/4	2,8
		Бутан	− 0,5		$0{,}60^{0}$	XXIV/16/5	5,2
		Ацетальдегид	21	1,3316	$0{,}7876^{16}$		
		Бутиральдегид	75	1,38433	$0{,}8170^{16}$	XXIV/3/2	8,5
		Метилэтилкетон	79,6	$1{,}3814^{15}$	0,8054		
		Кротиловый спирт (транс)	121	1,4289	0,8521	XXIV/3/3	13

№	β-Окись	Вещества	Т. кип. °С (мм Hg)	n_D^t	d	№ стати № Рис. № пика	Удерживаемое время, мин.
9	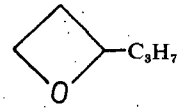	Пентан	36	1,35769	0,62632	XXIV/13/2	0,7
		Пентен-1	39	1,3711	0,6563	XXIV/13/3	1,0
		Гексан	68,95	1,37506	0,6603	XXIV/19/5	1,1
		Гексаналь	131		$0,8335^{20}$	XXIV/5/4	1,4
		Гексен-2-ол-1	159	$1,4403^{16}$	$0,8490^{16}$	XXIV/6/7	2,0
		Гексанон	123	$1,39899^{22}$	$0,81491^{22}$	XXIV/5/5	1,4
10	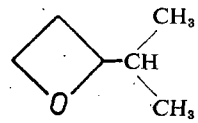	2-Метилбутан	30	$1,35796^{15}$	0,62007	XXIV/14/2	0,7
		3-Метилбутен	20,1	$1,3675^{16}$	$0,648^{0}$	XXIV/14/3	0,9
		2-Метилпентан	62,5	1,3735	0,6599	XXIV/17/5	1,1
		2-Метилпентен-3	57,7	1,38885	0,6709	XXIV/14/4	1,4
		4-Метилпентаналь	121 (743)			XXIV/9/4	7.1
		4-Метилпентен-2-ол-1	150	$1,4357^{21}$	$0,8348^{21}$		
11	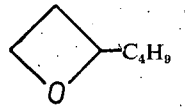	Бутан	– 0,5		$0,60^{0}$	XXIV/10/2	0,6
		Гексан	68,95	1,37506	0,6603	XXIV/15/2	1,2
		Гексен-1	63,35	1,3870	$0,6734^{20}$	XXIV/15/3	1,8
		Гептан	98,38	1,38777	0,68378	XXIV/15/4	3,5
		Гептаналь	152,4	1,4113	0,8219	XXIV/10/4	2,8
		Гептен-2-ол-1	178	1,4410	$0,8421^{10}$		
12	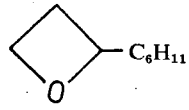	Винилциклогексан	131	$1,455^{19}$	$0,8166_4^{19}$		
		Этилбензол	135,5	1,49594	0,8669	XXIV/11/2	2,5
		Стирол	145	1,5462	0,9090	XXIV/11/3	3,9
		β-Циклогексилпропиональдегид	205	$1,4630^{24,5}$			
13	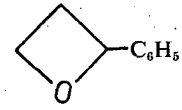	Бензол	80,4	1,50165	$0,8787_4^{15}$	XXIV/12/1	0,7
		Этилбензол	135,5	1,49594	0,8669	XXIV/12/2	2,5
		Стирол	145	1,5462	0,9090	XXIV/12/3	3,9

№	β-Окись	Вещества	Т. кип. °C (мм Hg)	n_D^t	d	№ стати № Рис. № пика	Удерживаемое время, мин.
14	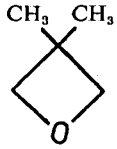	Пропан	−44,5		$0,536^0$	XXV/8/2′	1,5
		2-Метилпропан	−10,2			XXV/8/2	2,9
		2-Метилпропен-1	− 6,6			XXV/8/3	5,7
		2,2-Диметилпропан	79,4	$1,3513^0$	$0,613_0^0$		
		2,2-Диметилпропаналь	75		$0,7923^{17}$	XXV/1/4	0,8
		Метилизопропилкетон	93	$1,38788^{16}$	$0,8046^{16}$	XX/2/7	1,4
15	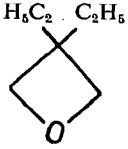	3-Метилпентан	65,2	$1,37929^{15}$	$0,6820_0^0$	XXV/6/2	0,8
		2-Этилбутен-1	67	$1,4028^{20,5}$	$0,6940^{20,5}$	XXV/6/3	1,5
		3,3-Диметилпентан	86	1,39114	0,6934	XX/3/4	1,0
		2-Метил-2-этилбутаналь				XXV/2/4	1,8
		3-Этилпентанон-2				XX/3/7	2,6
		4-Метилгексанон-3				XX/3/7	2,6
16		2-Метилпентан	62,3	1,3735	0,6599	XXV/7/2	0,8
		2-Метилпентен-1	61,5	1,3921	0,6817	XXV/7/3	1,3
		2,2-Диметилпентан	79,3	1,38233	0,6737	XX/4/4	0,8
		2,2-Диметилпентаналь				XXV/3/4	1,5
17	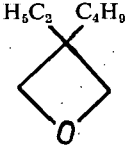	3-Метилпентан	120	1,398	0,7069		
		3-Этилгексен-1	120	1,4157	0,727	XXV/4/3	1,7
		3,3-диметилгептан	137,2	1,4087	0,7254	XX/5/4	1,8
		2-Метил-2-этилгексаналь-1				XXV/4/4	4,2
		3-Этилгептанон-2	176,9	$1,4223^{15}$	0,8246	XX/5/7	5,5
		3-Метилоктанон	182,4		0,8212	XX/5/7	5,5

18	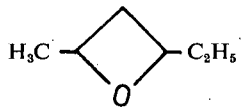	Метан	−164		$0{,}5547^{0}$	XXVI/6/2	0,4
		Этан	− 88,63		$0{,}5719^{0}$	XXVI/6/3	0,6
		Пропан	− 44,5		$0{,}536^{0}$	XXVI/6/5	1,2
		Пропен	− 47,8			XXVI/6/6	1,7
		Бутан	− 0,5		$0{,}60^{0}$	XXVI/6/7	3,2
		Бутен-1	− 6,1			XXVI/6/8	4,5
		Гексан	68,95	1,37506	0,6603	XXVI/7/9	1,2
		Гексен-1	63,34	1,3870	$0{,}6734^{20}$	XXVI/7/10	1,8
		Ацетальдегид	21	1,3316	$0{,}7876^{16}_{16}$		
		Пропиональдегид	47,5	1,3637	$0{,}79664^{25}_{25}$	XXVI/2/12	1,0
		Гексанон-2	126		$0{,}8298^{0}$	XXVI/2/14	2,4
		Гексанон-3	123	$1{,}39899^{22}$	$0{,}814914^{22}$	XXVI/2/14	2,4
19	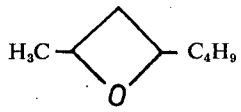	Метан	−164		$0{,}5547^{0}$	XXVI/8/2	0,4
		Пропан	− 44,5		$0{,}536^{0}$	XXVI/8/3	0,5
		Пропен	− 47,8			XXVI/8/4	0,5
		Бутан	− 0,5		$0{,}60^{0}$	XXVI/8/5	0,5
		Бутен-1	− 6,1			XXVI/8/6	0,6
		Гексан	68,75	1,37506	0,6603	XXVI/8/7	0,9
		Гексен-1	63,55	1,3870	$0{,}6734^{20}$	XXVI/8/8	1,3
		Октан	125,6	1,3975	0,7024	XXVI/8/9	2,7
		Октен-1	121,9	1,4080	0,7155	XXVI/8/10	4,0
		Ацетальдегид	21	1,3316	$0{,}7876^{16}_{16}$		
		Пентаналь	102,5	1,39436	0,80952	XXVI/3/12	1,5
		Октанон-2	173	1,41512	0,8202	XXVI/3/14	3,2
		Октанон-4	165,8			XXVI/3/14	3,2
20	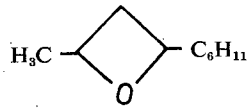	Метан	−164		$0{,}5547^{0}$		
		Пропилен	− 47,8				
		Винилциклогексан	151	$1{,}455^{19}$	$0{,}8166^{19}_{4}$		
		Этилбензол	135,5	1,49594	0,8669		
		Стирол	145	1,5462	0,9090		
		Бутилбензол	183,1	$1{,}494^{13}$	$0{,}279^{13}$		
		Ацетальдегид	21	1,3316	$0{,}7876^{16}_{16}$		
		Формилциклогексан	157	$1{,}4495^{19}$	$0{,}9263^{19}$		
		4-Фенилбутанон-2	218	1,532	$0{,}988^{20}_{20}$	XXVI/4/14	13

в) *Количественный анализ*

Количественный расчет хроматограмм проводился с помощью измерения площади и введения поправки определенной из калибровочной кривой.

В большинстве случаев превращение исходной β-окиси определялось на основании содержания этой β-окиси в катализате.

2. *Анализ катализатов, полученных на реакторе „препаративного" типа*

Жидкие катализаты, полученные на Pt/C взвешивались, сушились и перегонялись на эффективных колонках. Индивидуальные продукты идентифицировались с помощью определения физических констант, в некоторых случаях использовались методы элементарного анализа и газожидкостной хроматографии. Сырой катализат полученный при термическом разложении также взвешивался и для очистки от формальдехида несколько раз промывался раствором бисульфита натрия (большая часть образовавшегося формальдегида полимеризовалась в параформальдегид, выделявшийся в холодной части трубки реактора).

После высушивания катализат подвергался фракционированию на эффективной перегонной колонке. Олефины идентифицировались с помощью определения физических констант. В некоторых случаях были получены дибромпроизводные.

Литература

[1] *Байер, Э.:* Хроматография газов (Изд. И. Л., Москва, 1961).

STUDY OF THE CHEMICAL CHANGES OF DIOLS AND CYCLIC ETHERS. XVI

The analysis of products and experimental data of thermal and catalytic decomposition of oxetanes

By M. Bartók

The paper deals with the analysis of products formed in the thermal decomposition and catalytic changes of oxetanes studied in preparative dimensions and by microreactor-technique. Then experimental data are also tabulated.

ИЗУЧЕНИЕ ХИМИЧЕСКИХ ПРЕВРАЩЕНИЙ ДИОЛОВ И ОРГАНИЧЕСКИХ ОКИСЕЙ. XXI[1]

Исследование термического разложения 2,4-диалкил-замещённых β-окисей с применением микрореакторной техники

М. БАРТОК и К. КОВАЧ

Кафедра органической химии Университета им. Йожефа Аттилы, г. Сегед

(Поступило в редакцию 15-ого сентября, 1966 г.)

Было исследовано термическое превращение 2-метил-4-этил- и 2-метил-4-н. бутил β-окисей с использованием микрореактора, вмонтированного в газхроматограф. Скорость пиролиза последней окиси больше, чем 2-метил-4-этил-β-окиси. Эта разница связана с направлением термического распада. Главными продуктами пиролиза являются соответствующие олефины и альдегиды, которые образуются в результате обоих возможных направлений распада молекул окисей. Кроме распада наблюдалась и изомеризация в кетоны, вероятно, обусловлена влиянием стенки реактора. Первичные превращения сопровождаются различными вторичными процессами.

В изучении термического распада β-окисей раньше мы работали с 2-моно-, 3-моно- и 3,3-дизамещёнными гомологами оксациклобутана [1—3]. В этом сообщении мы хотим заниматься результатами, полученными при изучении пиролиза 2,4-диалкилзамещенных β-окисей. Термические превращения β-окисей этого типа до сих пор в литературы не описаны. Имеются лишь предположения Барбота [4], не подтвержденные экспериментально, о возможных направлениях превращения этих соединений.

Барбот, изучая термические превращения β, γ-ненасыщенных спиртов, на основании полученных продуктов предположил, что в качестве гипотеоических промежуточных продуктов могут образоваться β-окиси. Например, для гексилаллилкарбинола он предположил следующую схему:

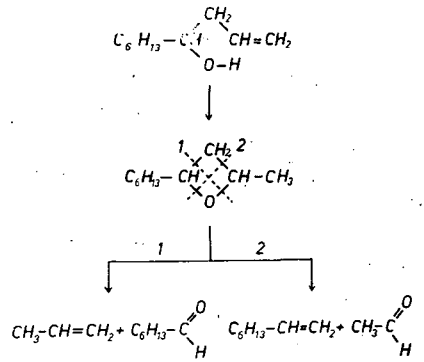

[1] Сообщение XX: Acta Chim. Hung. **52**, 83 (1967).

Из этого он сделал вывод (по нынешному мнению это не следует), что термические превращения указанных ниже структур протекают одинаково:

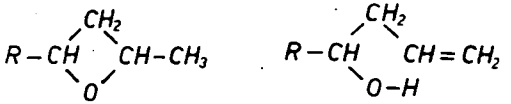

Мы изучили термические превращения из ряда 2,4-диалкилзамещенных β-окисей[2]: 2-метил-4-этил- и 2-метил-4-н. бутил- производных оксациклобутана с помощью микрореактора, уже описанного ранее [5].

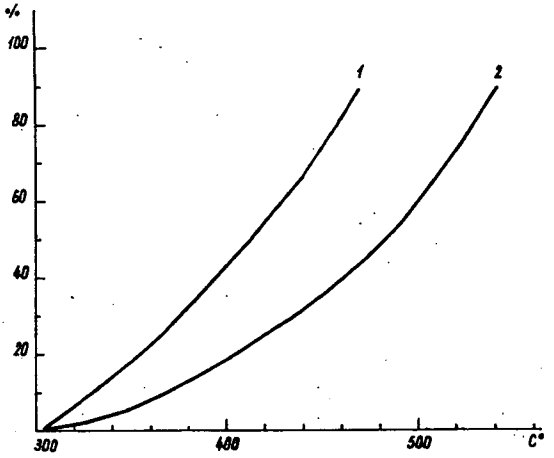

Рис. 1. Зависимость термического распада 2-метил-4-этил- (кривая 1) и 2-метил-4-н. бутилоксациклобутана (кривая 2) от температуры

На рис. 1. (см. кривую 1) представлена зависимость термического распада 2-метил-4-этил-β-окиси от температуры. Как видно из рисунка, разложение окиси начинается при 300°, причем с увеличением температуры скорость процесса увеличивается и при 480° достигается полное разложение исходной β-окиси. Пиролиз был проведен импульсным методом микрореакторной техники.

Данные хроматографического анализа позволили определить направления превращения β-окиси. На рис. 2 и 3. приведены типичные хроматограммы (1.[3] 1,1 К, 380, 480; 2. 1 АМ Al_2O_3; 3. 160; 4. 50 H_2; 5. 140; 6. 1/2; 7. 0,01), где

[2] Синтез β-окисей см. в сообщении XIV.

[3] Сокращения обозначают:

1. Количество (мл) и материал набивки микрореактора, температура опыта (°С). К: кварц (размер частиц: 0,2—0,4 мм).

2. Длина (м) и набивка или неподвижная фаза колонки, хроматографа Willy Giede GCHF 18/2. АМ — апиезоновое масло „L" 15% на термолите. 3. Температура термостата (°С). 4. Скорость (мл/мин) и качество газа-носителя. 5. Ток моста детектора (мА). 6. Чувствительность хроматографа (1 — предельное отклонение 2 мв, 1/2—4 мв и т. д.). 7. Количество пробы (мл).

пики обозначают: 1. CO, 2. метан, 3. этан, 4. этилен, 5. пропилен, 6. бутилен, 7. ацетальдегид, 8. гексен, 9. пропионовый альдегид, 10. 2-метил-4-этилоксациклобутан, 11. гексаноны-2 и -3.

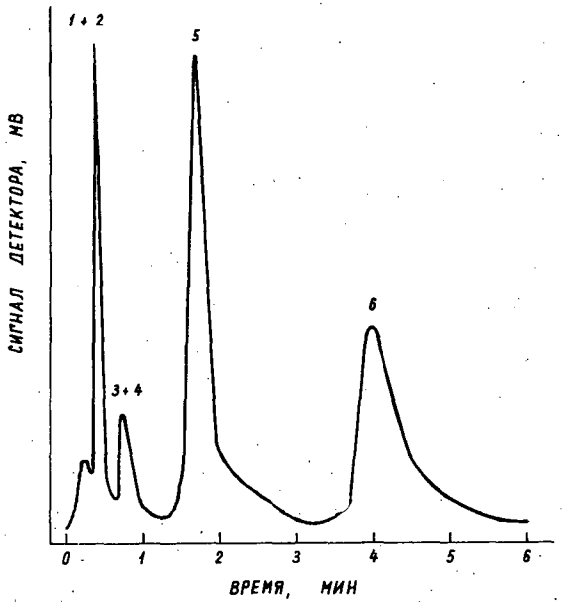

Рис. 2. Хроматограммы термического разложения 2-метил-4-этилоксациклобутана[3]

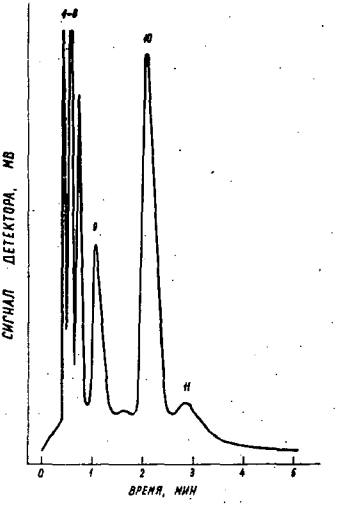

Рис. 3. Хроматограммы термического разложения 2-метил-4-этилоксациклобутана[3]

Таким образом, термический распад 2-метил-4-этилоксациклобутана можно представить следующей схемой:

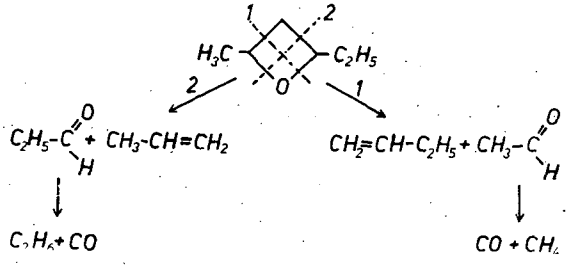

Как видно, главными направлениями пиролиза являются 1 и 2, в результате которых образуются: бутилен, ацетальдегид, пропилен и пропиональдегид. Основные процессы 1 и 2, протекают в соотношении 1:1. Изомеризация в кетоны и образование гексана и гексена, обусловлены — вероятно — влиянием стенки реактора. Как правило, первичные превращения сопровождаются вторичными процессами: при высокой температуре альдегиды декарбонилируются, происходит дегидрогенизация, изомеризация и крекинг углеводородов.

Зависимость распада 2-метил-4-бутилоксациклобутана от температуры показана на рис. 1 (кривая 2). Как видно из рисунка, разложение окиси начинается при 300°, но полное разложение достигается только при 550°. Следует указать, что разница между скоростью разложения 2-метил-4-этил- и 2-метил-4-н. бутил-β-окисей весьма значительна и отличается от других изученных β-окисей. По-видимому, помимо разницы индукционных эффектов заместителей и направлений пиролиза, большое значение имеет и различное содержание смеси стереоизомеров.

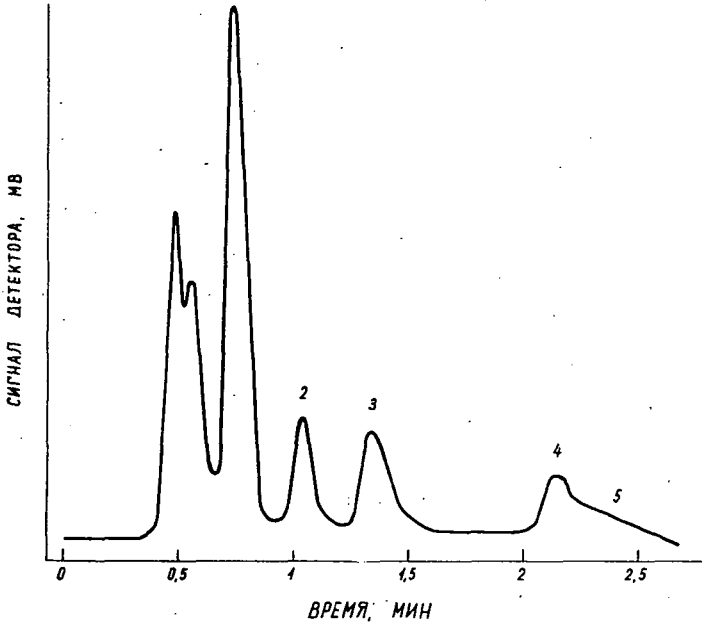

Рис. 4. Хроматограмма продуктов термического разложения 2-метил-4-н.-бутилоксациклобутана[3]

На рис. 4 приведена характерная хроматограмма термического распада 2-метил-4-н. бутилоксациклобутана (1.[3] 1,1 К, 520; 2. 1 силиконовое масло; 3. 160; 4. 50 Не; 5. 140; 6. 1/8; 7. 0,01), где пики обозначают: 1. гексен, 2. октен, 3. пентаналь, 4. 2-метил-4-н. бутилоксациклобутан, 5. октанон-2 и октанон-4.

Таким образом, направления пиролиза 2-метил-4-н. бутилоксациклобутана можно представить следующей схемой:

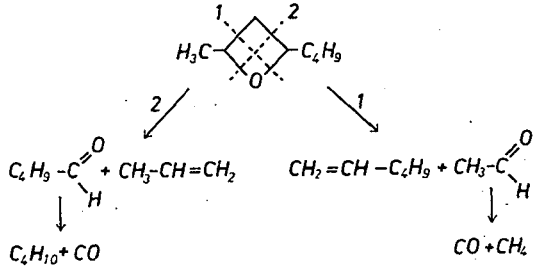

Соотношение основных процессов 1 и 2 при 500° составляет 2:1. Изомеризация, приводящая к кетону незначительна, однако она возрастает с увеличением поверхности загруженного в микрореактор кварца. Элиминирование кислорода в результате обеих C-O-связей, приводящее к образованию углеводородов с таким же числом углеродных атомов, как в исходной β-окиси, повидимому связано также с каталитическим влиянием стенок. В случаем 2-метил-4-н. бутилоксациклобутана в этом процессе образуются и углеводороды состава C_8.

Литература

[1] *Бартох, М., Б. Козма, Н. И. Шуйкин:* Изв. АН СССР, сер. хим. (в печати).
[2] *Bartók, M.:* Acta Chim. Hung. **51,** 403 (1967).
[3] *Bartók, M., B. Kozma:* Acta Chim. Hung. **52,** 83 (1967).
[4] *Barbot, A.:* Bull. Soc. chim. France **1936,** 1438.
[5] *Bartók, M., Sz. Fényi:* Acta Phys. et Chem. Szeged **12,** 157 (1966).

INVESTIGATIONS IN THE FIELD OF DIOLS AND CYCLIC ETHERS. XXI

Thermal decomposition of 2,4-dialkyloxetanes studied by microreactor technics

M. Bartók, K. Kovács

The thermal decomposition of 2-methyl-4-ethyl-oxetane and 2-methyl-4-n. butyloxetane has been studied. The apparatus consisted of a gas chromatograph connected to the microreactor. The rate of decomposition of the n. butyl derivative is higher than that of the corresponding ethyl derivative. The difference in rate is in connection with the direction of thermal decomposition. In accordance with the two possible ways of decomposition the main products of pyrolysis are the corresponding olefins and aldehydes. Besides the decomposition the formation of ketones isomer with the oxetane homologues could also be observed, probably owing to the wall-effect of the microreactor. The primary transformations are accompanied by different secondary processes.

PREPARATION OF STEREOISOMERIC 1,4-DISUBSTITUTED BUT-2-EN-1,4-DIOLS AND PROOF OF THEIR CONFIGURATION

By K. KOCZKA, P. AGÓCS and T. MEGYERI

Institute of Organic Chemistry Attila József University, Szeged

(Received November 30, 1966)

Experiments were carried out concerning the hydrogenation of 1,4-disubstituted but-2-in-1,4-diols and it was found that in the case of catalytically activated hydrogenation the rate and capability of hydrogenation, moreover the stereospecificity of the process is in connection with the space-requirement of the 1,4-substituents.

Comparative results were obtained with 10% Pd-charcoal catalyst: compound I was hydrogenated fast to yield a mixture, II took up hydrogen slowly to yield the cis.-olefin diol. Compound III could be hydrogenated very slowly and in case of less active catalyst no hydrogenation at all took place.

With $LiAlH_4$ 1,1,4,4-tetramethylbut-2-in-1,4-diol (I) gave 1, 1,4, 4,-tetramethylbutan-1,4-diol, while 1,2-bis-(1-hydroxycyclohexyl)-acetylene afforded stereospecifically cis-1,2-bis-(1-hyroxy-cyclohexyl)-ethylene.

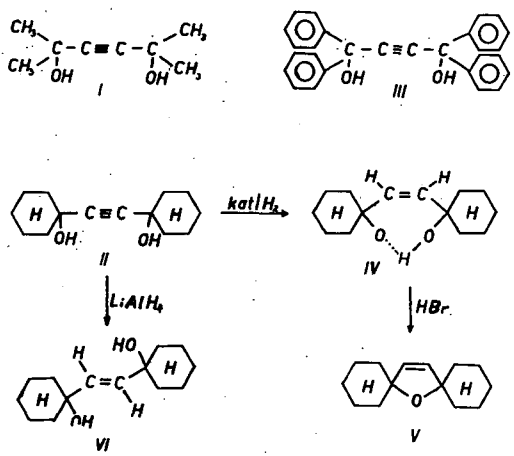

The steric structure of the geometrical isomer cis- and trans-1,2-bis-(1-hydroxycyclohexyl)-ethylene prepared in the course of our experiments was proved by means of their infrared spectra and application of BRUNI's rule.

The development of our earlier works [1a, b] necessitated the preparation of stereoisometric 1,4-disubstituted but-2-en-1,4-diols. Therefore we examined the hydrogenation of 1,1,4,4-tetramethylbut-2-in-1,4-diol (I) [2], 1,2-bis-(1-hydroxy-cycloexyl)-acetylene (II) [3], and 1,1,4,4-tetraphenylbut-2-in-1,4-diol (III) [4]. In the course of catalytic hydrogenation of similar compounds besides the two-stage saturation of the acetylenic bond multidirectional hydrogenolysis was observed

and studied in details [5]. In accordance with our purpose reduction experiments with catalitically activated hydrogen and $LiAlH_4$ were carried out.

The saturation reactions with catalitically activated hydrogen were carried out in the presence of Pd precipitated on barium sulphate [6], 10% Pd on charcoal [7], Adam catalyst [8], and Raney Ni.

No hydrogenation occurred with Pd catalyst precipitated upon $BaSO_4$ [6]. On the other hand, the experiments with Pd catalyst on charcoal carrier [7] were successful. In this case the hydrogenation was performed in the presence of 0,3% triethylamine, according to TEDESCHI [5] to minimize undesired hydrogenolysis. Instead of the expected cis-1,1,4, 4-tetramethylbut-2-en-1,4-diol the reaction yielded a mixture of cis- and trans-1,1,4, 4-tetramethylbut-2-en-1,4-diols. On the contrary, 1,2-bis-(1-hydroxycyclohexyl)-but-2-in-1,4-diol (II) afforded cis-1,2-bis-(1-hydroxycyclohexyl)-ethylene (IV) [9], the cis-structure of which was proved by its transformation to 2,5-di-spiro-dicyclohexylyden-2,5-dihydrofuran (V). A further piece of evidence concerning this result is added now by us: the infrared spectrum of the substance, taken in KBr, showed peaks at 1679 and 3200 cm^{-1}, characteristic of cis-olefin derivatives and indicating an intramolecular hydrogen bond, respectively, both supporting the cis structure of (IV).

The Bruni-rule [10], too, was applied and it was found that the compound (IV) is incapable of forming solid solution with 1,2-bis-(1-hydroxycyclohexyl)-ethane.

Under similar conditions the hydrogenation of 1,1,4, 4-tetraphenylbut-2-in-1,4-diol with Pd-charcoal catalyst proceeded only extremely slowly and the substrate was fully saturated to paraffin diol.

Attempts to obtain comparative experimental results with Adams Pt catalyst and Raney Ni failed, but our experiences indicate a decrease in the capability of hydrogenation in the order I' II and III, or rather the hydrogenation fails in case of III and a mixture is resulted from I.

Further on the preparation of 1,4-disubstituted trans-but-2-en-1,4-diols was attempted by reduction with $LiAlH_4$. Such reductions have already been studied [11] and generally the formation of the corresponding trans-isomers was observed [12]. The reduction of bis-1,2-(1-hydroxycyclohexyl)-acetylene with $LiAlH_4$ was carried out to yield a new compound (VI), m. 103—3·5°, having identical molecular formula with cis-bis-1,2-(1-hydroxycyclohexyl)-ethylene (IV), m. 153°. The steric structure of (VI) was proved by means of the Bruni-rule and infrared spectroscopy. It formed solid solution with the corresponding paraffin diol of similar structure and its infrared spectrum showed peaks at 1634 and 3380 cm^{-1}, characteristic of trans-olefin compounds and intermolecular hydrogen bonds, respectively.

The $LiAlH_4$ reduction of 1, 1,4, 4-tetramethylbut-2-in-1,4-diol was also accomplished, however, surprisingly the paraffin diol 1,1,4, 4-tetramethyl-butan-1,4-diol was yielded. In lack of comparative substance the reduction of 1, 1,4, 4-tetraphenylbut-2-in-1,4-diol with $LiAlH_4$ was not examined.

Experimental

Hydrogenation of 1,2-*bis-(*1-*hydroxycyclohexyl)-acetylene* (II) *in the presence of Pd-charcoal.*

0,02 mole 1,2-bis-(1-hydroxycyclohexyl)-acetylene (II) was hydrogenated in 60 ml. methanol-ethanol (1:1) with 0,03 g. 10% Pd-charcoal till the uptake of one

equivalent of hydrogen. The catalyst was filtered off, the filtrate was concentrated *in vacuo* and the residue crystallized from petrol ether, to yield cis-1,2-bis-(1-hydroxy-cyclohexyl)-ethylene [9], m.p. 152—153° C.

Hydrogenation of 1,1,4,4-*tetramethylbut*-2-*in*-1,4-*diol* (I) *in the presence of Pd-charcoal.*

Hydrogenation of 1,1,4,4-tetramethylbut-2-in-1,4-diol (I) under identical conditions as above yielded a product, which on basis of its infrared spectrum was a mixture. Namely, the bands characteristic of acetylene bonding were missing, but the peak characteristic of trans-olefin bond occurred together with a maximum at 1695 cm^{-1}, indicating a cis-olefin structure. The peak at 3290 cm^{-1} further indicated the inhomogeneous character of the substance.

Reduction of 1,1,4,4-*tetramethylbut*-2-*in*-1,4-*diol* (I) *and* 1,2-*bis*-(1-*hydroxycyclohexyl*)-*acetylene* (II) *with* $LiAlH_4$.

200 ml abs. ether and 3,8 g. $LiAlH_4$ were placed in a three-necked flask provided with a dropping funnel, a mechanical stirrer and a reflux condenser and the suspension was vigorously stirred for 5—6 hours. Then a solution of 0.1 mole 1,4.disubstituted but-2-in-1,4-diol (I, II) was added dropwise in 150 ml. ether, the mixture was stirred again for 4—5 hours and kept overnight. Excess $LiAlH_4$ was destroyed with 150 ml. 2N HCl, the ethereal phase was separated, dried, concentrated *in vacuo*, and the residue crystallized from carbon tetrachloride.

The reaction product of 1,1,4,4-*tetramethylbut*-2-*in*-1,4-*diol:*

1, 1,4, 4-tetramethylbutan-1,4-diol [13], m. 93—93.5°C. Anal.: Calc.: $C_8H_{18}O_2$ C 65,76 H 12,32; Found C 65,45 H 11,9. Bromine number O. According to infrared spectrum the substance contains neither acetylenic, nor olefinic double bond.

The reaction product of 1,2-*bis*-(1-*hydroxycyclohexyl*)-*acetylene:*

trans-1,2-bis-(1-hydroxycyclohexyl)-ethylene, m. 103—3.5° C (the cis-compound melts at 153° C). Anal.: Calc.: $C_{14}H_{24}O_2$ C 75,62 H 10,78; Found C 75,31 H 10,35.

Its infrared spectrum shows peaks at 1634 and 3380 cm^{-1}, characteristic of trans-olefin compounds and intermolecular hydrogen bond, respectively.

Formation of solid solution

(Application of Bruni's rule [10a, b]).

a, 1 g. cis-1,2-bis-(1-hydroxycyclohexyl)-ethylene (IV) (m.p. 153°) and 1 g. 1,2-bis-(1-hydroxycyclohexyl)-ethane (m. 128°) were dissolved in alcohol. The solution was kept overnight and the crystals deposited were collected and dried, m. 116—118 °C. Since the m.p. is depressed, no solid solution was formed.

b, 1 g. trans-1,2-bis-(1-hydroxycyclohexyl)-ethylene (VI) (m. 103 °C) and 1 g. 1,2-bis-(1-hydroxycyclohexyl)-ethane (m. 128° C) were dissolved as above. The deposited product melted at 102 °C; the absence of m. p. depression indicates solid solution formation.

The authors express their thanks to Prof. K. Kovács for his kind interest in the present work, to Dr. Kornélia L. Láng and Gizella B. Bozóki for the microanalises, to J. Szabó for the infrared spectra and to Miss Rozália Klonka for her technical assistance.

References

[1] *a) Koczka, K., G. Bernáth, A. Molnár:* Acta Chim. Hung., in print.
b) Koczka, K., P. Agócs: to be published in Acta Chim. Hung.
[2] *Bruson, H. A., J. W. Kroeger:* J. Am. Chem. Soc. **62**, 41 (1940).
[3] *Woods, G. F., L. H. Schwartzmann:* Org. Synth. **32**, 70 (1952).
[4] *Kazarian, L. Z., S. G. Avetkian:* Khim. Nauki **13**, No. 2—3, 129 (1960).
[5] *Tedeschi, R. J.:* J. Org. Chem. **27**, 2398 (1962).
[6] *Vogel, A. I.:* A Text-Book of Practical Organic Chemistry (Longmans, Green and Co. London, 1954) p. 997.
[7] Ibid. p. 996.
[8] Ibid. p. 457.
[9] *Chanley, J. D.:* J. Am. Chem. Soc. **71**, 829 (1949).
[10] *a) Bruni, G.:* Atti. R. Accad. Lincei **13**, (1) 625 (1904).
[10] *b)* Ibid.: p. 626.
[11] *Gaylord, N. G.:* Reduction with complex metal hydrides (Interscience, New York, 1956) p. 968—975.
[12] *Eliel, E. L.:* Stereochemistry of Carbon Compounds (McGraw Hill, New York, 1962) p. 346—349.
[13] *Zalkind, J. S., N. N. Visnyakov, L. Morev:* Zh. Obschch. Khim. **3**, 91 (1933).

ПРОИЗВОДСТВО СТЕРЕО-ИЗОМЕР-1,4-ЗАМЕЩЕННЫХ-БУТ-2-ЕН-1,4-ДИОЛОВ И ДОКАЗАТЕЛСЬТВО ИХ КОНФИГУРАЦИЙ

К. Коцка, П. Агоч и Т. Медери

Были сделаны эксперименты для гидрогенизации 1,4-замещенных-бут-2-ин-1,4-диолов и установлено, что при каталитически активированной гидрогенизации скорость гидрогенизации и способность к гидрорированию соединений и стереопецифичность процесса связаны с пространственным эффектом заместителей в положении 1,4.

Сравнительные данные получены на угле Pd 10%. Соединение I. при быстром гидрорировании даёт смесь. Соединение II. гидрорировая более медленно, даёт цис-олефин-диол, соединение же III. очень медленно, а при менее активном катализаторе совсем не гидрируется.

При востановлении $LiAlH_4$ было замечено, что 1,1,4,4-тетраметил-бут-2-ин гидрируется в 1,1,4,4-тетраметил-бутан-1,4-диол. А 1,2-бис-(I-гидрокси-циклогексил)-ацетилен стереоспецифично гидрируется в цис-1,2-бис (I-гидроксициклогексил)-этилен.

Пространственное строение полученных при экспериментах изомеров доказалось при помощи инфракрасной спектроскопии и применением правила Бруни.

UTILIZATION OF FURAN. V

Procedure and Apparatus for the Conversion of Furfurol to Furan by means of a Heterogeneous Catalytic Process in the Vapour Phase

By L. MÉSZÁROS and GY. SCHÖBEL

Institute of Applied Chemistry, Attila József University, Szeged

(Received November 30, 1966)

A catalytic laboratory has been developed for the oxidative decarboxylation of furfurol to furan. In contradistinction to the procedures known hitherto, the reaction was carried out in the vapour phase under oxidative conditions in the presence of the following catalysts: V_2O_5 on Al_2O_3, PbO on Al_2O_3, and PbO on aluminium grease supporter, respectively. The optimum parameters for the oxidative decarboxylation reaction have been determined.

Furan is one of the most important basic materials of modern organic chemical industry. Its utilization as basic material is made reasonable mainly by its accessibility from agricultural waste-materials and, on the other hand, by its numerous conversions to important industrial products.

All furan production procedures of industrial significance fall under either of the following two classes. Those methods belonging to the first one are characterized by catalytic decarbonylation of furfurol. The process max be illustrated by the following general equation (Equation 1):

(1)

In the processes of the second group fluoric acid intermediary product is formed, which, under the conditions applied, is unstable and decomposes to furan and carbon dioxide. In a number of cases the process takes place under reductive conditions, in hydrogen stream. These processes are characterized by the following general equation (Equation 2):

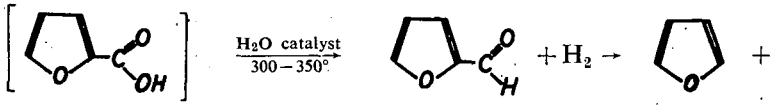

$$+CO_2 + 6{,}3\ \text{cal} \qquad (2)$$

1. *Catalytic decarbonylation of furfurol*

There are several methods known for the catalytic decarbonylation of furfurol. According to WILSON [1] the conversion may be accomplished in hydrogen atmosphere at 280—290° with nickel or cobalt catalyst. Generally, the oxides of the VIIIth

column of the periodic system proved suitable catalysts [2] under atmospheric or decreased pressure, in oxygen-free medium or in slight hydrogen stream.

According to ESCHINAZI's procedure [3] furfurol is heated in the presence of platinum catalyst and thus furan is yielded again.

A great number of catalytic furan production procedures are carried out in the presence of water vapours (steam). Among such conditions, with the simultaneous application of metal alloy catalysts at 300—500° furfural affords furan and carbon dioxide and hydrogen by-products. There are several assumptions concerning the formation of furan under the conditions given. According to the most obvious explanation the oxygen of water would oxidize the formyl group to carboxylic group and, since the process proceeds above the temperature of decarboxylation, the furoic acid decomposes to furan and carbon dioxide. The process is called decarbonylation, though the endgas contains only traces of carbon monoxide, while carbon dioxide and hydrogen are present near in stoichiometric ratio. Even the carbon monoxide traces present might be formed through the reduction of carbon dioxide [4]. According to WITHMAN's patent furan may be obtained from furfurol in 85—90% yield [4]. The catalyst applied was ZnO modified with Cs-, W-, Mo-, or V-oxides. The furfurol vapours were mixed with steam in molar ratio of 2:1—6:1 and passed through the catalyst above 200 °C. KARMILCIKS and HILLERS [5] succeeded in obtaining as high as 95% yields of furan from furfurol by passing water-furfurol 25:1 mixture through a catalyst consisting of a mixture of Al-, Cr-, Zn-, and Mn-oxides at 450°. The dilute aqueous furfural solution obtained by hydrolysis of pentosans proved a suitable starting material even without isolation of furan. However, in this case the activity of the catalyst was decreased because of the hydrocarbons deposited on its surface.

The processes catalysed by metal chromites provide lower yields. Passing furfurol and steam through Mn chromite catalyst containing K_2CrO_4 at 400° afforded only 50% yield of furan [6].

An interesting procedure is that of BÖLCS [7], who treated furfurol with hydrogen in the presence of steam at 260—280°. Simple pumice-stone was applied as catalyst. ALIEV and coworkers [8] used metal alloys for the decarbonylation of furfurol. Metal alloys exhibit a number of advantageous properties. In the first place these are easily accessible, recoverable, and they are handled more easily than metal oxide catalysts. Good results have been achieved with a catalyst containing 65.6% aluminium, 23.9% zincum, and 10.4% iron. In ALIEV's opinion [9] these processes are actually decarbonylation, to the effect that the metal catalyst forms complex with the carbonyl group and the decomposition of this complex at higher temperature results metal carbonyl and furan. The reaction of the metal carbonyl with water results in the formation of the metal and formic acid, the latter decomposing to CO_2 and H_2. The supposed mechanism of the reaction is as follows (Equation 3):

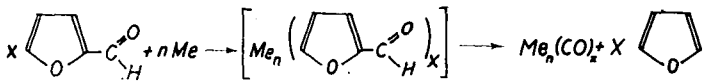

$$Me_n(CO)_z + X\,H_2O \rightarrow Me_n + X\,HCOOH$$
$$X\,HCOOH \rightarrow X\,CO_2 + X\,H_2 \qquad (3)$$

The mechanism of the decarbonylation reaction was also studied by VÁNDOR [10] in details. He stated that the decarbonylation reaction of furfurol gave only 30—40% yields of furan in the absence of steam, and the product contained mainly carbon monoxide. Since the low yield may be explained mainly by strong resinification, it seems obvious that in this case a direct decarbonylation takes place and the polymerization accompanied by resinification starts with the elimination of carbon monoxide. On the other hand, in the presence of steam 80—85% yields of furan are obtained and the end-product contains CO_2 and H_2 in equimolar amounts. The kinetic measurements of VÁNDOR have proved that the decarbonylation reaction of furfurol proceeds in the presence of excess steam approximately as a kinetically second order transformation. From this fact the conclusion may be drawn that the reaction is a Cannizzaro-type process, taking place in the vapour phase. The direct oxidation of furfurol to furoic acid followed by decarboxylation of the latter is not in accordance with the observed second order reaction, since furoic acid decarboxylates fairly fast and the partial pressure of water vapour is constant, as it may be expected at the Cannizzaro reaction. The authors wish to mention that the yields given in the literature could not be reproduced.

2. *Oxidative catalytic decarboxylation of furfurol*

The preparation of furan on a laboratory scale is carried out generally in the liquid phase through furoic acid. The procedure is based on the fact that furfurol transforms to 2-furoic acid in 90—95% yield in the presence of a catalyst consisting of NaOH, CuO, and some Ag_2O. 2-Furoic acid decarboxylates in quinoline in the presence of CuO catalyst in 70% yield [11]. The transformation of furfurol to 2-furoic acid proceeds also in the presence of other oxidizing agents. Thus, for instance, with H_2O_2 the reaction affords good yields [12]. There are also a number of procedures known for the decarboxylation process, to be carried out on a laboratory scale [13].

Contrary to the procedures known hitherto, the authors accomplished the production of furan from furfurol in the vapour phase under oxidative conditions [14]. The idea was taken from the investigations of MILAS and WALSH [15], who oxidized furfurol with the oxygen of air (with extremely high excess of oxygen) over V_2O_5 catalyst, to obtain maleic anhydride in good yields (Equation 4):

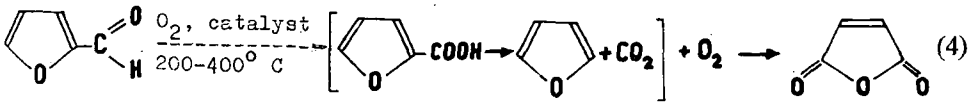

(4)

On basis of this result we concluded that as far as the process proceeds through furan, according to the mechanism described by the above authors [15], the selection of a suitable catalyst and reaction conditions would permit the elimination of further oxidation of furan. Accordingly furfurol was subjected to oxidative decaboxylation with air or oxygen; the reaction could be achieved without any significarnt over-

oxidation. The reaction carried out and studied in details by us is illustrated by Equation 5:

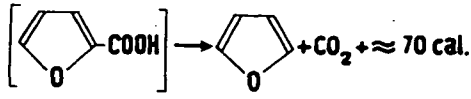

(5)

Comparison of the reaction heats of the processes represented by Equations 2 and 3 reveals that the reaction heat of the oxidative decarboxylation process carried out by us significantly higher than that of the preceeding reaction. Because of the high reaction heat a number of reactors of novel type have been developed by us for the effectuation of these reactions [16].

Experimental

I. Catalytic laboratory for the accomplishment of oxidative decarboxylation of furfural

The experiences of a number of apparatus have helped us in developing the present form of our vapour phase, heterogeneous catalytic laboratory.

Iron, glass and quartz reactors have been employed for carrying out the reaction. Iron reactors have the disadvantage that the catalytic effect of the reactor-wall can not be avoided. To eliminate wall-effects glass and quartz reactors were used. The drawback of such reactors lies in the low heat conductivity of the wall, moreover the inaccurate fitting of the heating block caused strong local over-heatings, resulting in resinification of the starting material.

In catalytic oxidation reactions, among the structural materials coming into consideration nickel has the least pronounced undesired catalytic effect, therefore the reactor (18) of our apparatus to be described later (Fig. 1) was made of nickel. The temperature and heating of the reactor was controlled according to the five temperature-zones of the reactor by devices and switches placed on an electric instrumentboard. On this electric instrument-board the electric heat-characteristics of the reactor-sectors could be read off. The temperature of the heating sectors of the reactor were controlled by means of phototransistoric temperature-regulators and thus the temperature of the reactor-wall was kept at the desired value. This value was measured with bent, L-shaped, nitrogen-pressure mercury thermometers and recorded in six different colours.

Fig. 1. Flow sheet of the catalytic laboratory

1. Steel distillation flask, *2.* Ground glass distillation headpiece, *3.* Thermometer, 20—200 °C, *4.* Bulb condenser, *5.* Spherical ground joint clamp, *6.* Three-finger flask-holder, *7.* Double clamp-nut, *8.* Receiver, *9.* Ground joint holder, *10.* Holding ring, *11.* Feeding pump, *12.* Pipe trundle stand, *13.* Separating funnels, *14.* Burettes, *15.* Illuminator, *16.* Y-shaped glass connection tubes, *17.* Capillary pipe systems, *18.* Reactor, *19.* Pneumatic stabilized reductor, *20.* Rotameter, *21.* Phototransistoric pressure gauge, *22.* Pneumatic reductor, *23.* Fine feeder, *24.* Differential manometer, *25.* Glass T-tube, *26.* U-tube manometer, *27.* Thermostat for thermoelements, *28.* Metal Liebig-condenser, *29.* Coil and bulb condenser, *30.* Distributing cock-system with water jackets, *31.* Carbon columns, *32.* Gas meter, *33.* Evaporator, *34.* Combined cooler, *35.* Cooling walls.

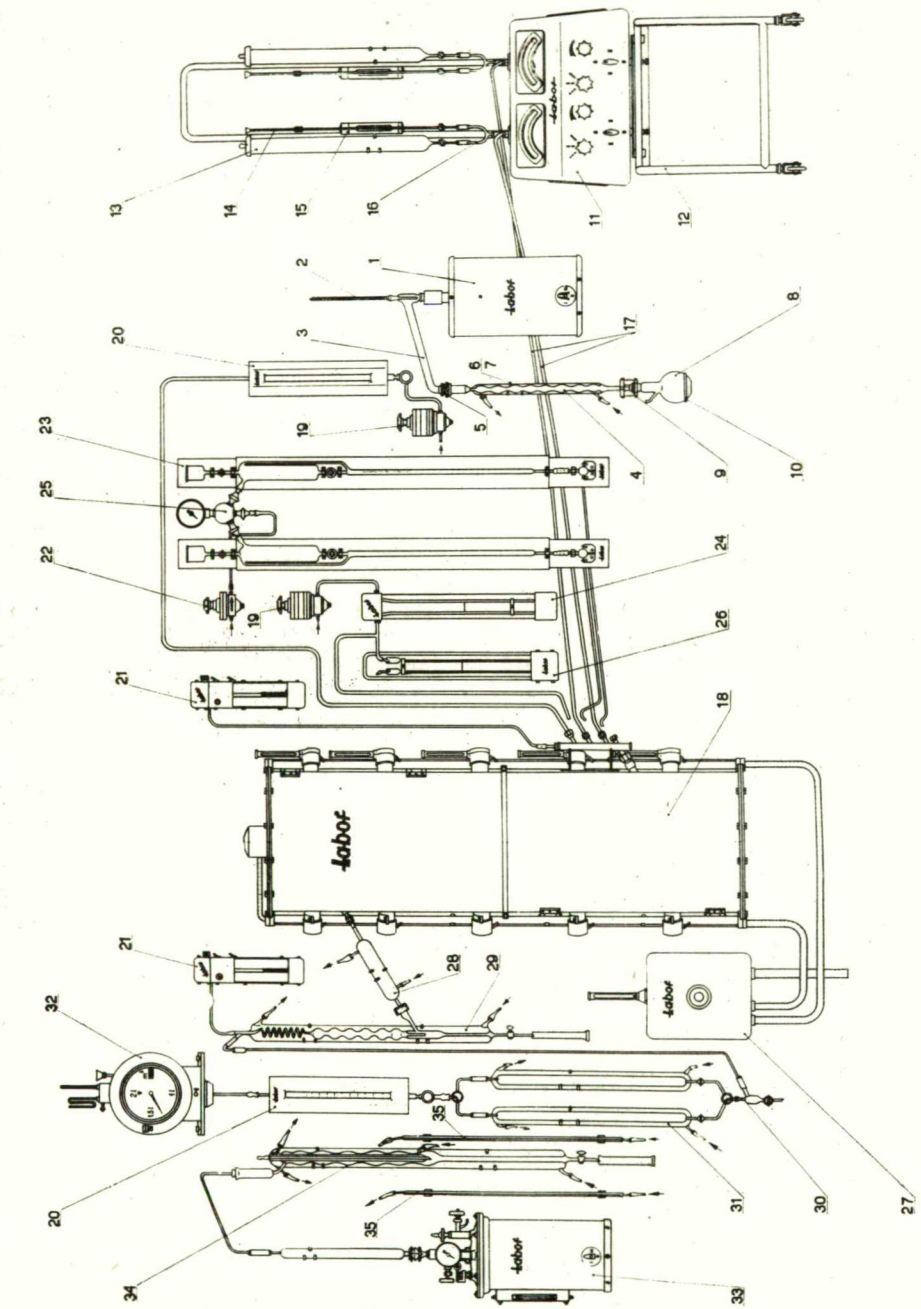
labor
1
2
3
4
5
6
7
8
9
10
11
12
13
14
15
16
17
18
19
20
21
22
23
24
25
26
27
28
29
30
31
32
33
34
35

The temperature in the axis of the reactor tube was measured with a three-fitting thermocouple and a connected millivoltmeter scaled in °C.

The freshly distilled furfural is introduced through the fine-dosing burette (23), the air through the stabilizing gauge (19) and differential manometer (24) into Sector I of the reactor. From the evaporator the reaction mixture enters catalyst-spaces II, III and IV. The reaction takes place here upon the contact surface and the vapours pass pre-cooler zone V and Liebig-cooler (28). The unreacted material condenses in the cooler and its amount can be read off in the lower part of the combined cooler-burette (29), wherefrom it can be let out through the tap to distill again for the next experiment. The uncondensed vapours and gases pass the bulb and coil condensers and reach the distributor head (30), from where in case of suitable tap-position they come to the carbon column (31). Furan is adsorbed here, while all the rest of the mixture goes further through rotameter (20) and gas-meter (32) to the exhausting equipment.

Desorption of furan is made with steam after saturation. The desorbed furan is collected in the furan-burette (34), where its volume, too, may be measured.

When larger amounts of fluid reaction-components are introduced, a motoric pump (11) is employed.

Experiments for the conversion of furfurol to furan

The oxidation of furfurol was carried out in the presence of the following catalysts: V_2O_5 on Al_2O_3, PbO on Al_2O_3, and PbO on aluminium grease, respectively. The temperature dependance of the reactions taking place on the above catalysts has been studied and expressed in yields and utilizations.

The definitions of the measure of value factors employed in our experiments are the following:

$$Te = \frac{\text{rate of feed of furfurol in ml/sec}}{\text{catalyst volume in liters}}$$

$$I = \frac{1}{\text{Te}}$$

$$A\% = \frac{\text{moles of furfurol converted}}{\text{moles of furfurol introduced}} \cdot 100$$

$$T\% = \frac{\text{moles of furan formed}}{\text{moles of furfurol introduced}} \cdot 100$$

$$K\% = \frac{\text{moles of furan formed}}{\text{moles of furfurol converted}} \cdot 100$$

a) Catalyst : V_2O_5 on Al_2O_3 (oxidation catalyst of the Hungarian Chemical Works)

Molar ratio of oxygen and furfurol:	2:1
Catalyst volume:	278 ml (V_2O_5)
Te (space velocity):	0,075 sec^{-1}
I (contact time):	13,0 sec
Temperature:	$a_1 = 250°$
	$a_2 = 300°$
	$a_3 = 350°$
	$a_4 = 400°$

	Temperature °C	A_{av}. %	T_{av} %	K_{av} %
a_1	250	22,6	—	—
a_2	300	30,8	0,55	1,8
a_3	350	54,8	15,2	27,4
a_4	400	68,1	2,4	3,5

b) Catalyst: PbO on Al_2O_3
Molar ratio of oxygen and furfurol: 2:1
Catalyst volume: 350 ml
Te (space velocity): 0,072 sec^{-1}
I (contact time): 13,8 sec
Temperature: $b_1=225°$
$b_2=250°$
$b_3=280°$
$b_4=300°$

	Temperature °C	A_{av} %	T_{av} %	K_{av} %
b_1	225	52,2	14,3	27,4
b_2	250	57,7	21,0	35,5
b_3	280	71,7	18,3	26,7
b_4	300	84,4	18,1	21,7

c) Catalyst: PbO on aluminium grease
Molar ratio of oxygen and furfurol: 1:0,8
Catalyst volume: 447 ml
Te (space velocity): 0,057 sec^{-1}
I (contact time): 17,6 sec
Temperature: $c_1=225°$
$c_2=250°$
$c_3=275°$
$c_4=285°$

	Temperature °C	A_{av} %	T_{av} %	K_{av} %
c_1	225	89,9	17,9	20,1
c_2	250	87,3	19,0	21,8
c_3	275	94,3	29,0	30,6
c_4	285	87,7	11,2	14,5

Preparation of the catalysts applied

a) V_2O_5 on Al_2O_3 supporter: the oxidation catalyst of the Hungarian Chemical Works

b) PbO on Al_2O_3 supporter: metal Al is dissolved in 50% NaOH solution and filtered to remove solid contaminations. A slow flow of CO_2 is passed through the solution at 80—90 °C, when crystalline $Al(OH)_3$ precipitates, which is then washed by decantation. The decanted product is mixed with 50(v)% minium to a homogeneous dough and partially dried. The obtained clay-like mass is passed through a hole of 3 mm. diameter and kept at room temperature until air-dry. The long rods are broken to pieces of 3—5 mm. length, dried with infra-lamp for

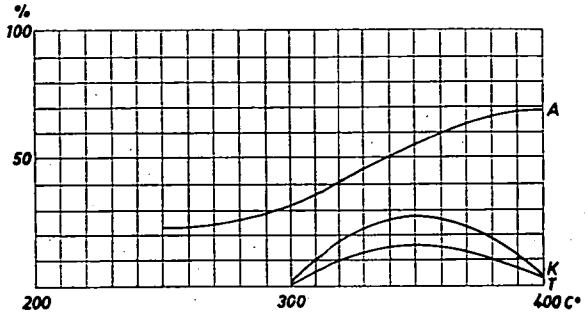

Fig. 2. Conversion of furfurol to furan. Temperature dependence of the measure of value factors. (V_2O_5 catalyst)

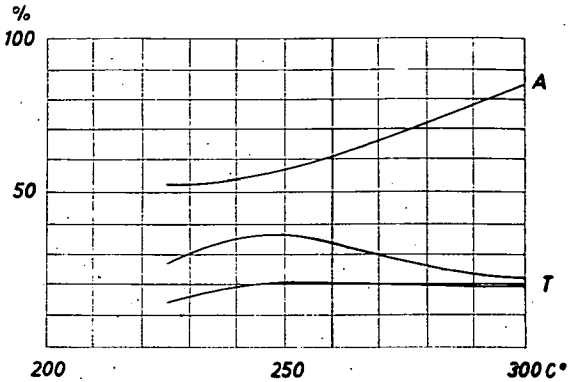

Fig. 3. Conversion of furfurol to furan. Temperature dependence of the measure of value factors. (PbO on Al_2O_3 catalyst)

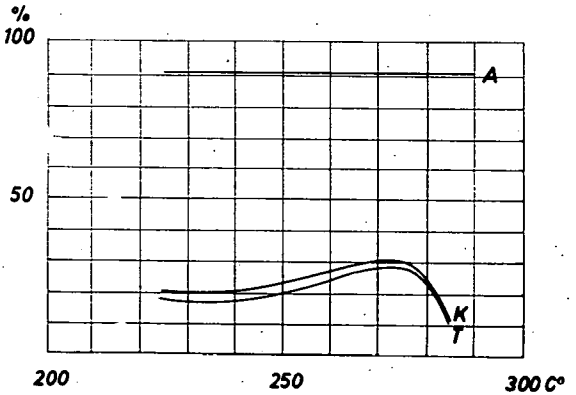

Fig. 4. Conversion of furfurol to furan. Temperature dependence of the measure of value factors. (PbO on aluminium grease catalyst)

5—6 hours, gradually heated at 350—450°, and kept at this temperature for 6 hours, the heating being repeated at 350—450° for a further 6 hours.

c) PbO on aluminium grease supporter: $Al(OH)_3$ is prepared as described above. The decanted product is mixed with 80(w)parts minium, the mixture is diluted with 20 parts water and shaken in a bolter for 30 minutes. Then aluminium grease is added, as to the suspension floods it and the whole is vigorously shaken for 1 hour again. After decantation the covered aluminium grease is dried with infra-lamp to air-dry and then gradually heated to 500—600 °C.

References

[1] *a) Wilson, Ch. L.:* J. Chem. Soc. **1945**, 61.
b) Wilson, Ch. L.: Brit. Pat. 553, 175, May 11, 1943; Chem. Abstr., **38**, 4963² (1944).
[2] *Codignola, F., M. Piacenza:* Ital. Pat. 421, 626, May 28, 1947; Chem. Abstr. **43**, 5047 g (1949).
[3] *Eschinazi, H. E.:* Bull. Soc. Chim. France **1952**, 967.
[4] *Whitman, G. M.:* U. S. Pat. 2, 374, 149, April 17, 1945; Chem. Abstr. **40**, 366 (1946).
[5] *a) Karmilciks, A., S. Hillers:* Trudy Inst. Lesokhoz., Problem, Akad. Nauk Litv. SSR., Voprosy Lesokhim. i Khim. Drevesiny **12**, 251 (1957); Chem. Abstr. **52**, 20773b (1958).
b) Karmilciks, A. Ya., S. Hillers: Voprosy Ispol'zovan. Pentozansoderzhaschego Syr'ya. Trudy Vsesoyuz. Soveshchaniya, Riga, **1955**, 327; Chem. Abstr. **53**, 15037a (1959).
[6] *Tyran, L. W.:* U. S. Pat. 2, 277, 981, Jan. 8, 1957; Chem. Abstr. **51**, 8143 e (1957).
[7] *Bölcs, Gy.:* Hung. Pat. 132, 763, May 16, 1944; Chem. Abstr. **43**, 4301i (1949).
[8] *a) Aliev, Ya. Yu., A. S. Sultanov:* Khim. Khlopchatnika, Akad. Nauk Uzbek. SSR **1959**, 105; Inst. Khim. Rastitel. Veshchestv **1959**, 105; Chem. Abstr. **55**, 12382a (1961).
b) Knunyants, I. L., A. S. Sultanov, Ya. Yu. Aliev: U.S.S.R. Patent 108, 708, Nov. 25, 1957; Chem. Abstr. **52**, 11945d (1958).
[9] *Aliev, Ya. Yu.:* Voprosy Ispol'zovan. Pentozansoderzhashchego Ser'ya, Trudy Vsesoyuz. Soveshcheniya, Riga, **1955**, 309; Chem. Abstr. **53**, 14077a (1959).
[10] *Vándor, J.:* Acta Chim. Acad. Sci. Hung. **3**, 169 (1953).
[11] *Narasaki, H., N. Ito:* Repts., Govt. Chem. Ind. Research Inst. Tokyo **46**, 199 (1951); Chem. Abstr. **46**, 4524b (1952).
[12] *Andrisano, R.:* Boll. Sci. facolta chim. ind. Bologna **7**, 66 (1949); Chem. Abstr. **44**, 9404h (1950).
[13] *Taniyama, M.:* Jap. Pat. 5679 ('53), Nov. 2.; Chem. Abstr. **49**, 8333 (1955).
[14] *a) Mészáros, L., Fodor, G.:* Lecture. Jubilarian Congress of the Hungarian Chemical Society, Budapest, May 15, 1958.
b) Mészáros, L., Fodor, G.: Hung. Pat. 146, 868, Oct. 4, 1959.
c) Mészáros, L.: Acta Phys. et Chem. Szeged, **6**, 97 (1960); Chem. Abstr. **55**, 25905a (1961).
[15] *Milas, N. A., W. L. Walsh:* J. Amer. Chem. Soc. **57**, 1389 (1935).
[16] *a) Mészáros, L.:* Lecture held at the D. I. Mendeléeff Technical University, Moscow, Sept. 22, 1960.
b) Mészáros, L.: Lecture. Series of lectures of the Hungarian Industrial Fair. Moscow, Aug. 29, 1960.
c) 'Labor' 3621 type apparatus for furan production. Foreign Trade Technical Information Circular (In Russian) Metrimpex, Budapest, 1960.
d) Vapour phase continuous Catalytic Laboratory. Foreign Trade Information Material (32 pages, in Russian) Metrimpex, Budapest, 1959.
[17] *Mészáros, L.:* Acta Phys. et Chem. Szeged, **8**, Supplementum I. Complete Catalytic Laboratories. Vol. I. Part I. Process and Equipment for the Production of Furan from Furfural by a Vapour-Phase Heterogeneous Catalytic Method. (300 pages, in English, Russian, German and Hungarian languages, Part 2. Apparatus informative (270 pages).

ПРИМЕНЕНИЕ ФУРФУРОЛА. V

Способ и аппаратура для получения фурана из фурфурола с парофазным гетерогенным каталитическим методом

Л. Месарош, Г. Шобэл

Разработана каталитическая лаборатория для получения фурана, методом окисьлительного декарбоксилирования фурфурола. В отличие от до сих пор известных методов реакция проводилась в окислительных условиях на катализаторах V_2O_5/Al_2O_3, PbO/Al_2O_3, PbO/Al. Установлены оптимальные экспериментальные параметры реакции.

ÜBER EINIGE KOLLOIDCHEMISCHEN EIGENSCHAFTEN VON UNGARISCHEN BENTONITEN. I

Peptisierbarkeit und Fraktionierung

Von F. SZÁNTÓ, B. VÁRKONYI, M. GILDE und J. BALÁZS
Institut für Kolloidchemie der Attila-József-Universität, Szeged

(Eingegangen Dezember 1, 1966)

Aus verschiedenen Fundstätten (Mád-Koldu, Istenmezeje, Nagytétény) stammende ungarische Bentonite wurden nach Aktivierung mit Soda durch Sedimentierung und Zentrifugieren in Fraktionen zerlegt. Dann wurde die Untersuchung der mengenmäßigen Verteilung und mineralischen Zusammensetzung dieser Fraktionen durchgeführt. Auf Grund dieser Untersuchungen folgerten wir auf die Peptisierbarkeit der verschiedenen ungarischen Bentonite und der aus diesen gewonnenen Montmorillonite.

Einleitung

Bekanntlich bildet der Montmorillonit das wichtigste Mineral der natürlichen Bentonite, sie enthalten jedoch außer diesem häufig in ansehnlichen Mengen auch andere Tonmineralien (wie Kaolinit und Illit) sowie weitere Beimineralien (z.B. Quarz, Kristobalit, Feldspat, Kalzit etc.). Da für bestimmte praktische Zwecke, so z.B. zur Herstellung von organophylen Bentoniten guter Qualität nur der Montmorillonit in Betracht kommen kann, müssen die Beimineralien von diesem nach Möglichkeit abgetrennt werden. Als ungarische Bentonitvorkommnisse gibt es vorwiegend Ca-Bentonite, zu deren Fraktionierung jedoch allein in dem Fall Möglichkeit besteht, wenn sie vorerst mit Natriumkarbonat in eine gut peptisierbare Na-Bentonit-Form übergeführt werden. Auf diese Weise kann man nämlich sonstige Ton- und Beimineralien mehr oder weniger vollständig vom Montmorillonit sondern [1—3].

In diesem Zusammenhang taucht die Frage auf, wie sich die peptisierte Menge, die Verteilung und Zusammensetzung der Fraktionen, vor allem aber die abgetrennte Montmorillonitmenge bei Variierung der Menge des Natriumkarbonat-Zusatzes gestaltet. Obgleich diese Frage sowohl in theoretischer als auch in praktischer Hinsicht zu Interesse kommt, wurden in dieser Beziehung wenig systematische Untersuchungen durchgeführt.

In der vorliegenden Arbeit soll über einen Teil unserer Ergebnisse im Zusammenhang mit der Peptisation und Fraktionierung der wichtigsten ungarischen Bentonite Bericht erstattet werden.

Tabelle I
Mineralische Zusammensetzung der untersuchten Bentonite %

Mineral	Bentonit von		
	Istenmezeje	Mád-Koldu	Nagytétény
Montmorillonit	75,0	53,6	90,0
Illit	2,9	1,7	9,0
Kaolinit	—	8,3	—
Quarz	2,3	29,1	1,0
Kristobalit	13,3	—	—
Kalzit	6,5	—	—
Sanidin	—	7,3	—
Insgesamt	100,0	100,0	100,0

Versuchsmaterialien und Methoden

Die Versuche wurden an den Bentoniten von Istenmezeje (creme), Mád-Koldu und Nagytétény vorgenommen. Tabelle I gibt ihre durch Röntgenanalyse ermittelte mineralische Zusammensetzung wieder[1].

1. *Die Aktivierung der Ca-Bentonite*

Die ursprüngliche rohe Bentonite wurden bei Zimmertemperatur getrocknet, in der Kugelmühle vermahlen und durch eine Siebe DIN 30 durchgelassen. Die Bestimmung des Feuchtigkeitsgehalts geschah nach 5 stündiger Trocknung im Trockenschrank bei 110 °C Temperatur. Danach erfolgte mit je 200 ml Wasser die Verrührung bis zu homogener Massenkonsistenz der Bentonite von je 100 g Trockenstoffgehalt. Zu diesen Breien wurde unter weiterem ständigen Rühren in Form 5%-iger wäßriger Lösung soviel Natriumkarbonat hinzugegeben, daß die Proben auf das Trockensubstanz bezogen 2 bis 8% Natriumkarbonat enthalten sollten. Die zu Gelen erstarrten Systeme wurden mit dest. Wasser auf je 500 ml ergänzt, mehrmals umgerührt und einen Tag lang ruhen gelassen, danach auf dem Wasserbad eingedampft, vermahlen und wie oben gesiebelt.

2. *Die Fraktionierung der Na-Bentonite*

Es wurden von den Bentoniten verschiedenen Natriumkarbonatgehalts 1%-ige wäßrige Suspensionen dargestellt; die Dosierung der Na-Bentonite in dest. Wasser erfolgte in kleinen Zusatzmengen unter ständigem Rühren der Systeme mit einem Vibromischer. Dann wurden die Suspensionen nach eintägigem Stehenlassen zwei Stunden lang in der Vibrationsmaschine geschüttelt und in großen Flaschen sedimentiert.

Die sechstägige Sedimentation der Suspensionen geschah bei einer Sedimentationshöhe von 25 cm. Diese Sedimente (grobe Fraktionen III) setzen sich überwiegend aus Teilchen mit einem Aequivalentradius von $>0{,}4$ µm zusammen. Die weitere Zerlegung der übergebliebenen Suspensionen in zwei Fraktionen verschiedenen Dispersitätsgrades wurde mit einer Superzentrifuge Type FS—45 durchgeführt. Die bei einer Durchflußgeschwindigkeit von 400 ml/Min und einer Umlaufgeschwindigkeit von 30 000 Umdreh./Min abzentrifugierten Bestandteile lieferten die mittleren Fraktionen (II) mit Teilchen von 150 bis 400 nm Radiengrößen; die feinen Fraktionen (I) bestanden aus den durchgegangenen Solteilchen mit Radien von weniger als 150 nm.

[1] Die Analysen wurden von I. NÁRAY-SZABÓ und Frau ÉVA PÉTER nach ihrer neuerdings entwickelten Methode [4] durchgeführt, wofür wir ihnen unseren aufrichtigen Dank aussprechen.

Tabelle II
Bentonit von Istenmezeje

Natrium-karbonat-menge %	Fraktionsmenge %		
	I.	II.	III.
2	30	22	48
3	57	16	27
5	55	19	26
6	46	20	34
7	45	21	34
8	42	24	34

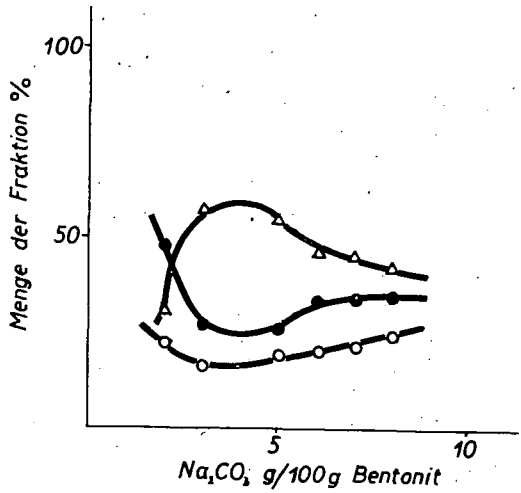

Fig. 1. Verteilung der Fraktionen des Bentonits von Istenmezeje in Abhängigkeit der Natriumkarbonatmenge
△ Feine (I) Fraktion
○ Mittlere (II) Fraktion
● Grobe (III) Fraktion

Tabelle III
Bentonit von Mád-Koldu

Natrium-karbonat-menge %	Fraktionsmenge %		
	I.	II.	III.
2	31	15	54
3	33	21	46
4	35	25	40
5	39	29	32
6	40	32	28
7	40	32	28
8	35	27	38

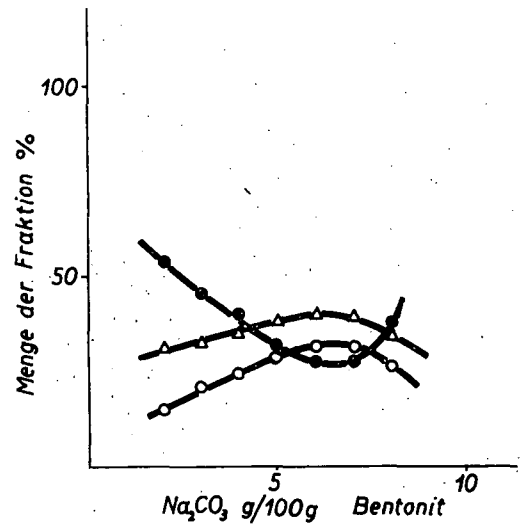

Fig. 2. Verteilung der Fraktionen des Bentonits von Mád-Koldu in Abhängigkeit der Natriumkarbonatmenge
△ Feine (I) Fraktion
○ Mittlere (II) Fraktion
● Grobe (III) Fraktion

Versuchsergebnisse

Die Tabellen II—IV sowie die Abbildungen 1—3 veranschaulichen die mengenmäßige Verteilung der Fraktionen I—III verschiedenen Dispersitätsgrades. Es geht aus diesen Abbildungen hervor, daß sich die Menge der Fraktionen nach Maximum-bzw. Minimumkurven mit der Natriumkarbonatmenge verändert. Bei allen drei untersuchten Bentoniten decken sich die Maxima der mittleren Fraktionen mit den Minima der groben Fraktionen.

Tabelle IV
Bentonit von Nagytétény

Natrium-karbonat-menge %	Fraktionsmenge %		
	I.	II.	III.
2	13	12	75
3	45	15	40
4	52	16	32
5	50	29	21
6	50	33	17
7	46	31	23
8	24	23	53

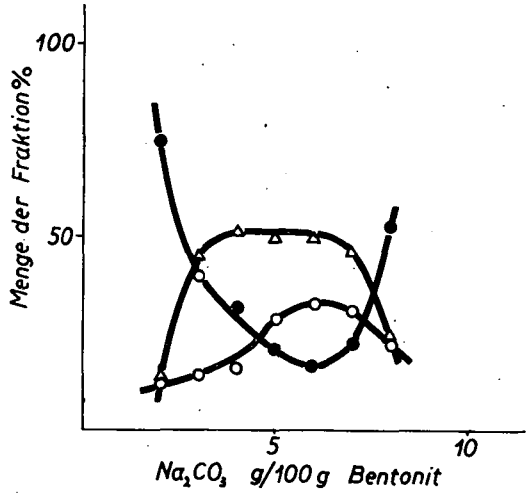

Fig. 3. Verteilung der Fraktionen des Bentonits von Nagytétény in Abhängigkeit der Natriumkarbonatmenge
△ Feine (I) Fraktion
○ Mittlere (II) Fraktion
● Grobe (III) Fraktion

Tabelle V zeigt die Ergebnisse der Röntgenanalysen von Bentonitfraktionen, die mit 5 prozentigen — in der Praxis am besten bewährten — Natriumkarbonatmenge peptisiert wurden[2]. Demnach bestehen die feinen Fraktionen praktisch aus reinem Montmorillonit, obgleich es für die Bentonite aus Istenmezeje charakteristisch ist, daß auch die kolloide Fraktion bedeutende Mengen an Kristobalit enthaltet. Die Hauptmenge des Montmorillonits läßt sich also — wie aus Tabelle VI hervorgeht — durch einmalige Behandlung mit Soda in den Solzustand überführen, allein gibt einen Teil des Montmorillonits, der sich mit dieser Methode nicht peptisieren läßt.

[2] Siehe Fußnote 1.

Tabelle V
Mineralische Zusammensetzung der Fraktionen %

Mineral	Bentonit von								
	Istenmezeje			Mád-Koldu			Nagytétény		
	I.	II.	III.	I.	II.	III.	I.	II.	III.
Montmorillonit	86,7	78,1	48,2	100	32,2	16,4	100	96,5	57,0
Illit	—	3,3	8,8	—	—	5,2	—	3,5	38,0
Kaolinit	—	—	—	—	22,4	5,6	—	—	—
Quarz	—	1,0	8,0	—	36,9	57,6	—	—	5,0
Kristobalit	10,6	17,6	16,0	—	—	—	—	—	—
Kalzit	2,7	—	14,0	—	—	—	—	—	—
Sanidin	—	—	—	—	8,5	15,2	—	—	—
Insgesamt	100	100	100	100	100	100	100	100	100

Tabelle VI
Die Verteilung des Montmorillonits in den Fraktionen

Fundort	Montmorillonitgehalt in Prozent	Montmorillonitgehalt der					
		Fraktion I		Fraktion II		Fraktion III	
		in Prozent des Ausgangsmaterials	in Prozent des Gesamtmontmorillonits	in Prozent des Ausgangsmaterials	in Prozent des Gesamtmontmorillonits	in Prozent des Ausgangsmaterials	in Prozent des Gesamtmontmorillonits
Istenmezeje	75,0	47,7	63,6	14,8	19,7	12,5	16,7
Mád-Koldu	53,6	39,0	72,8	9,3	17,4	5,3	9,8
Nagytétény	90,0	50,0	55,6	28,0	31,1	12,0	13,3

Bewertung der Versuchsergebnisse

In den natürlichen Erdalkali-Bentoniten finden sich die Teilchen verschiedenartiger mineralischer Zusammensetzung in aggregiertem Zustand vor. Um die groben Tonmineralien und ihre Beimineralien trennen zu können und zur Peptisierung des Montmorillonits benötigt man den Natriumkarbonat in optimalen Mengen [1, 2]. Bei Erhöhung derselben vergrößert sich nämlich vorerst das Ausmass der Desaggregierung und Peptisierung, um nach Erreichung eines Maximums wieder abzunehmen. Nach BUZÁGH und SZEPESI [1] sowie WEBLUS [5] findet dies seine Erklärung in der koagulierenden Wirkung des im Überschuß angewendeten Peptisators. Bei mittleren und feinen Fraktionen kann dieser Umkehrpunkt auf Einwirkung verschiedener Elektrolitmengen in Erscheinung treten. Offensichtlich steht dies mit der verschiedenen Oberflächenladung der Montmorillonite verschiedener Herkunft und verschiedenen Dispersitätsgrades im Zusammenhang, die theoretische Bereinigung dieser Fragen würde indessen viel eingehendere Forschung erforderlich machen.

Man findet die Desaggregations- und Peptisierungsmaxima bei 3 bis 7 prozentigen Natriumkarbonatmengen. Dies bedeutet also größere Mengen an Natriumkarbonat als der Ionenaustauschkapazität entspricht. Zugleich aber läßt sich allerdings ein bedeutender Teil des mit Natriumkarbonat behandelten Bentonits nicht vollständig peptisieren bzw. verursacht die zur Aktivierung benötigte Sodamenge bereits eine Koagulation der feinen Fraktionen. All dies weist darauf hin, daß die Wechselwirkung des Montmorillonits mit Natriumkarbonat nicht auf einfachem Ionenaustausch beruht — wie z.B. von WEBLUS [5] und anderen Autoren angenommen wird — sondern diese Wirkung einen komplizierten Vorgang bedeutet. Mit den Fragen der Wirkungsweise des Natriumkarbonats werden wir uns in einer nächsten Arbeit befassen.

Wir beabsichtigen mit den hier rezensierten Ergebnissen darzulegen, daß die Hauptmenge des Montmorillonits durch Behandlung mit Soda und entsprechendes Abtrennungsverfahren aus Ca-Bentoniten erhalten werden kann, zwischen den Bentoniten aus verschiedenen Fundorten charakteristische Unterschiede bestehen und daß sich die von uns angewendete Methode zur praktischen Beurteilung der mannigfaltigen Bentonite resp. Montmorillonite als geeignet erweist.

Literatur

[1] *Buzágh, A., K. Szepesi:* Acta Chim. Acad. Sci. Hung. **5**, 287 (1955).
[2] *Buzágh, A., F. Szántó:* Annales der Loránd-Eötvös-Universität, Budapest **3**, 85 (1961).
[3] *Szántó, F., B. Várkonyi:* Kolloid-Z. und Z. Polymere **191**, 123 (1963).
[4] *Náray-Szabó, I., É. Péter:* Tschermaks mineralogische und petrographische Mitteilungen **10**, 120 (1965).
[5] *Weblus, B.:* Kolloid-Z. **132**, 16 (1953).

КОЛЛОИДХИМИЧЕСКИЕ СПОСОБНОСТИ ВЕНГЕРСКИХ БЕНТОНИТОВ. I

Ф. Санто, Б. Варконьи, М. Гилде, Я. Балажс

Венгерские бентониты из различных месторождений (Mád-Koldú, Istenmezeje, Nagytétény) после активирования в соде разложились осаждением и центрифугированием на фракции. Рассмотрелись количественное распределение и минеральный состав фракций. На основе исследований сделаны выводы о пептизационной способности различных венгерских бентонитов и монтмориллонитов, полученных из них.

SCIENCE CITATION INDEX, 1965

Issued by the

INSTITUTE FOR SCIENTIFIC INFORMATION*

The Science Citation Index (SCI) represents a new form in the development of scientific information. Its basic idea of covering all natural sciences and informing about titles, authors and references in practically all periodicals of scientific importance is a new feature which enables to have information about the widest field of topics connected by the references in the papers reviewed. By these means, it facilitates new connections between workers not only on the same field, but also on contiguous subjects in a very general sense.

The SCI contains four basic parts:

Citation index (alphabetic in cited authors, 4 volumes)

Patent index (1 volume)

Source index (alphabetic in journals, 3 volumes)

Guide and Journal List,

which by cross-references render possible a basic literature search by informing about papers and authors referred to in the articles reviewed.

The growing interest in this really valuable tool led to a steady increase in bulk as well as coverage since the first issue for the year 1961. This increase amounted in a single year (from 1964 to the present issue) to 48,6%, *i. e.* the total amount of source journal items in the cumulative issue of 1965 was 296,293 covering 1147 journals and the 60,492 U. S. Patents in 1965.

Among the special services of Institute for Scientific Information we wish to mention the Search Service intended for those who need not use SCI regularly. By this service the Institute provides informations about citations, *etc.* in SCI, which are delivered within 72 hours.

We are looking forward for the 1966 issue of SCI under preparation, and we are convinced that it will render further important services to its users.

J. Gyulai

* Institute for Scientific Information 325 Chestnut St Philadelphia Pa 19106 USA.

INDEX

J. I. Horváth: Zero-Point Kinetic Energy of Relativistic Fermion Gases 3
Л. Козма: К вопросу выхода антистоксовой флуоресценции 21
J. Gyulai, V. K. Subashiev, G. A. Chalikyan: On the Photoconductivity of GaP Crystals 25
I. Hevesi: On Diffuse Reflection Spectra of V_2O_5 39
F. Márta, L. Szirovicza: The Thermal Decomposition of *n*-Propyl Nitrite 43
E. Horváth, M. Gécseg: Über die Permanganat-Oxalat Reaktion 51
М. Бартох: Изучение химических превращений диолов и органических окисей. XVI. Анализ продуктов и экспериментальные данные по термических и каталитических превращений β-окисей 59
М. Бартох, К. Ковач: Изучение химических превращений диолов и органических окисей. XXI. Исследование термического разложения 2,4-диалкил-замещённых β-окисей с применением микрореакторной техники 67
K. Koczka, P. Agócs, T. Megyeri: Preparation of Stereoisomeric 1,4-Disubstituted But-2-en-1,4-Diols and Proof of Their Configuration 73
L. Mészáros, Gy. Schöbel: Utilization of Furan. V. Procedure and Apparatus for the Conversion of Furfurol to Furan by means of a Heterogeneous Catalytic Process in the Vapour Phase 77
F. Szántó, B. Várkonyi, M. Gilde, J. Balázs: Über einige kolloidchemischen Eigenschaften von ungarischen Bentoniten. I. Peptisierbarkeit und Fraktionierung 87
Book review: Science Citation Index, 1965 (J. Gyulai) 93

TOMI PRIORES

Acta Chemica, Mineralogica et Physica,	Tom. I,	Fasc. 1—2,	1928—29.
Acta Chemica, Mineralogica et Physica,	Tom. II,	Fasc. 1—2,	1932.
Acta Chemica, Mineralogica et Physica,	Tom. III,	Fasc. 1—3,	1934.
Acta Chemica, Mineralogica et Physica,	Tom. IV,	Fasc. 1—3,	1934.
Acta Chemica, Mineralogica et Physica,	Tom. V,	Fasc. 1—3,	1937.
Acta Chemica, Mineralogica et Physica,	Tom. VI,	Fasc. 1—3,	1938.
Acta Chemica, Mineralogica et Physica,	Tom. VII,	Fasc. 1—3,	1939.
Acta Chemica et Physica,	Tom. I,	Fasc. 1—2,	1942.
Acta Chemica et Physica,	Tom. II,	Fasc. 1—6,	1948—50.
Acta Physica et Chemica, Nova series,	Tom. I,	Fasc. 1—4,	1955.
Acta Physica et Chemica, Nova series,	Tom. II,	Fasc. 1—4,	1956.
Acta Physica et Chemica, Nova series,	Tom. III,	Fasc. 1—5,	1957.
Acta Physica et Chemica, Nova series,	Tom. IV,	Fasc. 3—4,	1958.
Acta Physica et Chemica, Nova series,	Tom. V,	Fasc. 1—2,	1959.
Acta Physica et Chemica, Nova series,	Tom. V,	Fasc. 3—4,	1959.
Acta Physica et Chemica, Nova series,	Tom. VI,	Fasc. 1—4,	1960.
Acta Physica et Chemica, Nova series,	Tom. VII,	Fasc. 1—2,	1961.
Acta Physica et Chemica, Nova series,	Tom. VII,	Fasc. 3—4,	1961.
Acta Physica et Chemica, Nova series,	Tom. VIII,	Fasc. 1—2,	1962.
Acta Physica et Chemica, Nova series,	Tom. VIII,	Fasc. 3—4,	1962.
Acta Physica et Chemica, Nova series,	Tom. IX,	Fasc. 1—2,	1963.
Acta Physica et Chemica, Nova series,	Tom. IX,	Fasc. 3—4,	1963.
Acta Physica et Chemica, Nova series,	Tom. X,	Fasc. 1—2,	1964.
Acta Physica et Chemica, Nova series,	Tom. X,	Fasc. 3—4,	1964.
Acta Physica et Chemica, Nova series,	Tom. XI,	Fasc. 1—2,	1965.
Acta Physica et Chemica, Nova series,	Tom. XI,	Fasc. 3—4,	1965.
Acta Physica et Chemica, Nova series,	Tom. XII,	Fasc. 1—2,	1966.
Acta Physica et Chemica, Nova series,	Tom. XII,	Fasc. 3—4,	1966.

A kiadásért felelős: Budó Ágoston

1967

A kézirat nyomdába érkezett: 1967. január. Megjelenés 1967. június

Példányszám: 480 Ábrák száma: 37 Terjedelem: 8,4 (A/5) ív

Készült monó szedéssel, íves magasnyomással, az MNOSZ 5601—54 és az MNOSZ 5602—50 A szabványok szerint

Szegedi Nyomda 67-5519